AD-A142 619 NONLINEAR REAL-TIME OPTICAL SIGNAL PROCESSING(U) 1/2
UNIVERSITY OF SOUTHERN CALIFORNIA LOS ANGELES IMAGE
PROCESSIN.. A A SAWCHUK ET AL. 01 DEC 83 USCIPI-1100
UNCLASSIFIED AFOSR-TR-84-0538 AFOSR-81-0082 F/G 20/6 NL

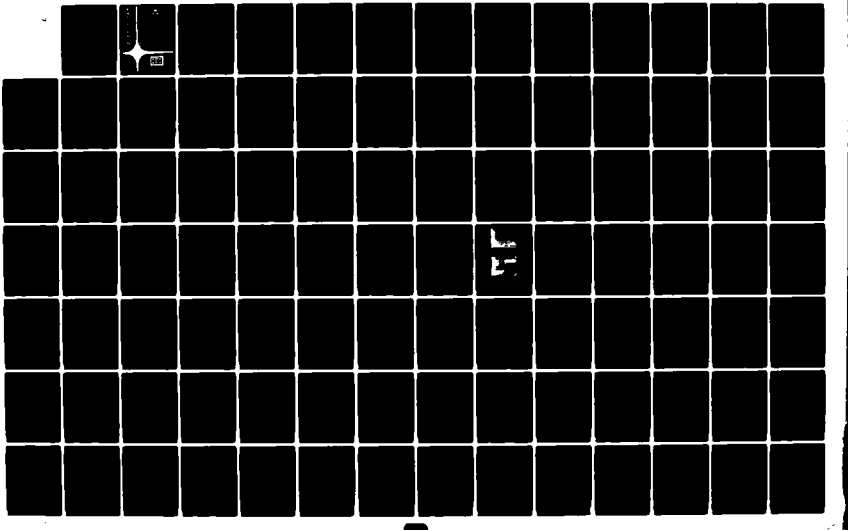

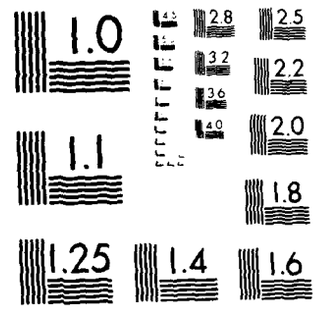

AFOSR-TR- 84-0538

USCIPI Report 1100

(4)

UNIVERSITY OF SOUTHERN CALIFORNIA

ANNUAL TECHNICAL REPORT

April 15, 1982 - April 14, 1983

NONLINEAR REAL-TIME OPTICAL SIGNAL PROCESSING

A.A. Sawchuk, Principal Investigator
T.C. Strand, and A.R. Tanguay, Jr.

December 1, 1983

Department of Electrical Engineering
Image Processing Institute
University of Southern California
University Park - MC 0272
Los Angeles, California 90089-0272

Research Sponsored by the
Air Force Office of Scientific Research
Electronics and Solid State Sciences Division
Under Grant No. AFOSR-81-0082

IPI

IMAGE PROCESSING INSTITUTE

USCIPI Report 1100

ANNUAL TECHNICAL REPORT

April 15, 1982 - April 14, 1983

NONLINEAR REAL-TIME OPTICAL SIGNAL PROCESSING

A.A. Sawchuk, Principal Investigator
T.C. Strand, and A.R. Tanguay, Jr.

December 1, 1983

Department of Electrical Engineering
Image Processing Institute
University of Southern California
University Park - MC 0272
Los Angeles, California 90089-0272

Research Sponsored by the
Air Force Office of Scientific Research
Electronics and Solid State Sciences Division
under Grant No. AFOSR-81-0082

UNCLASSIFIED

SECURITY CLASSIFICATION OF THIS PAGE (When Data Entered)

REPORT DOCUMENTATION PAGE	READ INSTRUCTIONS BEFORE COMPLETING FORM
1. REPORT NUMBER ~~AFOSR-TR- 84-0538~~ ~~USCIPI Report 1100~~	2. GOVT ACCESSION NO. AD-A143 629	3. RECIPIENT'S CATALOG NUMBER
4. TITLE (and Subtitle) NONLINEAR REAL-TIME OPTICAL SIGNAL PROCESSING	5. TYPE OF REPORT & PERIOD COVERED Annual Technical Report 4-15-82 to 4-14-83
	6. PERFORMING ORG. REPORT NUMBER USCIPI 1100
7. AUTHOR(s) A.A. Sawchuk, T.C. Strand, and A.R. Tanguay, Jr.	8. CONTRACT OR GRANT NUMBER(s) AFOSR-81-0082
9. PERFORMING ORGANIZATION NAME AND ADDRESS Department of Electrical Engineering Image Processing Institute University of Southern Calif., L.A.,CA 90089-0272	10. PROGRAM ELEMENT, PROJECT, TASK AREA & WORK UNIT NUMBERS 61102F 2305/A1
11. CONTROLLING OFFICE NAME AND ADDRESS Air Force Office of Scientific Research Bldg. 410, Bolling AFB Washington, D.C. 20332	12. REPORT DATE December 1, 1983
	13. NUMBER OF PAGES 128
14. MONITORING AGENCY NAME & ADDRESS(if different from Controlling Office) as above	15. SECURITY CLASS. (of this report) Unclassified
	15a. DECLASSIFICATION/DOWNGRADING SCHEDULE

15. DISTRIBUTION STATEMENT (of this Report)

Approved for public release; distribution unlimited.

17. DISTRIBUTION STATEMENT (of the abstract entered in Block 20, if different from Report)

18. SUPPLEMENTARY NOTES

19. KEY WORDS (Continue on reverse side if necessary and identify by block number)

Optical Information Processing
Nonlinear Optical Processing
Optical Computing
Light Valves
Optical Digital Computing

20. ABSTRACT (Continue on reverse side if necessary and identify by block number)

The results of the second year of a two year research program in nonlinear real-time optical signal processing are described. The research has concentrated on optical sequential logic systems for parallel digital processing and on variable grating mode (VGM) liquid crystal real-time spatial light modulators. The goal of the program is to extend fast parallel nonlinear operations to optical processing systems with large time-bandwidth and space-bandwidth products. Parallel and twisted nematic liquid crystal light valve (LCLV) devices have been used as a nonlinear element in a feedback arrangement in the binary sequential logic

DD FORM 1 JAN 73 1473 EDITION OF 1 NOV 65 IS OBSOLETE

UNCLASSIFIED

SECURITY CLASSIFICATION OF THIS PAGE (When Data Entered)

system. A computer generated hologram fabricated on an e-beam system serves as a beamsteering interconnection element. A completely optical oscillator and frequency divider have been experimentally demonstrated, and various circuit interconnection techniques have been explored. Research has continued on variable-grating mode (VGM) liquid crystal devices that perform local spatial frequency modulation as a function of the incident intensity. These devices can be used for nonlinear processing by selection and recombination of these spatial frequency components. These devices have many interesting physical effects with useful applications in both analog and numerical optical signal processing. Results on the physical modeling of VGM devices are given, with particular emphasis on experimental measurements of the Jones matrix describing polarized light propagation through the VGM cell.

TABLE OF CONTENTS

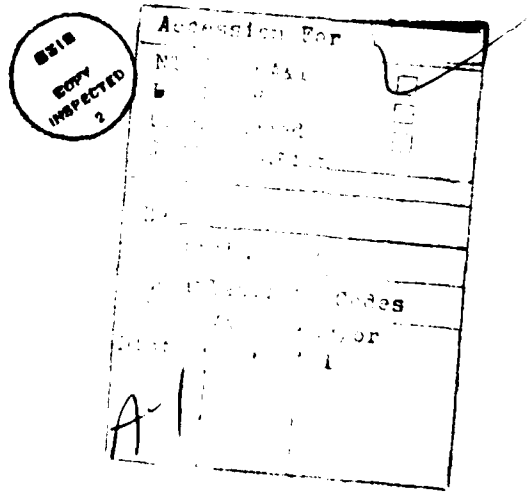

ABSTRACT

The results of the second year of a two year research program in nonlinear real-time optical signal processing are described. The research has concentrated on optical sequential logic systems for parallel digital processing and on variable grating mode (VGM) liquid crystal real-time spatial light modulators. The goal of the program is to extend fast parallel nonlinear operations to optical processing systems with large time-bandwidth and space-bandwidth products. Parallel and twisted nematic liquid crystal light valve (LCLV) devices have been used as a nonlinear element in a feedback arrangement in the binary sequential logic system. A computer generated hologram fabricated on an e-beam system serves as a beamsteering interconnection element. A completely optical oscillator and frequency divider have been experimentally demonstrated, and various circuit interconnection techniques have been explored. Research has continued on variable-grating mode (VGM) liquid crystal devices that perform local spatial frequency modulation as a function of the incident intensity. These devices can be used for nonlinear processing by selection and recombination of these spatial frequency components. These devices have many interesting physical effects with useful applications in both analog and numerical optical signal processing. Results on the physical modeling of VGM devices are given, with particular emphasis on experimental measurements of the Jones matrix

describing polarized light propagation through the VGM cell.

1. RESEARCH OBJECTIVES AND PROGRESS

1.1 Introduction and Project Overview

This report summarizes the results of the second year of a two year research effort in performing nonlinear operations in optical signal processing and achieving operation in real time using various input transducers. This section contains an introduction, motivation for the work and an overview of the research program.

The recent research described in this report addresses the need for signal processing systems that can perform high throughput parallel multi-dimensional operations on signals with large time-bandwidth and space-bandwidth products. In many of these applications, digital hardware is inadequate. One goal of this research has been to explore numerical optical computing using binary or residue arithmetic. In these systems, signals exist as discrete levels rather than as analog signals. This new approach holds much promise for the future if real-time processing speed, accuracy, and flexibility can be maintained.

During this past year of research we have concentrated on optical sequential logic systems that directly rely on the input-output characteristics of LCLV devices, and on variable grating mode (VGM) devices and their applications.

Nonlinear optical functions can be achieved directly using

the inherent transfer characteristics of an optical recording medium or real-time image transducer. With this type of nonlinear processing, there is no pulse-width modulation, intensity-to-spatial frequency conversion or other type of intermediate mechanism. Thus, these techniques offer the potential of simple systems that avoid the noise problems associated with many optical filtering techniques and have much less stringent space-bandwidth product requirements than systems which must modulate the input data. Such systems can implement parallel combinatorial logic and, with the addition of feedback, parallel sequential logic. Section 1.2 of this report describes recent results on this subject.

Another convenient method of obtaining point nonlinearities is through intensity-to-spatial frequency conversion. The idea is to encode each resolution element of an image with a grating structure where the period and/or the orientation of the grating is a function of the image intensity at the point in question. Assuming certain sampling requirements are met, each intensity level of interest is uniquely assigned to a different point in Fourier space and all points with a given intensity in the image are assigned to the same point in Fourier space (assuming space-invariant operation is desired). Then a pure amplitude spatial filter can alter the relative intensity levels in an arbitrary way, and combination of the filtered components produces various nonlinear functions. Both continuous-level (analog) nonlinear functions and various numerical logic

functions (binary or residue) are possible. This method relies on the behavior of variable-grating mode (VGM) liquid crystal real-time devices which have been developed under this AFOSR program. Section 1.3 of this report describes work on physical modeling and measurements of VGM liquid crystal devices. The goal of this work is to improve their temporal response, uniformity, lifetime, etc. Several new types of electrically and optically activated VGM devices have been constructed and evaluated.

This past year has been very productive; a number of oral presentations have been made and many written papers have been submitted describing recent results. Four of the most significant of these papers are reprinted as part of this report.

1.2 Optical Sequential Logic

1.2.1 Introduction

There has been considerable work in recent years in developing optical systems that perform essentially digital processing functions. The reasons for this interest include extending the flexibility of optical processing systems and the possibility of using the parallel capabilities of optical systems for digital signal processing. The first steps in this digital optical computing research have included parallel A/D conversion and optical combinatorial logic implementation. Each of these have been demonstrated in real-time systems at USC [1, 3].

The next step in this progression of experiments is to demonstrate the feasibility of optical sequential logic. Here the basic logic gates are interconnected in a circuit which generally includes some form of feedback. In this system the temporal response characteristics of the system become very important. We have developed an optical system which demonstrates the feasibility of optical sequential logic. In particular we have implemented a totally optical system which includes a clock driving a master-slave flip-flop. The basic elements of a sequential logic system are a nonlinear element that performs the desired logic function and an interconnection system to route the outputs of the nonlinear device to the appropriate inputs.

Two recent papers that contain the details of this work are reprinted here. The first paper is "Sequential Optical Logic Implementation", by B.K. Jenkins, A.A. Sawchuk, T.C. Strand, R. Forchheimer and B.H. Soffer. This paper has been submitted to Applied Optics and concentrates on experimental results from the sixteen gate clocked master-slave optical flip-flop.

A second paper "Architectures for a Sequential Optical Logic Processor" by P. Chavel, R. Forchheimer, B.K. Jenkins, A.A. Sawchuk and T.C. Strand, was presented at the Tenth International Optical Computing Conference in Cambridge, Ma., in April 1983. This paper is also included. It describes various interconnection techniques for optical sequential logic systems, including space-variant, space-invariant and hybrid computer-generated holograms.

SEQUENTIAL OPTICAL LOGIC IMPLEMENTATION

B.K. Jenkins, A.A. Sawchuk, T.C. Strand, R. Forchheimer

and B.H. Soffer

Abstract

An optical system that performs sequential binary logic operations is described. The system consists of a spatial light modulator (SLM) used to provide a nonlinear threshold response, and a computer-generated hologram to provide interconnections between logic gates. A two-dimensional array of logic gates with binary inputs and outputs is formed on the active surface of the SLM. These gates are interconnected by a two-dimensional array of subholograms, one for each gate. Arbitrary logic circuits consisting of NOR gates and inverters can be implemented, and the system can be reconfigured by changing a single holographic element. The system is demonstrated using a twisted-nematic liquid crystal light valve as the SLM. A test circuit has been implemented that includes a synchronous master-slave flip-flop and an oscillator consisting of five inverters in a feedback loop. Experimental results of this test circuit are presented.

B.K. Jenkins, A.A. Sawchuk, T.C. Strand, and R. Forchheimer were at the University of Southern California, Department of Electrical Engineering, Los Angeles, Ca. 90089 when this work was done. T.C. Strand is now with IBM Corp., San Jose, Ca. 95193, and R. Forchheimer is now with Linkoping University, Linkoping, Sweden. B.H. Soffer is at Hughes Research Laboratories, Malibu, Ca. 90265.

I. Introduction

The vast majority of optical processing systems to date have operated with analog signal levels. While many of these systems can perform specific operations with extremely high throughput rates, at the same time they suffer from two basic limitations: the variety of operations that can be performed and the accuracy of the results. These limitations preclude the use of optical processing systems in certain application areas that could otherwise benefit from some of the inherent advantages of optics. These advantages include a high degree of parallelism, both in processing and input/output, and a high density and number of interconnections. Two approaches have been taken to eliminate or at least substantially reduce these limitations. Both approaches utilize discrete, instead of analog, signal levels. One approach is based on residue arithmetic operations, and optical systems utilizing this principle have been studied [1-7]. The other approach is based on binary logic operations, such as used in conventional electronic computers.

The first step in the binary approach has been to demonstrate Boolean operations optically. Two-dimensional arrays of some of these operations such as OR, NOR, AND, NAND, XOR, and XNOR have been demonstrated using a variety of optically-addressed two-dimensional spatial light modulators (SLMs). These include the Pockels readout optical modulator (PROM) [8,9], the microchannel spatial light modulator (MSLM)

[10,11], the Hughes liquid crystal light valve (LCLV) [12-14], and a segmented liquid crystal light valve used as an optical parallel logic (OPAL) device [15,16]. These operations have also been demonstrated using light-emitting diodes with optical masks [17]. Other schemes, too numerous to mention here, have also been used to implement logic gates optically. A review of optical computing systems, including these combinatorial operations, is given in reference [18]. Very recently, fast individual optical logic gates have been demonstrated in InSb [19] and in GaAs [20].

Although these operations form the basic building blocks for combinatorial logic, in order to build a sequential circuit or an optical computer, memory is also needed. This can be achieved using optical feedback. An array of optical flip-flops has been demonstrated using an LCLV in an optical system with feedback [21,22], and an array of optical latches has been demonstrated by using an OPAL device with optical feedback [23]. Fast individual bistable elements have also been demonstrated in many materials using feedback by means of a Fabry-Perot cavity [24].

These elements, however, have not been combined to form an all-optical logic circuit. Such a circuit may have the potential of combining the high degree of parallelism and interconnection density found in optical processors with the flexibility and accuracy of digital electronic computers. A method for combining these binary elements using fiber optics has been described [25],

but a complete system has not been demonstrated experimentally. A system with an array of optical gates and some optical memories, under electronic control, has been demonstrated [26]. This system is particularly useful for operations requiring only local communication, as is the case for many image processing operations, e.g. cellular logic machines.

In this paper a system is presented which interconnects optical logic elements to form a sequential logic circuit. Every signal in this system is represented optically, and at the same time the system permits the implementation of arbitrary connections between the individual logic gates. Because this system is digital, the accuracy limitation mentioned above can be overcome by selecting the number of bits per data element to yield the desired accuracy. In addition, the arbitrary interconnections of the system presented here permit the implementation of a very large variety of processing operations. Finally, the advantages of parallelism and interconnection density are retained to a large degree [27].

In the system presented here, a spatial light modulator (SLM) is used as a two-dimensional array of independently-acting logic gates. These gates are interconnected via an optical system that utilizes a computer-generated hologram. In this paper we discuss the SLM implementation of logic gates in section II, the interconnection system in section III, and some experimental results of the implementation of a test circuit to

demonstrate the feasibility of the optical logic system in sections IV and V. Finally, in section VI we point out some of the limitations involved in using optical devices as arrays of logic gates, and discuss the relevance of these limitations to the system presented here.

II. LOGIC GATES

Binary logic gates may be implemented optically through the use of a point nonlinearity. The general scheme used for each gate in our system is depicted in Fig. 1. First the two binary input lines to the gate are added to yield a single three-level signal. The value of this 3-level signal (or (N+1)-level signal for the case or N-input gates) is then equal to the number of input lines that are true (i.e., that have a value of 1). This signal is then operated on by a nonlinear function with a binary-valued output. As will be shown below, any logic operation can be performed in this manner by choosing the appropriate nonlinear function. Figure 2 shows the extension of this method to N-input gates. To implement this scheme optically, the binary values are represented by intensity levels with a high intensity level representing a 1 and a low intensity level representing a 0. The addition is done merely by optically superimposing the input line signals. With a detector that integrates the signal over the input spot, this has the effect of adding the intensity levels regardless of the coherence properties of the light (see section III). In this paper, the

term "gate input" will refer to this superimposed signal (i.e., the input to the nonlinearity) and the term "input lines" will refer to the binary inputs before superposition.

Possible choices of the nonlinear functions for some of the common logic operations are shown in Fig. 3. In the case of 2-input gates, there are a total of 16 possible operations. The operations AND, NAND, OR, NOR, XOR, XNOR, TRUE, and FALSE may be implemented with this scheme directly (Table 1a). The remaining logic functions require the ability to distinguish between the two input lines A and B. These operations are A, B, $\bar{A}$, $\bar{B}$, $\bar{A}\cdot B$, $A\cdot\bar{B}$, $\bar{A}+B$, and $A+\bar{B}$. These operations can be implemented with a single gate by doubling the signal level of one of the input lines, say, A (Table 1b); this is conceptually equivalent to using a 3-input gate with A going into two of the input lines.

However, several subsets of the operations which are realizable with a 2-input gate form logically complete sets, obviating the need for these asymmetric functions. For example, all logic operations can be built out of NOR gates.

The nonlinearity required for optical logic may be implemented with any of a variety of optical devices. Fast switching times (nsec-psec) may be obtained by using a bistable optical device [19,20,24,28]. This prospect is discussed in section VI. While in principle these devices can be built as two-dimensional spatial light modulators (SLMs), at present they are not available. Other optically addressed SLMs are presently

available, however. While their characteristically slow response times may appear to be a major drawback, they provide a practical means for demonstrating the system concept. The same sequential optical logic system described and demonstrated here may be used with other SLMs, including much faster ones, so long as they can provide a suitable nonlinearity, and satisfy the following requirements. First, the inputs and outputs of the gates must be the same wavelength. This eliminates such devices as the Pockels readout optical modulator (PROM) [9], with which the write illumination must be a different wavelength than the read illumination. Second, we assume the device has no memory, although in some cases devices with memory could also be used. Finally, we assume here that the gate inputs and outputs appear on opposite sides of the SLM, although it is worth noting that with a slight rearrangement of the system components, SLMs with gate inputs and outputs on the same side can also be accommodated.

Given these requirements, there are still a variety of SLMs that can be used. The microchannel spatial light modulator [11] could be used in this system, as could various types of liquid crystal light valves (LCLVs) [12-14]. For the demonstration of the system presented in this paper, a Hughes LCLV was used. An LCLV with liquid crystal molecules exhibiting a uniform parallel alignment in the off state may be used to implement nonmonotonic nonlinearities, which are needed for such operations as XOR [14]. In this system, NOR gates were used, and LCLVs with liquid

crystal molecules in a variety of configurations can provide the appropriate nonlinearity. For example, Fig. 4 shows the steady-state response for an LCLV with a twisted nematic liquid crystal layer, biased to implement the NOR operation.

The input/output characteristic of an SLM, when used in this system, essentially serves as an approximation to the corresponding ideal nonlinearity (e.g., Fig. 3). An important criteria in determining whether a particular nonlinearity is a sufficiently accurate approximation, is the regeneration or "restandardization" of the signal level at each pass through a gate. The general requirement is that a signal should not degenerate in passing through a large number of gates in series. Assuming a transition time of zero, the signal level at each pass through a gate may be read off the SLM input/output curve. If f(x) represents this curve and x is the signal level at the gate input, then for the case of a simple inverter, the following requirement ensures that the signal will not degenerate (Fig. 5):

$$a_{1-i} < kf(x) < b_{1-i} \quad \text{for all } x \in (a_i, b_i), \quad i=0,1$$

where k = the gain from the output of one gate to the input of the next and $a_i<x<b_i$ defines the range of gate input signal levels interpreted as the discrete level i. This can be generalized to include the other Boolean operations, by defining output intervals as the (union of the) mapping through f of the corresponding gate input intervals. One then requires appropriate combinations of output intervals (i.e., all possible

sums of the elements) to map into the corresponding gate input intervals. The input/output curve of the LCLV used in the experiment does satisfy these criteria for the NOR and NOT operations.

III. INTERCONNECTIONS

The previous section dealt with the optical implementation of logic gates, and in this section we address the problem of interconnecting these gates optically. The general problem is to be able to implement an arbitrary connection pattern between gate outputs and gate inputs. Since gate outputs correspond to inputs of the interconnection system and outputs of the interconnection system become gate inputs, for the remainder of this section the words input and output will be used with respect to the interconnection system only unless explicitly stated otherwise.

In direct analogy to the use of wires in an electrical circuit, optical fibers could be used for the interconnections. Although the idea is simple when there is a one-to-one correspondence between inputs and outputs, the method is less obvious when there is not. A possible scheme is described here. Assuming each input illuminates enough fibers, the fibers that are illuminated by an input, j, that addresses more than one output can be split up such that an equal number of fibers, P_j, go to each output. Since all outputs may not have the same number of fibers, a mask is needed at the input plane, with an

intensity transmittance at each input that is inversely proportional to P_j. Alternatively, the same (albeit small, perhaps) number of fibers could be used to address all outputs, making P_j independent of j. The problem of fabricating fiber optic bundles for large, arbitrary interconnection patterns, however, is a serious drawback unless one has an automated system to do so.

The interconnections in the system presented here are implemented with a holographic element instead of the fiber optic assembly. The holographic element consists of an array of subholograms in a one-to-one correspondence with the gates, or pixels of the input array. The interconnection system is shown schematically in Fig. 6. This is only one of several holographic systems that could be used to interconnect the gates [27]. In this system, the input array is imaged onto the subhologram array. The hologram is encoded in the Fourier domain. A Fourier transform is then taken optically to obtain the output array. Each subhologram reconstructs a set of dots, one dot for each connection to a pixel of the output array. Because of the Fourier transform relationship, the coherence area of the illumination at the hologram must be larger than or equal to the subhologram size. If the coherence area is much larger, then fringe patterns will appear in each pixel in the reconstruction plane. This occurs when different subholograms, whose separation is less than the coherence area, reconstruct dots at the same location in the output array. Spatial averaging over each

pixel in the output array then results in an effective intensity summation, as desired for gate inputs (Figs. 1 and 2).

This interconnection system is essentially a space-variant filter, providing a different point spread function for each input pixel. Because of the Fourier transform relationship, each subhologram stores the absolute position of the output pixels it addresses. This absolute addressing scheme implies the system does not distinguish between global and local interconnections, but discriminates only on the basis of the position of the output array pixels, relative to the origin of the output array.

In order to avoid a manufacturing problem similar to that of the fiber optic system, the hologram can be recorded optically using an automated system under computer control [29,30], or can be generated entirely by computer. In this experiment the hologram was generated by computer. Many types of computer-generated Fourier-transform holograms have been demonstrated [31] and many of them would suffice for this application. To demonstrate the operation of the sequential logic system we used a binary version of the hologram proposed by Lee in 1970 [32] for reasons of simplicity, diffraction efficiency, and signal-to-noise ratio in the reconstruction [33]. Because of the coding process used in the hologram, the desired output array appears in the (1,0)-diffracted order in the reconstruction plane, leaving the spatially inverted (-1,0) order available for probing the system.

The effect of the hologram on the input array may be represented by the matrix equation

$$\underline{O} = \underline{\underline{M}}\ \underline{I} \tag{2}$$

Here $\underline{I}$ is a vector representing the two-dimensional input array, lexicographically ordered. This input array is actually the gate output array augmented by the system inputs. Similarly, $\underline{O}$ is a vector representing the lexicographically ordered output array (which is the gate input array augmented by the system outputs). Each element of the vector $\underline{I}$ is binary valued and represents the signal of the corresponding pixel in the input array. Each element of $\underline{O}$ is a nonnegative integer representing the signal level of the corresponding output array pixel. This integer is between 0 and N if the output pixel represents a gate with N input lines, and is binary if the output pixel represents a system output. $\underline{\underline{M}}$ is a matrix representation of the interconnect pattern - each matrix element m_{ij} is nonzero if and only if there is a connection between pixel j of the input array and pixel i of the output array. m_{ij} is an integer equal to the signal level created at output pixel i due to a signal level of 1 at input pixel j.

Using this notation, the fan-in to gate i (or number of input lines to gate i) is equal to the sum of the elements in row i of $\underline{\underline{M}}$. The fan-out of gate j (or number of gate input lines, plus the number of system outputs, that come from the output of gate j) is equal to the sum of the elements in column j of $\underline{\underline{M}}$.

The fan-out is limited only by such parameters as the power of the illumination source, hologram efficiency, and SLM input sensitivity. The maximum fan-in is a function of the SLM intensity input/output characteristic.

With this interconnection technique, the hologram or equivalently the elements of M, completely define the circuit. Within the limit of the number of gates available, any operation that can be represented by a digital circuit can be implemented optically with this system by encoding the appropriate interconnection pattern into the hologram.

IV. EXPERIMENTAL DEMONSTRATION

For the experimental demonstration of this system, an LCLV with liquid crystal molecules in a 45° twisted nematic configuration was used as the SLM. The light valve is read out between crossed polarizes and is biased to implement a NOR operation. Its steady-state input/output relationship is shown in Fig. 7. This response, together with the attenuation of the interconnection system, satisfies the regeneration criteria stated in Section II.

The gates are interconnected with a binary version of the Lee (1970) computer-generated hologram [32]. In a Lee hologram, each complex-valued sample is described by a linear combination of four real nonnegative numbers. i.e., is decomposed into its components along each of the four half-axes in the complex plane.

Each cell of the hologram is divided into four subcells, one subcell for each of these four components. One complex-valued sample is taken at the center of each subcell. Stored in each subcell is the corresponding component of its complex-valued sample. Because of the locations of these subcells, upon taking the optical Fourier transform, these four components are added with the correct phases to obtain the reconstruction in the (1,0) diffracted order. If the transmittance of the hologram is binary valued, each subcell actually contains a rectangle whose width is equal to the subcell width and whose height is proportional to the value of the corresponding sample component (Fig. 8).

For the hologram used in this experiment, the transmittance is binary valued and these values are represented by different optical path lengths, i.e, a phase hologram. If the optical path lengths differ by a phase of π, the theoretical efficiency of the hologram is four times that of the equivalent absorption hologram [31]. A possible tradeoff is that the (0,0)-order intensity may increase by more than a factor of four.

The hologram was written onto photo resist via electron-beam lithography. Surface relief of the photo resist provides the optical path length difference in the hologram. The electron-beam machine used has a step size of 0.125 μm and has written patterns with line widths as small as 0.5 μm. It writes 1.024x1.024mm fields and can stitch them together to cover a maximum area of 102x102mm. The machine provides a far greater

space-bandwidth product than was needed for our test circuit.

Our test circuit comprises 16 gates so the hologram comprises 16 subholograms, which are laid out in a 4 by 4 array. Each subhologram covers a circular area and has diameter of 1.04mm. Each cell is a square 62.5 μm on a side, so there are a maximum of 17 cells (68 subcells) across each subhologram in the horizontal direction. Each subcell has a width of approximately 15.6 μm, or 125 steps of the electron-beam system, and has a height of 500 steps; both dimensions have more steps than were needed. 251 quantization levels were used for each subcell sample, keeping the apertures centered in each subcell.

Figure 9 shows pictures of one subhologram, taken with a scanning electron microscope. Figure 9a shows the entire subhologram. The rectangles are pits, the exteriors of which are photo resist, and the interiors of which are just glass substrate. Figure 9b shows a close-up of the top edges of two rectangles. The rectangle interiors (no photo resist) are located below these edges. The thickness of the photo resist is 1.25 μm and the edges are inclined at approximately 32^{o} with respect to the substrate normal. The pictures reveal that the photo resist is slightly rough near the edges but is otherwise quite smooth (except for an occasional defect). Defects are apparent on the glass but are too small to affect the optical quality. Line widths down to approximately 1 μm were obtained.

Defining efficiency as the power in the desired reconstruction pixels due to one subhologram divided by the power incident on that subhologram, the maximum efficiency over all subholograms was measured to be 5%. The efficiencies of the other subholograms were intentionally reduced in order to normalize the intensities in the reconstruction plane. This measurement was taken using an illumination wavelength of 514.5 nm, the wavelength used in the sequential logic system. This is close to the optimum wavelength for this hologram. Aside from efficiency, we must consider the noise appearing in the desired reconstruction order, of which there are three sources: (1) the encoding process used to represent the complex-valued function on the hologram, (2) scattering from the photoresist and glass substrate, and (3) the tail of the (0,0) order. The pictures of Fig. 9 indicate that the contribution due to scattering should be small, and this is verified by experiment. The effect of the (0,0) order could be substantial with a phase hologram, but can be filtered out spatially if the location of the limiting aperture is chosen appropriately. This leaves the encoding process as the major source of noise. The effect of the encoding process on noise is discussed in [33,34]. For the case of an interconnection hologram, we can define the signal-to-noise ratio in each reconstruction pixel as the ratio of the power in the reconstruction pixel when it represents a maximum signal level, to the maximum power in the same reconstruction pixel when it represents a signal level of 0. Measurements on our test

hologram indicate a typical signal-to-noise ratio of approximately 60.

A diagram of the main components of the sequential logic system is shown in Fig. 10. An expanded Ar laser beam is incident on the readout side of the LCLV (gate output plane). It is reflected off the internal mirror of the LCLV and is imaged from the liquid crystal (gate output) plane to the hologram via L_2. The liquid crystal plane is situated between crossed polarizers. The Fourier transform of the field transmitted by the hologram appears at the write side of the LCLV (gate input plane) via L_3. The phase of the illumination at the gate input plane is not correct, but only the intensity is of interest. Note that the Fourier transform relationship provides for complete regeneration of spot location during each pass through the feedback loop. In addition, since the subholograms are not contiguous, a mask is effectively incorporated into the hologram. This provides regeneration of the size and shape of each pixel, and also facilitates alignment.

A diffuser is placed just in front of the LCLV gate input plane in order to average over the fringe patterns mentioned in Section III. This is not necessary when the pixels are small enough for the fringe patterns to be beyond the resolution limit of the device. Since a phase hologram was used and the effects of the (0,0) diffracted order were of concern, an aperture was used as a spatial filter at P, to filter out diffraction effects

from the limiting aperture. The (-1,0) diffracted order in the hologram reconstruction can be used to monitor the gate inputs during system operation. The gate outputs can also be probed by using a reflection off of the analyzer or the hologram.

For purposes of demonstration, a test circuit needs to be chosen. A gate may be used in two different classes of circuits: (1) with feedback, e.g., to achieve oscillation or to achieve memory, or (2) with no feedback. A test circuit was chosen that includes both classes (Fig. 11) and a hologram with the appropriate interconnection pattern was then generated (Fig. 12). The test circuit includes a synchronous master-slave flip-flop and a driving clock. The clock circuit is a ring oscillator consisting of an odd number of inverters. Clock circuits with three gates and with five gates have been implemented. The flip-flop functions as a frequency divider and outputs a signal whose frequency is half that of the clock and whose duty cycle is close to 50%. The outputs of some of the gates in the test circuit are shown in Figs. 13-14. A discussion of them follows.

V. DISCUSSION OF RESULTS

The clock circuit, consisting of five gates in a feedback loop, will be considered first. The phase delay of the signal in passing through one gate is expected to be 180^{o} (for inverting gates) plus an additional $36^{o}+72^{o}n$, n=integer, to insure that the total delay through all 5 gates is a multiple of 360^{o}. The phase

delay in passing through gate 12 is measured to be 216° (Fig. 13) within experimental error. The frequency of oscillation was 2.65 Hz. (Speed is device-dependent and is discussed in sections II and VI). An oscillator has also been constructed out of 3 gates, in which case the expected phase delay through each is $240^{\circ}+120^{\circ}n$, and was measured to be close to 240°. Although nonuniformities across the spatial extent of the LCLV caused variations in characteristics from one gate to another yielding a slightly different phase delay through each gate, the sum of the 3 phase delays was 720° to within the accuracy of the measurement, as expected.

The frequency of oscillation of the clock circuit can be changed by changing the number of gates in the feedback loop. The five-gate clock circuit oscillated at a frequency of 2.64 ± 0.07 Hz (measurement error). If we assume the temporal behavior of the LCLV can be modeled by a simple RC circuit, the above measurement implies that the three-gate clock should oscillate at a frequency of 6.32 Hz. We observed 6.40 ± 0.12 Hz. No attempt to measure the frequency stability was made. The system did, however, sustain oscillations for periods lasting eight hours. Given the number of gates in the clock circuit, the frequency of oscillation is determined solely by the temporal characteristics of the LCLV. For sufficiently fast SLMs, the optical path length of the interconnection system will also have an effect.

Measurements we have taken indicate that the LCLV response time is limited by the photoconductor and that the response time of the liquid crystal is much faster [14]. Improvements in LCLV photoconductor response times [35] should yield higher clock frequencies. Use of optical bistable devices could improve clock frequencies by many orders of magnitude (see Section VI).

The test circuit (which has five gates in its clock circuit) functions correctly. The output waveforms (Fig. 13-14) are not expected to be square. The gates are operating near their maximum speed, so their rise and fall times are substantial in comparison with their pulse widths. With one minor exception, all gates in the test circuit output the expected waveforms. The exception is that the pulse widths of the outputs of gates 5 and 6 are less than those of the outputs of gates 1 and 2. They were expected to be the same. This is a result of unequal interconnection losses among different gates in the clock circuit (due to an error in the hologram), which caused gate 11 to output larger pulse widths than gate 12.

VI. DEVICE LIMITATIONS

We have mentioned in section II the possibility of using much faster devices in place of the LCLV, for example an optical bistable device. We must consider the potentials and limitations involved in using such devices as optical logic gates, as well as how they might compare with their electrical counterparts. A

number of people have studied this subject [36-43].

A very important consideration is power dissipation of these devices. This takes the form of heat which must be removed from the device to keep its temperature within operating bounds. Earlier works have indicated that optical logic gates may suffer from a higher power dissipation than electronic gates, and in particular noted the unfavorable trend on fundamental limits in optical logic of increasing power dissipation with decreasing delay time, versus a fundamental limit of power dissipation that is independent of delay time in the case of semiconductor electronic devices [37,38]. More recently it has become evident that most of the power dissipation in a practical integrated circuit is due to the on-chip interconnections instead of the transistors themselves, and that the lower limit on this power dissipation also increases with decreasing delay time [41]. his limit is essentially the same, when plotted on a power vs. delay time graph, as the lower limit on power of an optical switching device using an absorptive nonlinearity given in [42]. Furthermore, the limit on power in the case of an optical switch using a reactive nonlinearity increases more slowly (than the optical absorptive and electrical cases) with decreasing delay, although its power level is higher in the region of common delay times (>1 psec). While lowering the operating temperature of semiconductor logic will lower its power dissipation limit to a point [41], use of an optical resonator can, in some cases, reduce the limits on the power dissipation of the optical switch

[42,43]. Finally, we point out that in the optical case much of the power can potentially be dissipated external to the device, permitting the operation of switches at significantly higher power levels than would otherwise be possible.

While these fundamental limits on optical switches can be approached with known materials [42], significant progress, some of a relatively fundamental nature, would have to be made for these switching devices to become competitive with electronics [42,43]. Optical gates will not replace electronic gates for use in general-purpose computers in the near future, but their use in an optical special-purpose computer could permit the realization of a number of architectural advantages over semiconductor electronics [27]. These advantages include parallel input-output, global as well as local interconnections, and the implementation of interconnection-intensive circuits and processors without reducing the active device area available for gates.

CONCLUSIONS

In conclusion, we have presented an all optical sequential logic system. It is all optical in that every signal is represented optically, and it is sequential in that it can include memory elements and clocks. We demonstrated the operation of the system using a test circuit consisting of a synchronous master-slave flip-flop and its driving clock. The

circuit functioned properly and the output of each gate was as expected, for the given interconnection hologram.

On this system, any digital circuit can be implemented, up to limitations in the total number of gates. The circuit is encoded in the hologram. Since the hologram represents a fixed interconnection pattern, the circuit or processor is not reconfigurable in real time. This does not eliminate the possibility of software control however, as can be seen by noting that the interconnections between gates in a general-purpose electronic computer are also fixed. As in an electronic sequential circuit, software control is obtained by changing the inputs to appropriate control lines.

The speed of operation of the processor depends on the device. While an LCLV was used to demonstrate the system concept, much faster SLMs in the same system will yield much faster processors. Recent progress in optical bistability provides hope for an extremely fast optical logic system.

The maximum number of gates that can be implemented is limited by the space-bandwidth product of the hologram. However, this restriction can be alleviated by using a different interconnection technique [27].

Aside from the question of speed and number of gates, this optical system has some architectural advantages over conventional digital electronic systems. First, parallel inputs

(and outputs) can easily be incorporated into the system. This permits large amounts of parallel data to be input to and output from the system, alleviating the pin-out constraints found in semiconductor electronics. Second, communication intensive operations may be performed easily with the optical system. And finally, the optical system cannot tell the difference between global and local interconnections. It is the lack of these features that is becoming a substantial limiting factor in the design and development of state-of-the-art semiconductor electronic systems. These points are treated more fully in the subsequent paper [27].

ACKNOWLEDGMENTS

The holograms used in this work were fabricated at the Microelectronics Research and Development Center of Rockwell International by R. Imerson and A.B. Jones. The authors gratefully acknowledge their assistance. This work was supported by the Air Force Office of Scientific Research under grant AFOSR-81-0082. Portions of this paper were presented at the 1982 Annual Meeting, Optical Society of America, Tucson, Az., October 1982 [44].

References

1. A. Huang, "The Implementation of a Residue Arithmetic Unit via Optical and Other Physical Phenomena," Proc. 1975 Int. Optical Computing Conf., 14 (1975)

2. A. Huang, Y. Tsunoda, J.W. Goodman, S. Ishihara, "Optical Computation Using Residue Arithmetic," Appl. Opt. 18, No. 2, 149 (1979).

3. D. Psaltis and D. Casasent, "Optical Residue Arithmetic: A Correlation Approach", Appl. Opt. 18, No. 2, 163 (1979).

4. A. Tai, I. Cindrich, J.R. Fienup, C.C. Aleksoff, "Optical Residue Arithmetic Computer with Programmable Computation Modules," Appl. Opt. 18, No. 16, 2812 (1979).

5. S.A. Collins, Jr., J. Ambuel, E.K. Damon, "Numerical Optical Data Processing," Proc. 1978 Intl. Optical Computing Conf., IEEE CAT. No. 79CH 1305-2, 194 (1978).

6. F.A. Horrigan and W.W. Stoner, "Residue-Based Optical Processor," Proc. SPIE 185, 19 (1979).

7. C.C. Guest and T.K. Gaylord, "Truth-Table Look-up Optical Processing Utilizing Binary and Residue Arithmetic," Appl. Opt. 19, No. 7, 1201 (1980).

8. B. Horowitz, F. Corbett, Opt. Eng. 17, 353 (1978).

9. S. Iwasa, J. Feinleib, "The Prom Device in Optical Processing Systems," Opt. Eng. 13, 235 (1974).

10. C. Warde, A.D. Fisher, J.I. Thackara, A.M. Weiss, Image Processing Operations Achievable with the Microchannel Spatial Light Modulator," SPIE 252 (1981).

11. C. Warde, A.M. Weiss, A.D. Fisher, J.I. Thackara, "Optical Information Processing Characteristics of the Microchannel Spatial Light Modulator," Appl. Opt. 20, No. 12, 2066 (1981).

12. S.A. Collins, Jr., M.T. Fatehi, K.C. Wasmundt, "Optical Logic Gates Using a Hughes Liquid Crystal Light Valve," SPIE 232 (1980).

13. B.H. Soffer, D. Boswell, A.M. Lackner, P. Chavel, A.A. Sawchuk, T.C. Strand, and A.R. Tanguay, Jr., "Optical Computing with Variable Grating Mode Liquid Crystal Devices," Proc. SPIE 232 (1980).

14. A.A. Sawchuk, T.C. Strand, and A.R. Tanguay, Jr., "Nonlinear Real-Time Optical Signal Processing," USCIPI Report 1080, USC Image Processing Institute (1982).

15. R.A. Athale, S.H. Lee, Opt. Eng. 18, 513 (1979).

16. R.A. Athale, H.S. Barr, S.H. Lee, B.J. Bartholomew, Proc. SPIE 241, 149 (1980).

17. J. Tanida and Y. Ichioka, Optical Logic Array Processor," Proc. Tenth Intl. Optical Computing Conf., IEEE Cat. No. 83CH1880-4, 18, (1983).

18. A.A. Sawchuk and T.C. Strand, submitted to Proc. IEEE.

19. C.T. Seaton, F.A.P. Tooley, M.R. Taghizadeh, W.J. Firth, S.D. Smith, "Optical Logic Operations in InSb Bistable Devices," Conf. on Lasers and Electro-Optical Technical Digest, IEEE Cat. No. 83CH1852-3, 92 (1983); D.A.B. Miller, S.D. Smith, C.T. Seaton, IEEE J. Quantum Electron. QE-17, 312 (1982).

20. J.L. Jewell, M.C. Rushford, H.M. Gibbs, and N. Peyghambarian, "Nonlinear-Etalon Optical Logic Gates," Presented at the 1983 Annual Meeting, Optical Society of America, New Orleans, La., October 1983; JOSA 73, (1983).

21. V.K. Sengupta, U.H. Gerlach, S.A. Collins, "Bistable Optical Spatial Device Using Direct Optical Feedback," Optics Letters 3, No. 5 (1978).

22. U.H. Gerlach, S.A. Collins, V.K. Sengupta, Opt. Eng. 19, 452 (1980).

23. R. Athale, S.H. Lee, Appl. Opt. 20, 1424 (1981).

24. H.M. Gibbs, S.L. McCall, T.N.C. Venkatesan, "Optical Bistable Devices: The Basic Components of All-Optical Systems?" Opt. Eng. 19, No. 4, 463 (1980).

25. D.H. Schaefer and J.P. Strong III, "Tse Computers," Proc. IEEE 65, No. 1., (1977).

26. H. Barr and S.H. Lee, "A Digital Optical Processing System," Proc. Tenth Intl. Optical Computing Conf., IEEE CAT. No. 83CH1880-4, 171 (1983).

27. P. Chavel, R. Forchheimer, B.K. Jenkins, A.A. Sawchuk, T.C. Strand, "Architectural Implications of Digital Optical Processors," Submitted to Appl. Opt.

28. P.W. Smith and W.J. Tomlinson, "Bistable Optical Devices Promise Subpicosecond Switching," IEEE Spectrum, 26 (June 1981).

29. S.K. Case, P.R. Haugen, and O.J. Lokberg, "Multifacet Holographic Optical Elements for Wave Front Transformations," Appl. Opt. 20, No. 15, 2670 (1981).

30. S.K. Case, P.R. Haugen, "High Efficiency Multifacet Holographic Optical Elements for Image Formation, " Proc. Soc. Photo-Opt. Instr. Eng. 437 (1983).

31. W.J. Dallas, "Computer-Generated Holograms," in The Computer in Optical Research: Methods and Applications, B.R. Frieden, ed. (Springer-Verlag, New York, 1980), p. 291.

32. W.H. Lee, "Sampled Fourier Transform Hologram Generated by Computer," Appl. Opt. 9, No. 3, 639 (1970).

33. J. Bucklew and N.C. Gallagher, Jr., "Comprehensive Error Models and Comparative Study of Some Detour-Phase Holograms," Appl. OPT. 18, 2861 (1979).

34. J.P. Allebach, "Representation-Related Errors in Binary Digital Holograms: A Unified Analysis," Appl. Opt. 20, No. 2, 290 (1981).

35. V. Efron, P.O. Braatz, M.J. Little, R.N. Schwartz, Jan Grinberg, "Silicon Liquid Crystal Light Valves: Status and Issues," SPIE Advances in Optical information Processing 388 (1983).

36. R.W. Keyes, "Physical Problems and Limits in Computer Logic," IEEE Spectrum, 36 (May 1969).

37. R.W. Keyes and J.A. Armstrong, "Thermal Limitations in Optical Logic," Appl. Opt. 8, 2549 (1969).

38. R.W. Keyes, "Power Dissipation in Information Processing," Science 168, 796 (1970).

39. R. Landauer, "Optical Logic and Optically Accessed Digital Storage," in Nesterikhin, Stroke, and Kock, eds., Optical Information Processing (Plenum Press, New York, 1975), p. 219.

40. R.W. Keyes, "Physical Limits in Digital Electronics," Proc. IEEE 63, 740 (1975).

41. R.W. Keyes, "Fundamental Limits in Digital Information Processing," Proc. IEEE 69, 267 (1981).

42. P.W. Smith, "On the Physical Limits of Digital Optical Switching and Logic Elements," Bell System Technical Journal 61, 1975 (1982).

43. R.L. Fork, "Physics of Optical Switching," Phys. Rev. A 26, 2049 (1982).

44. B.K. Jenkins, A.A. Sawchuk, T.C. Strand and B.H. Soffer, "Sequential Optical Logic Implementation," Presented at 1982 Annual Meeting, Optical Society of America, Tucson, October 1982; JOSA 72, p. 1721A. (1982).

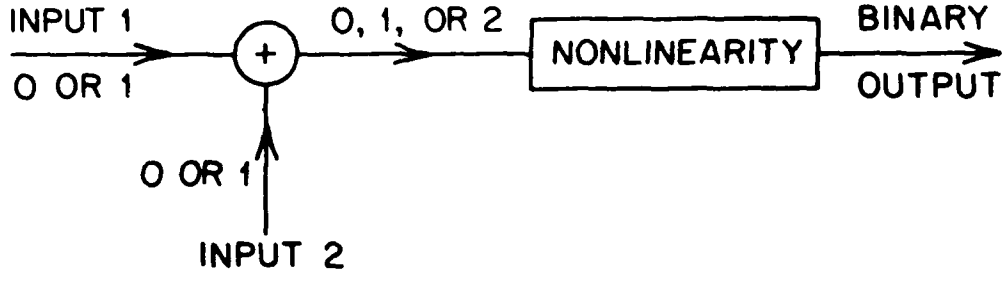

Fig. 1. Implementation of a logic gate.

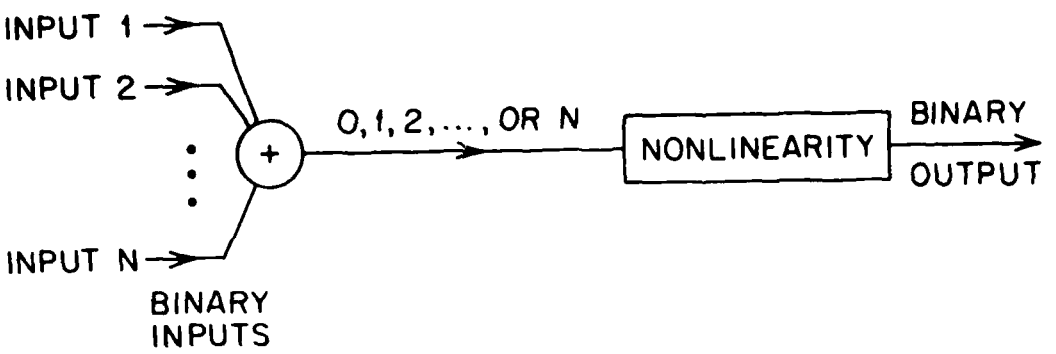

Fig. 2. Generalization of Fig. 1 to N-input gates.

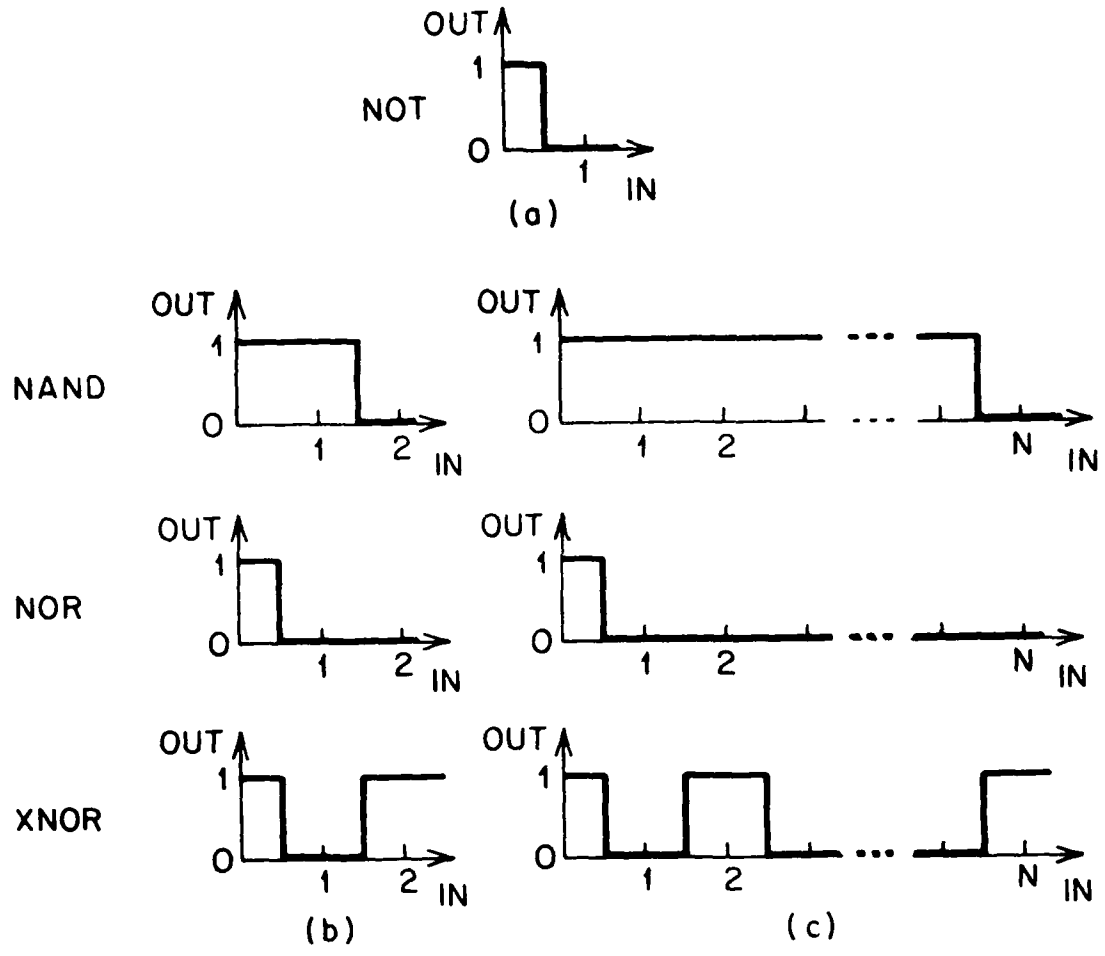

Fig. 3. Nonlinearities for implementation of logic operations. (a) 1-input gates; (b) 2-input gates; (c) N-input gates (N is assumed to be even in the XNOR case).

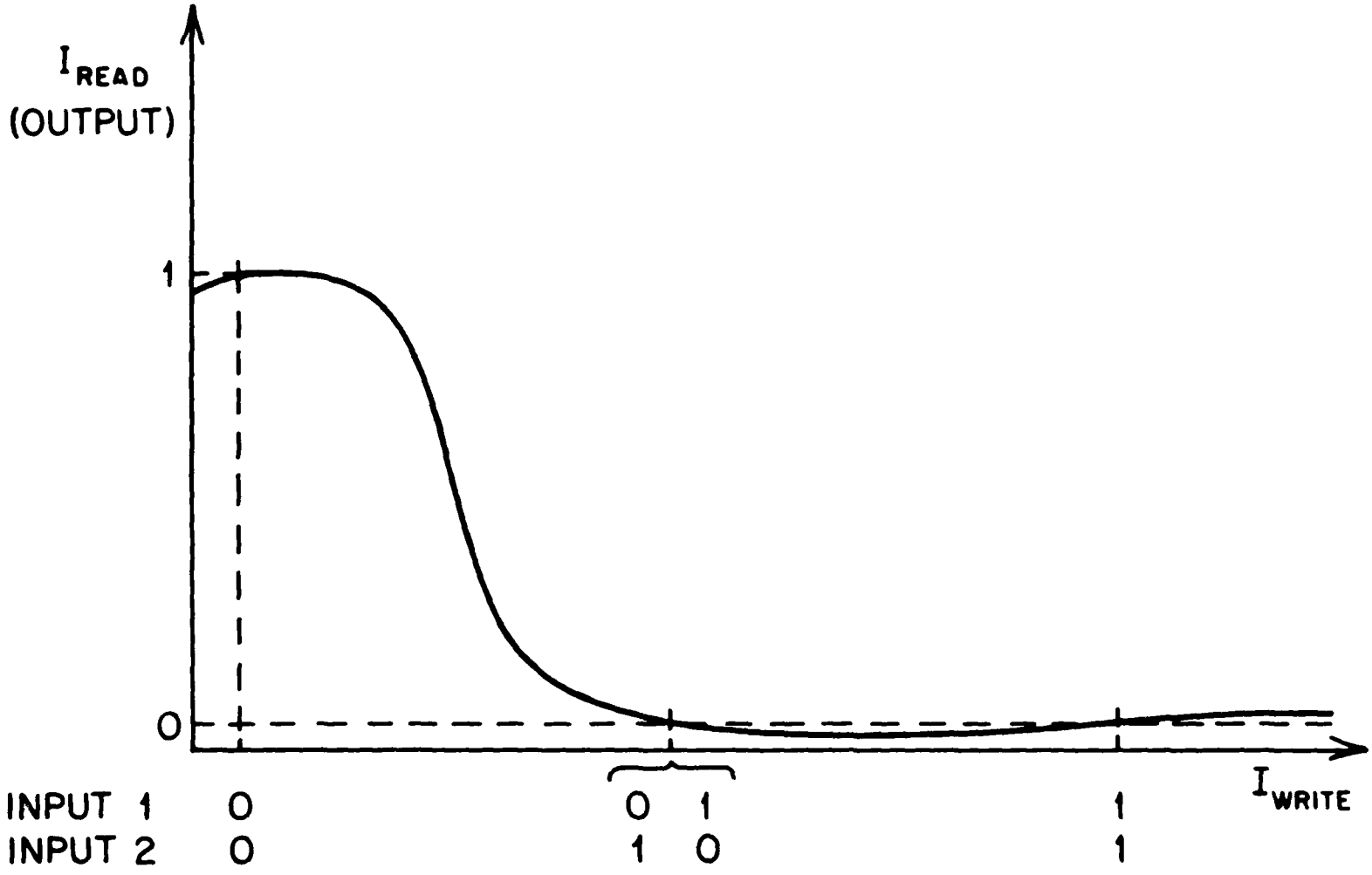

Fig. 4. LCLV input/output characteristic used to implement the NOR operation.

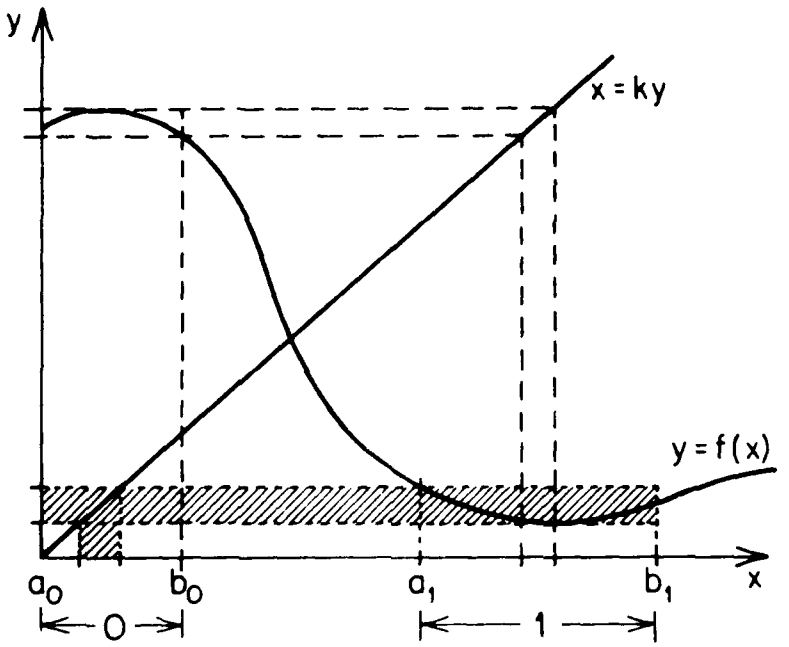

Fig. 5. Gate output, y, vs. gate input, x, for an inverter that satisfies the regeneration criterion. The shaded region shows the criterion for a 1 input and a 0 output.

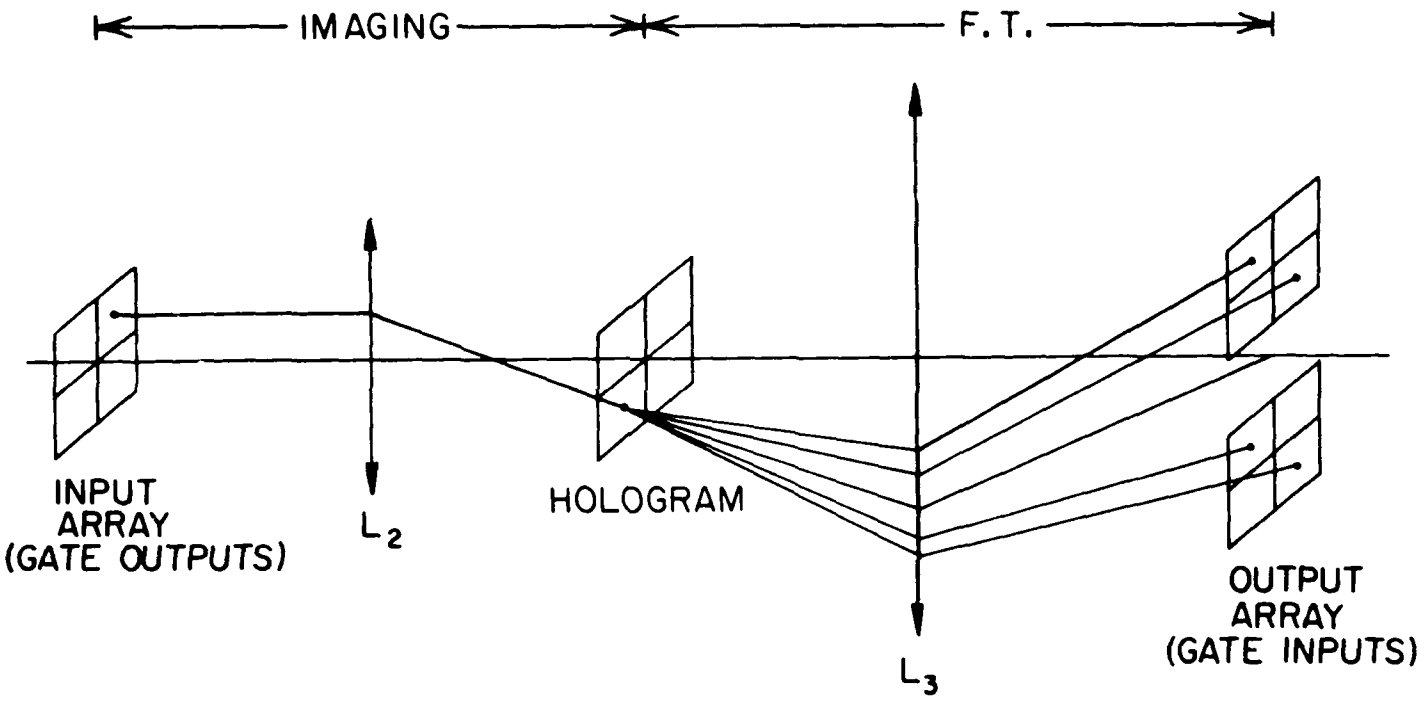

Fig. 6. System for interconnecting gates. Each pixel of the input and output arrays corresponds to a gate. The input array is the SLM output (gate output array), and the output array is the SLM input (gate input array). In general the hologram produces multiple diffraction orders, only one of which is used.

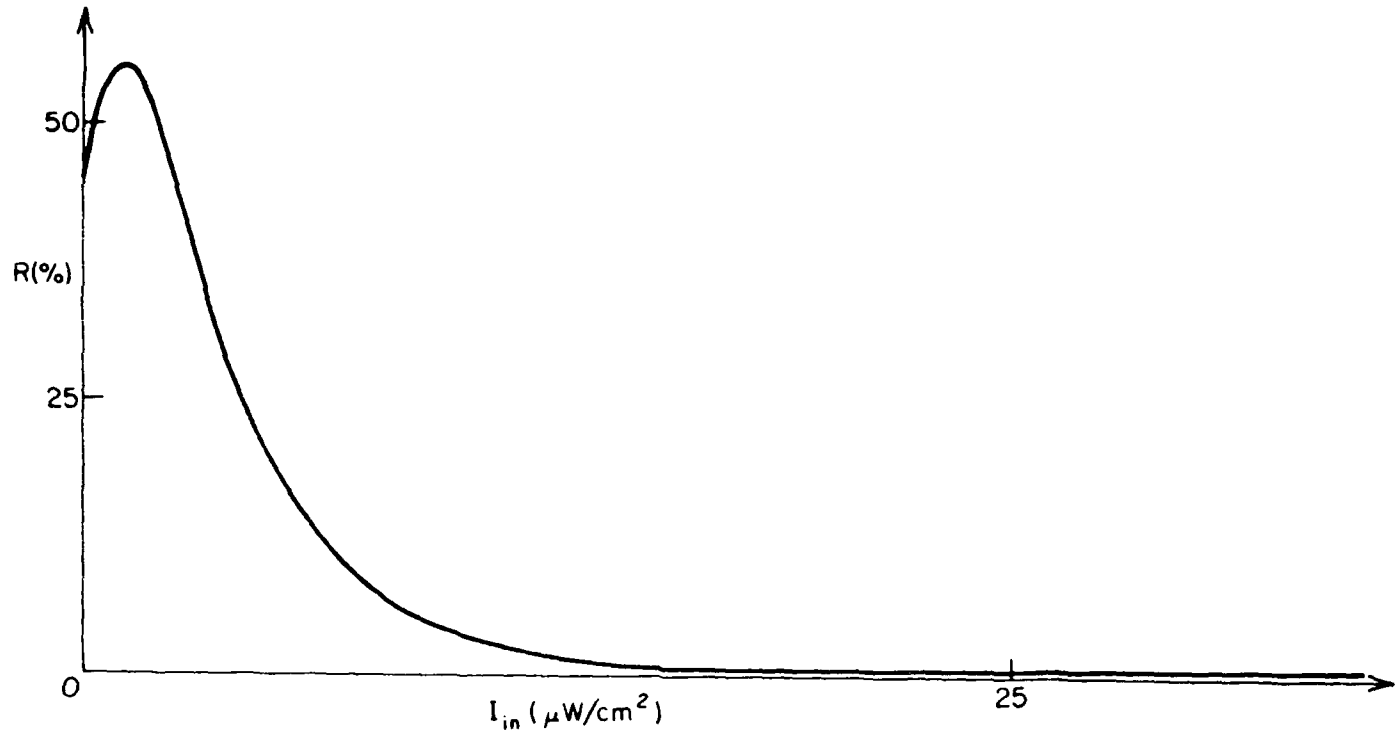

Fig. 7. Steady-state output vs. input relationship of LCLV used to implement the NOR operation in the experimental system.

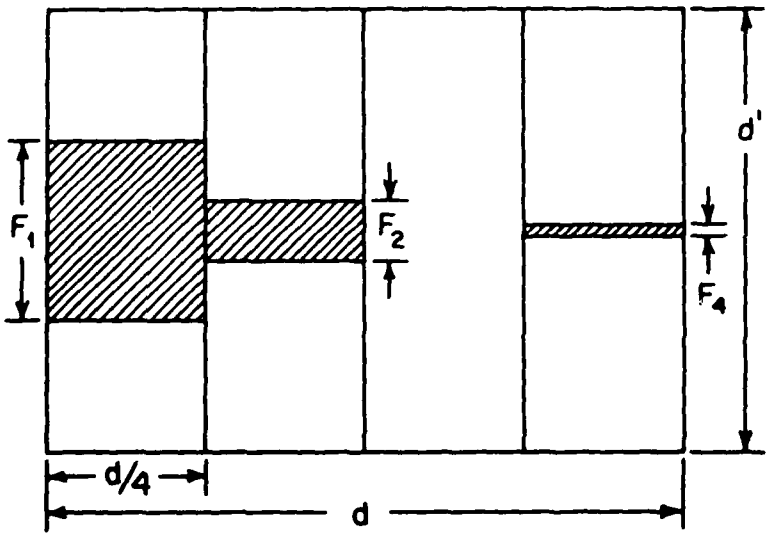

Fig. 8. Resolution cell of the 1970 Lee computer-generated hologram with binary-valued transmittance. Usually d=d'.

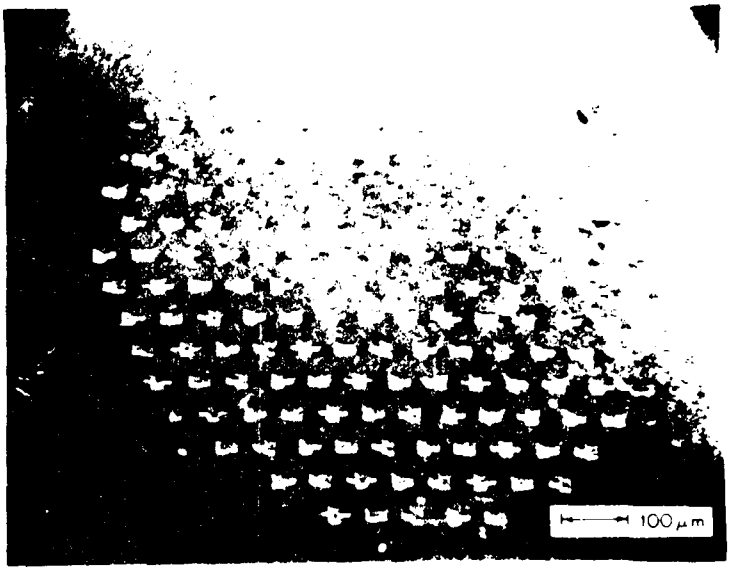

(a)

(b)

Fig. 9. Scanning electron microscope pictures of the interconnection hologram.

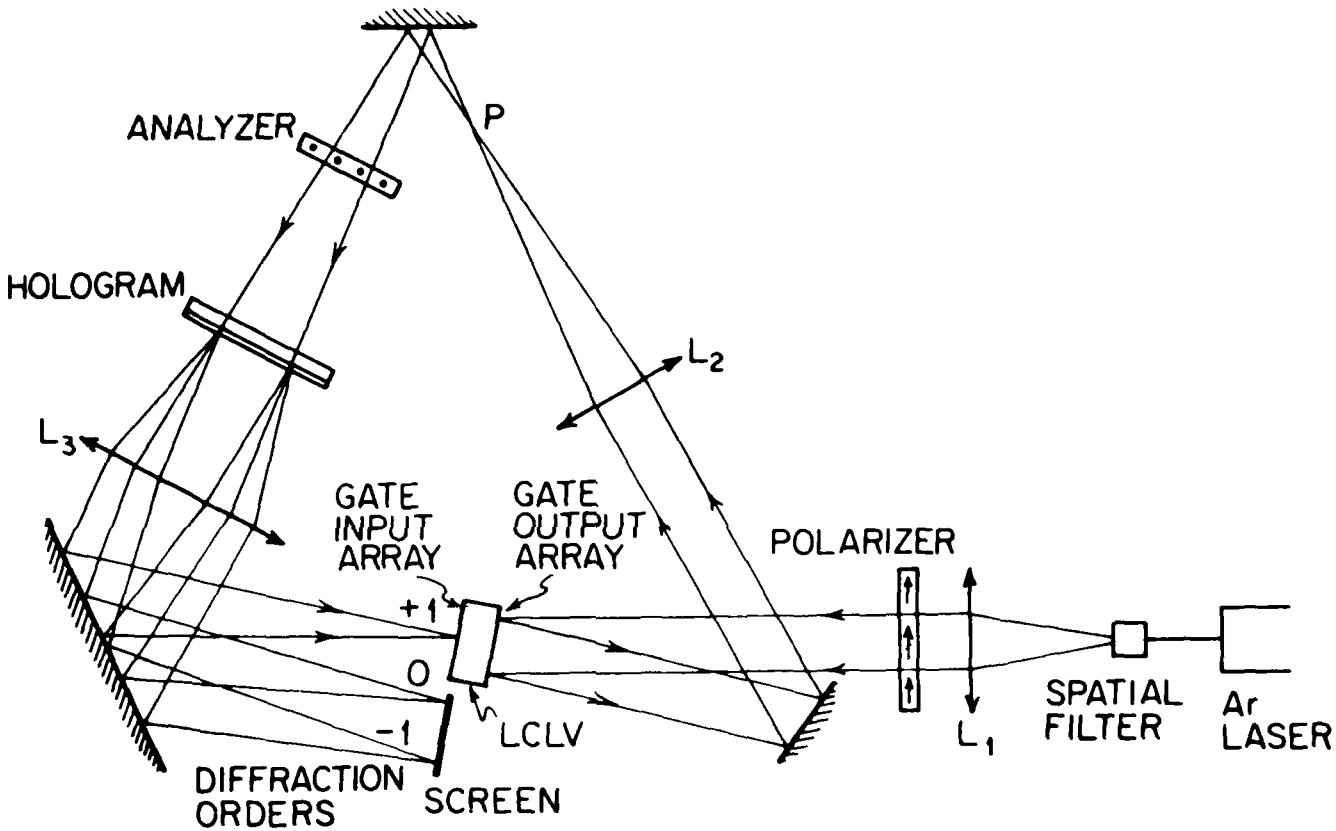

Fig. 10. Experimental system. Lens L_2 images from the LCLV gate output plane (liquid crystal plane) to the hologram plane. Lens L_3 provides a Fourier transform from the hologram plane to the LCLV gate input plane. The hologram comprises an array of subholograms.

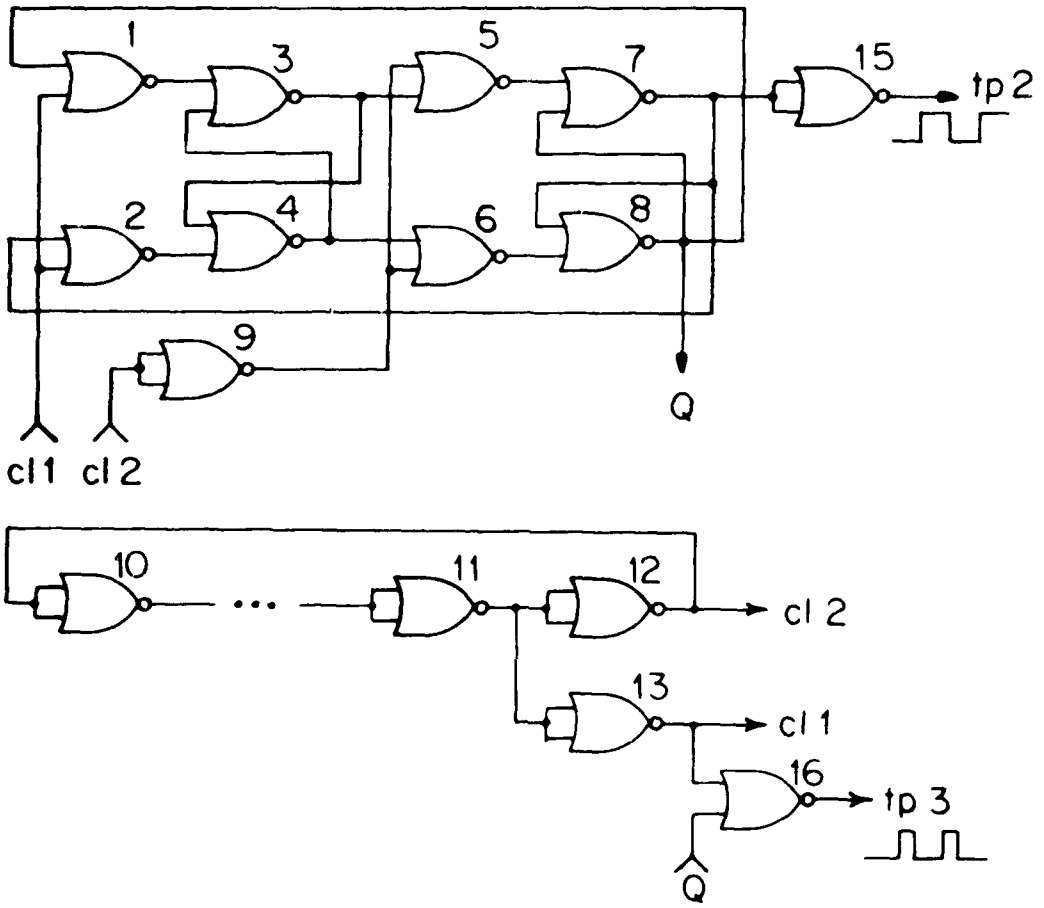

Fig. 11. Test circuit consisting of a synchronous master-slave flip-flop with driving clocks.

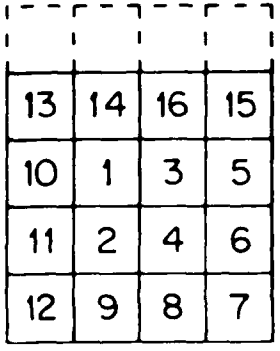

13	14	16	15
10	1	3	5
11	2	4	6
12	9	8	7

(a)

	tp1	tp2	tp3
(2,0) (1,-1) (1,-2)	(0,1)	(0,1)	(0,1)
(1,1) (0,-1)	(1,0)	(1,0) (0,-1)	(0,-2)
(0,2) (0,-1)	(1,0)	(0,1) (1,0)	(-1,-1)
(0,2) (1,0)	(2,2) (2,1)	(-1,2) (0,3) (1,0)	(-1,0) (-2,1) (0,3)

y ↑ , → x

(b)

Fig. 12. (a) layout of test-circuit gates on the hologram. (b) interconnection patterns stored in each subhologram. Each ordered pair represents the relative x and y coordinates of a pixel, or gate input, that is addressed.

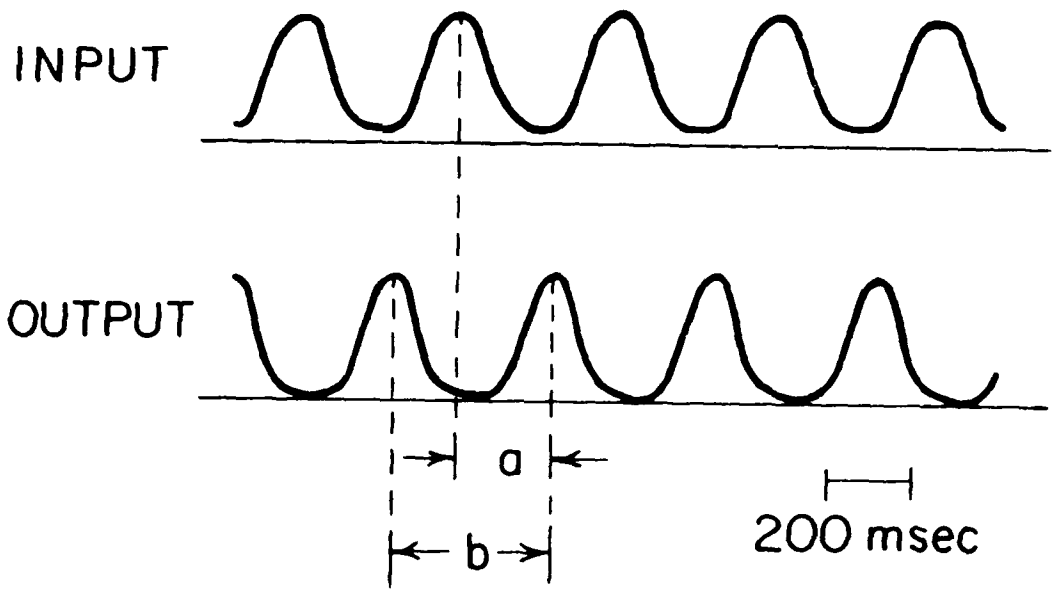

Fig. 13. Input and output of one of the five gates in the clock circuit (gate 12). Each trace represents intensity vs. time. The period is b and the phase delay is $360^{o} \cdot a/b$.

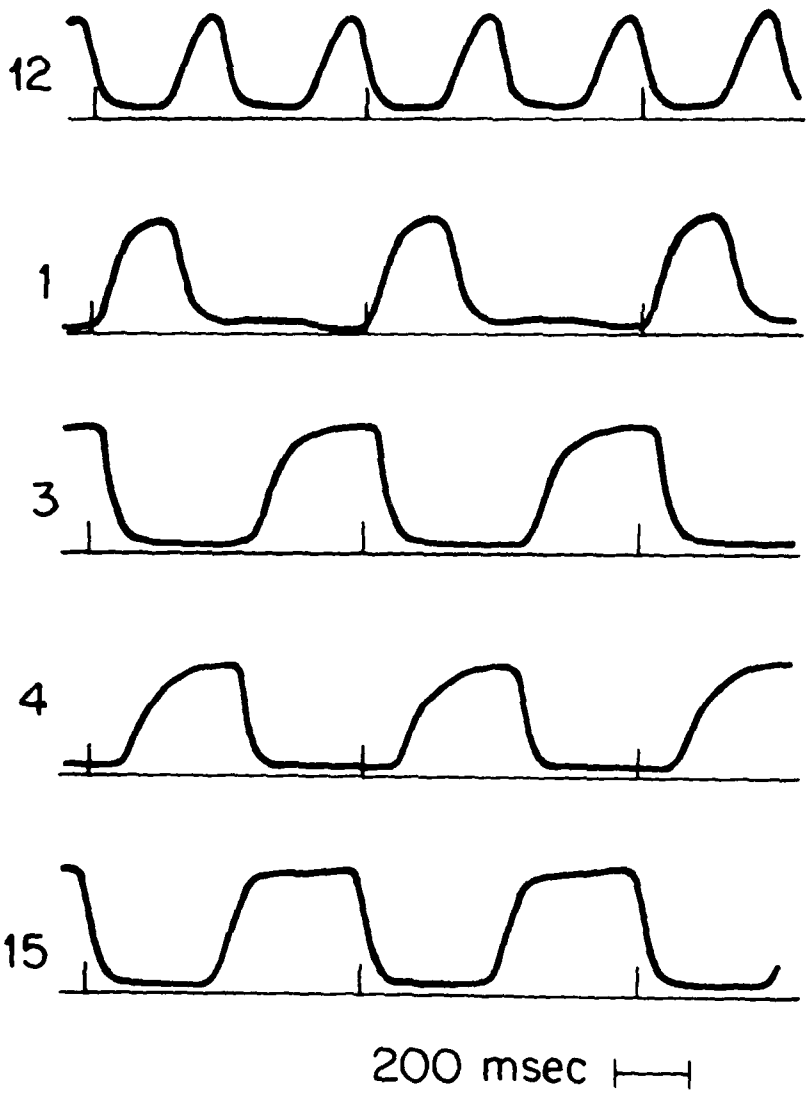

Fig. 14. Test circuit outputs.

Input Lines		Gate Input	Outputs							
A	B	(A+B)	AND	NAND	OR	NOR	XOR	XNOR	TRUE	FALSE
0	0	0	0	1	0	1	0	1	1	0
0	1	1	0	1	1	0	1	0	1	0
1	0	1	0	1	1	0	1	0	1	0
1	1	2	1	0	1	0	0	1	1	0

(a)

Input Lines		Gate Input	Outputs							
A	B	(2A+B)	A	B	$\bar{A}$	$\bar{B}$	$A\cdot\bar{B}$	$\bar{A}\cdot B$	$A+\bar{B}$	$\bar{A}+B$
0	0	0	0	0	1	1	0	0	1	1
0	1	1	0	1	1	0	0	1	0	1
1	0	2	1	0	0	1	1	0	1	0
1	1	3	1	1	0	0	0	0	1	1

(b)

Table 1. The desired values of the nonlinearity for the 16 possible logic operations on two binary inputs. Also listed are the gate inputs. The inputs to the adder are A and B in (a), and are 2A and B in (b).

ARCHITECTURES FOR A SEQUENTIAL OPTICAL LOGIC PROCESSOR

P. Chavel
Institut d'Optique, Orsay, France

R. Forchheimer
Linkoping University, Linkoping, Sweden

B.K. Jenkins, A.A. Sawchuk, and T.C. Strand
Image Processing Institute-MC 0272
University of Southern California
Los Angeles, California 90089

Abstract

A general technique is described for implementing sequential logic circuits optically. The system consists of a nonlinear transducer which provides a two-dimensional array of gates and one or more computer generated holograms (CGHs) to interconnect the gates. The limitations on the number of gates which can be implemented in an optical system is affected by the interconnection method. We describe three interconnection methods and their respective limitations. One method, which is a hybrid of space-variant and space-invariant CGH elements, provides high gate densities and high gate-utilization rates.

1. Introduction

There has recently been considerable research in optical systems for parallel digital computing with applications in signal processing. The advantages of optical and hybrid optical-electronic systems for high throughput, parallel multi-dimensional processing on signals with large time-bandwidth and space-bandwidth products are well known. Nearly all of these systems to date are basically analog and have severe limitations in accuracy, programmability and flexibility in comparison to electronic digital systems.

Our recent research has concentrated on optical combinatorial and sequential logic systems for parallel digital processing. Some of this work has included parallel A/D conversion [1] and two different implementations of optical combinatorial logic [2], [3]. More recently, we have implemented a parallel optical sequential logic circuit including a clock and a master-slave flip-flop used as a frequency divider [4]. The main components of the sequential logic system are a nonlinear spatial light modulator (SLM) (ideally having a threshold or bistable response function) and a computer generated hologram (CGH) used as a beamsteering element for interconnections. The SLM functions as a two-dimensional array of independent logic gates, and the CGH (or set of them) contains a two-dimensional array of subholograms that interconnect the gates to form a circuit. In the current system the nonlinear element is a Hughes liquid crystal light valve (LCLV) with a 45 degree twisted orientation of the nematic liquid crystal molecules [5]. Although a major limitation of this current SLM is its slow response time (10-100 ms), we feel that recent improvements in both LCLV technology [6] and the exploration of new technologies such as all-optical bistability [7], [8] will significantly improve this. We will not directly consider the question of device speed in this paper.

The main emphasis in this paper is on processor architectures for optical sequential logic. Section 2 of this paper briefly reviews the fundamentals of optical sequential logic. Sections 3 through 5 describe details of CGHs used as interconnection elements. Two basic interconnection methods, space-variant and space-invariant are described. The main limitation on the number of gates is due to space-bandwidth limitations of the CGH and SLM. A hybrid interconnection system having both space-variant and space-invariant elements is described in Section 5, and various types of processors that utilize each type of architecture are described.

2. Fundamentals of 2-D Optical Sequential Logic

In order to implement any logic system, we require two fundamental elements: a nonlinear device to provide the gate function or basic combinatorial operations and an interconnection element (Fig. 1). Furthermore, if we want to provide for sequential logic, the interconnection path must include feedback paths for generating clock signals and for obtaining memory elements. The introduction of feedback and of timing signals makes this work significantly different from previous work with combinatorial logic [2], [3] because the dynamic behavior of the nonlinear device now plays a critical role in the operation of the circuit.

We use the Hughes LCLV as the nonlinear component, although other nonlinear devices could also be used. This device produces a pointwise nonlinear behavior which can to some extent be modified, and in particular can take a shape adequate for our present needs. For example, Fig. 2 depicts a response function for a 45 degree twisted nematic device operated in the backslope

CH1880-4/83/0000/0006$01.00 © 1983 IEEE

mode. We have used the device in this mode to implement the NOR function. If we consider the total input to the device as the sum of two binary inputs, the output will be a binary valued NOR of the inputs. Other binary operations can be performed by altering the characteristic curve of the device [2]. The possible input and output values are indicated in Fig. 2.

The parallelism in the system is evident in the fact that the nonlinearity is applied simultaneously to all points on the device. Thus each resolution element or pixel on the light valve acts as an independent gate. Using resolution figures quoted for current SLMs [5], arrays of 10^5-10^6 pixels can be anticipated.

The remaining problem is how to interconnect the gates. Although several techniques are possible, CGH elements seem to offer the best solution. By using CGH elements in an optical feedback system, the output from any gate can be directed to the input of any other gate or combination of gates. Given that CGH components are to be used for interconnections, there are still a multitude of possible systems for achieving the desired circuit. In the following sections we describe three basic interconnection methods. Naturally, each method offers certain design tradeoffs and limitations. It is the purpose of this paper to examine those tradeoffs and describe how they affect system design.

3. Space-variant Interconnection Method

The most general interconnection system is one in which any gate output can be connected to the input of any gate or combination of gates. If we think of the interconnection scheme as imaging the gate output array plane onto the gate input array plane, this approach represents a space-variant imaging system. The "image" of a gate output consists of a collection of spots (the impulse response of the system for that particular point) which illuminate the appropriate gate inputs, and form the circuit interconnections. Because each object point (gate output) sees a different impulse response (interconnection pattern) this represents a general space-variant system. A space-variant system has been built to demonstrate the concept of sequential optical logic. The demonstration circuit which was implemented comprises a ring oscillator which generates a clock signal and a master-slave flip-flop which is driven by the clock. This system is operational and is described in another paper [4].

A schematic diagram of the optical system used for the space-variant interconnections is shown in Fig. 3. First, the gate outputs are imaged onto the interconnection hologram. This CGH consists of an array of subholograms, one subhologram for each gate. When illuminated by its corresponding gate output, a subhologram will reconstruct an image on the "write" side, or gate input side, of the light valve. The reconstructed images are simple dot patterns, each bright dot illuminating a gate input. Since the

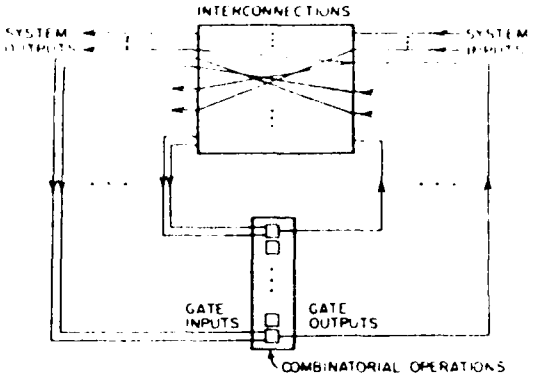

Fig. 1. Functional block diagram of sequential optical logic.

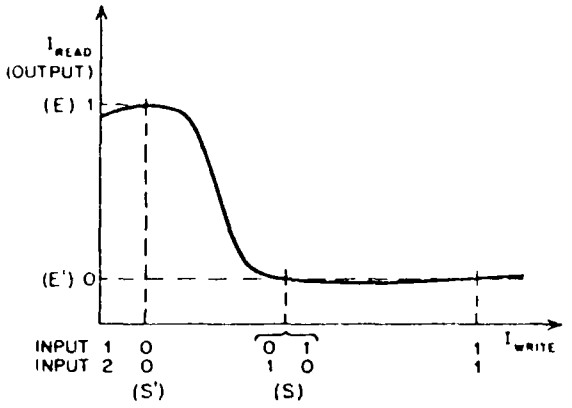

Fig. 2. LCLV input/output characteristic.

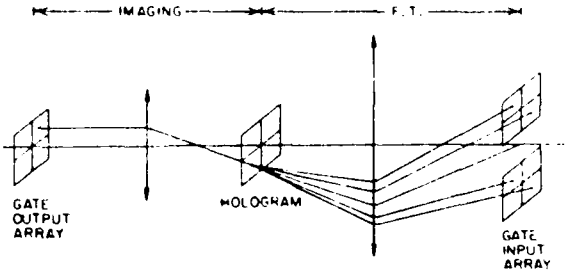

Fig. 3. Space-variant interconnection system. In general the hologram produces multiple diffraction orders, only one of which is used.

reconstructed images can be designed to illuminate any combination of gate inputs, arbitrary interconnections are possible. As shown in Fig. 3, the desired interconnections are formed in one particular diffraction order. Typically, a conjugate image will also be produced, in which case it can be used to probe the system without affecting system operation or to access the system outputs.

While this interconnection scheme allows complete generality, a price is paid in terms of

the space-bandwidth requirements on the CGH. Let there be an NxN array of subholograms on the CGH and an NxN array of gates on the light valve. Each subhologram must have the capability of addressing any of the N^2 gate inputs. The number of addressable points in the reconstruction of a subhologram is equal to the number of complex-valued sample points in the subhologram, assuming a Fourier hologram. Thus the actual space-bandwidth product (SBWP) of each subhologram is

$$S_S = p^2q^2N^2 \qquad (1)$$

where p^2 is the number of resolution elements in the hologram used to represent one complex-valued sample and q^2 is a factor representing the amount of oversampling in the hologram plane. Generally $p^2>1$ because the complex sample values must be encoded into the hologram, e.g., as real values. Also we generally have $q^2>1$ to avoid crosstalk. These problems are discussed further below.

The entire interconnection hologram consists of N^2 subholograms, one for each gate. Thus the total SBWP of the hologram is S_T where

$$S_T = N^2S_S = p^2q^2N^4. \qquad (2)$$

Because $S_T \geq N^4$, we expect that the hologram SBWP, S_T, will quickly become the limiting factor as N increases. We will verify that below, but first we need to study the crosstalk in the gate-input plane to get a feeling for the expected values of q^2.

The crosstalk can be represented by ϵ, the ratio between gate inputs of the worst-case (largest) "zero" value, I_0, and the worst-case (smallest) "one" value, I_1:

$$\epsilon = I_0/I_1. \qquad (3)$$

We require $\epsilon<1$ in order to distinguish all possible zero and one states. Assume that the intensity profile of a single gate input reconstructed from a subhologram is F(x,y). (The reconstruction of a subhologram can be represented by a set of Dirac delta functions (one for each addressed gate input) convolved with the Fourier transform, W(x,y), of the aperture function of the subhologram. Then $F(x,y) = |W(x,y)|^2$.) Thus the worst-case "one" value is the integral of F over the defined area, a, of the gate input

$$I_1 = \iint_a F(x,y)\ dxdy \qquad (4)$$

The worst-case zero level occurs when all gates have their maximum input levels except for the gate in question which has a zero input level. If each gate has m inputs (a fan-in of m) and gates are contiguous, then the worst-case zero can be shown to be

$$I_0 = m\left[\iint_A F(x,y)\ dxdy - \iint_a F(x,y)dxdy\right] \qquad (5)$$

where A is the area of the entire gate array. This assumes that the spatially integrated sum of gate inputs from different subholograms is effectively an incoherent sum. Note that such inputs may actually add coherently in which case they produce interference fringes. Spatial integration over these fringes results in an effective incoherent summation. Similarly, the above equation assumes that the gate inputs reconstructed from a single subhologram also can be modeled as adding incoherently. This will be essentially true if a pseudorandom phase is applied to the m distinct gate inputs. Combining the above equations we get

$$\epsilon = m(1/E_0-1) \qquad (6)$$

where E_0 is the fraction of the single-gate input intensity profile which falls within the defined area of that gate

$$E_0 = \iint_a F(x,y)\ dxdy \Big/ \iint_A F(x,y)\ dxdy \qquad (7)$$

If we define a_0 as the minimum gate area determined by the Nyquist theorem and the subhologram area, then

$$a = q^2a_0 \qquad (8)$$

with q^2 being the oversampling factor as defined above. Obviously, as q increases, E_0 approaches unity and ϵ approaches zero.

We now consider an example. If we use a triangle function in x and in y for the aperture (window) function of each subhologram, then its Fourier transform is a two-dimensional $sinc^2$ function, and

$$F(x,y) = sinc^4(x/2)sinc^4(y/2) \qquad (9)$$

Choosing q=2 yields a crosstalk $\epsilon=(0.11)m$, so that 3-input gates cause a crosstalk of 0.33. Thus for NOR gates the thresholding of the nonlinear device can be performed anywhere between relative input levels of 0.33 and 1.0. In this case the sampling rate is twice the Nyquist rate. Increasing q permits a larger fan-in, e.g., q=3 implies $\epsilon=(.0082)m$ and a crosstalk of 0.33 permits 40-input gates to be used. Also note that the use of a more appropriate aperture function could permit smaller values of q.

In order to estimate the SBWP that can be written onto a CGH, we assume the CGH is written using electron-beam lithography, as was the case for the experimental demonstration of the optical logic system [4]. This electron-beam system has written linewidths down to 0.5 μm, and has a maximum file size of 1.024 mm on a side. Files can be stitched together to yield a maximum size of 10 cm on a side. If we minimize the stitch error by making the file boundaries coincident with subhologram boundaries, a SBWP of $4x10^{10}$ is attainable.

The hologram coding parameter p, defined in Eq. 1, for the case of a Burckhardt hologram [9], has a minimum value of 3, assuming square cells. Having found that q will typically be in the range of 2-3, we conclude that the maximum feasible number of gates corresponds to a value of pq on the order of 10. From Eq. 2 and the above SBWP, we find that the gate array dimension is NxN where

$$N \approx 100\text{-}200 \qquad (10)$$

for space-variant interconnections. Because this is less than the SBWP capabilities of some spatial light modulators, the CGH is the limiting element.

Since the space-variant system allows arbitrary interconnections, the only other possible limitation on the circuits that can be implemented is the requirement that all gates must perform the same binary operation, e.g., NOR in this case. However, since all the Boolean operations may be constructed out of NOR gates, this does not limit the types of processing operations that can be performed. Another feature is that circuits with any degree of inherent parallelism, or lack thereof, can be implemented with approximately equal ease.

4. Space-invariant Interconnection Method

If one is willing to compromise on the arbitrariness of the gate interconnections, a substantial increase in the possible number of gates results. The extreme case is a totally space-invariant interconnection. This is the idea behind the processor suggested by Huang [10]. Here we extend this concept to include sequential circuits. This interconnection method is implemented optically by an imaging system with a space-invariant filter, using one simple hologram for the entire circuit (Fig. 4). The filter has an impulse response consisting of a series of spots which illuminate the appropriate gate inputs as in the space-variant case. However, in this case, the impulse response (interconnection pattern) is the same for every gate output, and the gate inputs are addressed relative to the position of the gate output. The space-variant method worked on the basis of absolute addressing.

An example of a space-invariant interconnection pattern is shown in Fig. 5. Each dot in the figure represents a (NOR) gate, and each arrow represents an interconnection from the output of one gate (dot) to the input of another. Each gate is considered to have one additional, unconnected input for an enable/disable signal. A particular circuit is implemented by disabling the appropriate gates. In the NOR case, a gate is disabled by projecting light onto it (i.e., putting a 1 onto the unconnected input). With the illustrated interconnection pattern it is possible to transfer data in various directions without getting unintended feedback loops. The major limitation of this interconnection method is that the implementation of many circuits will require a large number of gates to be disabled. Obviously, circuits with very regular interconnections can utilize the gates more efficiently than irregular circuits.

Since the holographic element used in this interconnection system is simple, a very large number of gates can be interconnected. Even allowing the PSF to simultaneously address any set of points in the array, the SBWP required of the hologram is of order $p^2q^2N^2$ (see Eq. 1 above). Thus if the full SBWP available with the CGH could be exploited in this system and if $p^2q^2 \approx 100$ approximately 4×10^8 gates could be interconnected. The hologram for this system could also be recorded optically. In either case, the number of gates with the space-invariant interconnection method is limited by the SBWP of the spatial light modulator.

As mentioned above, the method of disabling gates to implement circuits decreases the number of gates that are actually used, and therefore severely restricts the types of operations that can be performed efficiently. It also adds a degree of complexity to the system. However, this method of optically disabling gates also provides a potential advantage - it provides a means of easily "re-wiring" the system in real time by changing the disable signals. This could offer considerable flexibility in making an adaptive system.

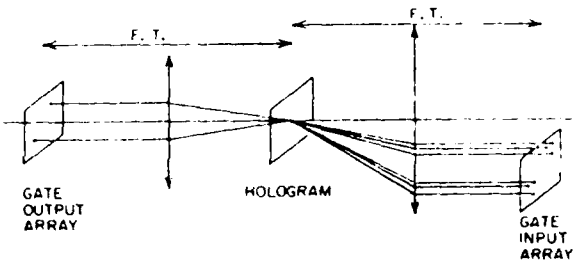

Fig. 4. Space-invariant interconnection system.

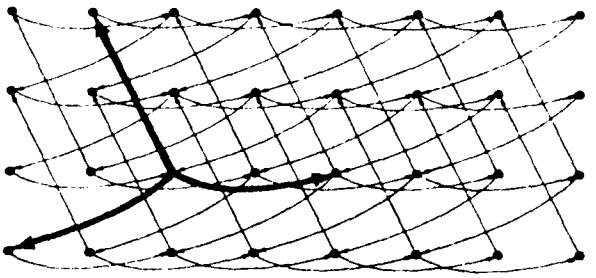

Fig. 5. An example of a space-invariant interconnection network. Nodes represent gates and arrows are the (optical) interconnections.

5. Hybrid Interconnection Method

At this point we have seen two approaches to interconnecting gates. In the space-invariant case there is only one interconnection pattern which is applied to all gates whereas in the

space-variant case the number of distinct interconnection patterns is in general equal to the number of gates. These two approaches represent the extreme cases in terms of the space-bandwidth requirements they place upon the CGH element. The tradeoffs between these two is increased flexibility at the cost of increased hologram complexity. Since the space-invariant case generally suffers from inefficient gate utilization and the space-variant system is limited by the hologram to the number of gates it can address, it is worthwhile considering if there is a combination of techniques which can achieve high gate utilization efficiency and at the same time be limited in gate count only by the space-bandwidth product limitations of the spatial light modulator.

Our approach to this has been to consider a hybrid system which combines space-variant and space-invariant interconnections. The idea is to define a finite number, M, of distinct interconnection patterns. We then assemble our circuit using only these M interconnection patterns. If the total number of gates is N^2 we assume

$$1 << M << N^2 \tag{11}$$

so that this system is truly intermediate between the space-variant and space-invariant cases. If M is large, we anticipate that we have almost complete flexibility in designing our circuit.

The optical implementation of this system is schematically diagrammed in Fig. 6. Here the gate output array is imaged onto a space-variant filter element as in Fig. 3. The purpose of this element is to deflect the light from each gate output through one of M subholograms in the second CGH element (Fig. 6). These subholograms act as space-invariant filter elements which produce the M different interconnection patterns in the gate input plane.

Although the space-variant element would appear to have the same space-bandwidth limitations as in the simple space-variant case, we note that the SBWP of each subhologram in this plane is now of order M rather than of order N^2. Thus the total SBWP requirement in this element is much less than in the previous space-variant case. The holograms in the space-invariant element generally have a relatively low SBWP.

The SBWP, S_{S_1}, of a subhologram in the first hologram, H_1, is

$$S_{S_1} = p_1^2 q_1^2 M \tag{12}$$

where M is the number of subholograms in the second (space-invariant) hologram, H_2, and p_1 and q_1 represent coding and oversampling factors, respectively, as in the space-variant interconnection section. Similarly, the SBWP of a subhologram of H_2 is, in the worst case,

$$S_{S_2} = p_2^2 q_2^2 N^2 \tag{13}$$

where N^2=number of gates. This worst case allows the H_2 subhologram to address any n gates in the array. If the gates it addresses are localized, i.e., are all contained in the same portion of the array, then its SBWP can be significantly reduced by the introduction of a carrier frequency [16]. Since H_1 consists of N^2 subholograms and H_2 consists of M subholograms, their total SBWPs are given by

$$S_{T_1} = p_1^2 q_1^2 MN^2 \qquad S_{T_2} = p_2^2 q_2^2 MN^2 \tag{14}$$

and here, again, S_{T_2} is a worst-case estimate. If we assume both holograms are written in the same manner, then $S_{T_1} = S_{T_2} = S$ and $p_1 = p_2 = p$, from which it follows that $q_1 = q_2 = q$, thus

$$S_T = p^2 q^2 MN^2. \tag{15}$$

As in the space-variant case, we need to analyze the crosstalk in order to estimate q.

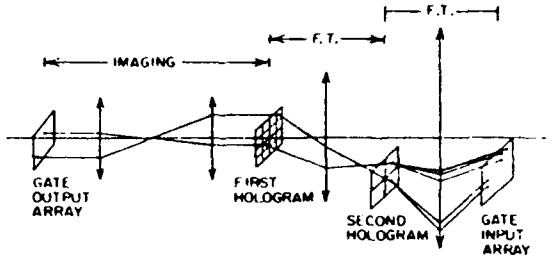

Fig. 6. Hybrid interconnection system. The first holgoram is a space-variant element as in Fig. 3. The second element is an array of space-invariant filters.

For the hybrid interconnection scheme, two sources of crosstalk exist. Inter-pixel crosstalk occurs between pixels in the gate-input plane, and is analogous to the crosstalk treated in the space-variant interconnections section. Inter-hologram crosstalk occurs between subholograms in the second hologram and also contributes to noise in the gate-input plane. (We assume neglible crosstalk at the first hologram because it is in the image plane of the gate output array.)

The inter-pixel crosstalk is completely analogous to the crosstalk in the space-variant interconnection case when applied to H_2 and the gate-input array, and the same equations apply.

In order to analyze the inter-hologram crosstalk, we have to find the effect of this crosstalk in the gate input plane. We assume that each H_1 subhologram addresses only one H_2 subhologram. Through a given H_2 subhologram k, there are only n_k subholograms of H_1 that can address a given gate input ρ, where n_k is the fan-out of subhologram k. Any unintentional illumination of k from one of these H_1 subholograms will contribute crosstalk to gate ρ.

The worst-case (maximum) zero input to ℓ_1 then occurs when all n_k of these H_1 subholograms illuminate the nearest-neighbor subholograms of k. We then sum this result over all H_2 subholograms k, to obtain the worst-case zero-level input,

$$\ell_0 = \left[\sum_{k=1}^{M} n_k\right] \iint_{\sigma_{NN}} g(x,y)\, dxdy \qquad (16)$$

where g(x,y) is the intensity profile in the H_2-plane due to the illumination of one H_2 subhologram by one H_1 subhologram and is analogous to F(x,y) in our previous derivation. σ_{NN} is a nearest-neighbor subhologram to the illuminated H_2 subhologram. The coefficient is the total fan-out of the H_2 array, and is equal to nM, where n is the mean fan-out over the H_2 array. All additions here are incoherent because we are effectively averaging over fringe patterns again. The worst case one-level input is simply the integral of g(x,y) over the illuminated subhologram σ, so the inter-hologram crosstalk α_H is

$$\alpha_H = \frac{\ell_0}{\ell_1} = \frac{nM \iint_{\sigma_{NN}} g(x,y)\, dxdy}{\iint_{\sigma} g(x,y)\, dxdy} \qquad (17)$$

Now we look at an example. Again taking a two-dimensional triangle function as the subhologram aperture function in the H_1 plane, g(x,y) in the H_2 plane is given by F(x,y) of Eq. 9. Now the intensity profile F(x,y) in the gate input plane is the squared modulus of the convolution of this triangle aperture function with the sinc function resulting from the rect aperture function in the H_2 plane. Taking for example q=3, the total crosstalk, α, given by the sum of the inter-pixel crosstalk α_P, from Eq. 6, and the inter-hologram crosstalk α_H, from Eq. 17, is

$$\alpha = \alpha_P + \alpha_H = m(.0025) + nM(.0018) \qquad (18)$$

where m is the fan-in to each gate. For example, if 8-input gates are used and we allow $\alpha = .50$, we can have 50 different interconnection patterns with an average fan-out of 5.2. These numbers are strongly dependent on the aperture function used. Since no attempt to optimize the aperture function was made, one can expect a significant improvement in these numbers by using a more appropriate aperture function.

Thus, as in the space-variant case, we conclude that the maximum number of gates corresponds to a value of pq on the order of 10. Again using $S_T = 4 \times 10^{10}$, from Eq. 15 we get

$$MN^2 \simeq 4 \times 10^8$$

and thus for $M \simeq 50$ different interconnection patterns, we get on the order of 10^7 gates, or an NxN array with

$$N \simeq 2{,}000\text{-}3{,}000$$

which is above the SBWP capabilities of presently available spatial light modulators.

In order to implement an arbitrary circuit with the hybrid interconnection method, the M interconnection patterns may be considered to be a basis set from which one constructs the desired interconnections. With a large enough M, any circuit can be implemented. However, the potential of this architecture can be exploited more fully by implementing circuits with a high degree of regularity or symmetry. Examples include parallel arrays such as systolic arrays and cellular automata. The principle motivation behind the systolic array concept is the adaption to the limitations of VLSI structures.

A more appropriate application of our hybrid interconnection scheme is that of cellular logic arrays. A conceptual diagram of such an array is shown in Fig. 7. Each block represents a cell, or processing element, made up of a number of gates connected in some arbitrary manner. Each block may be identical to the others or different, although the more similarities there are between blocks, the fewer interconnection patterns are needed. The connections between blocks will typically be space-invariant. Although the figure depicts only nearest-neighbor connections between blocks, much more complicated interconnection patterns, without regard to the physical distance between connected blocks, may be made almost as easily. Thus we have a cellular logic machine with global, as well as local, interconnections. Of course, if the cellular logic machine is used for image processing, we have the additional advantage of not requiring electronic-optical conversions on the inputs and outputs.

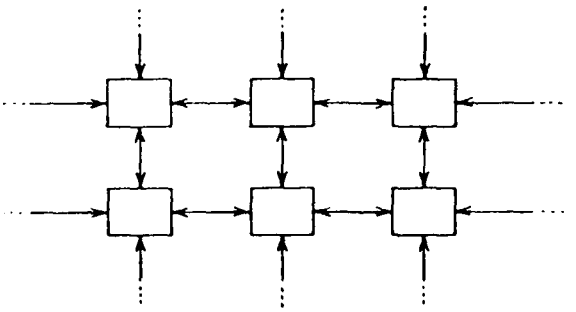

Fig. 7. A cellular logic array as an example of the use of the hybrid interconnection system of Fig. 6. Connections within each block are space-variant, and connections between blocks are space-invariant.

This concept may also be applied to computational algorithms that require global interconnections, which are often difficult or inefficient to implement using VLSI. In this case, the blocks in the figure are often identical, but the interconnections between the blocks are space-variant. Frequently, however, as in the case of the fast Fourier transform algorithm, for example, there is still a high

degree of symmetry among the connections between blocks. Thus this class of algorithms is also particularly well-suited to the hybrid interconnection scheme.

6. Conclusion

We have described some of the architecture and design considerations which affect the implementation of sequential logic in an optical system.

Whereas in VLSI systems, communication costs are the major limiting design factor, in the optical system, the communication costs are much less severe. Thus many architectures which may be impractical in VLSI due to communication problems, may be easily implemented in an optical system.

The interconnection network can be produced in several different ways. We discussed three ways: a space-variant technique which allows arbitrary interconnections but is limited by the SBWP of the CGH; a space-invariant system which requires only simple CGH elements but suffers from low gate-utilization rates; and a hybrid of these two techniques which provides large gate counts with high gate-utilization rates.

The major limitations of the system at this point relate to the device used as a gate array. In particular, the speed of current devices is a major bottleneck. Current work in optical bistability may alleviate that restriction although significant progress will have to be made before that technology develops into functional devices.

Acknowledgements

We thank A.R. Tanguay, Jr., B.H. Soffer, and S.-Y. Kung for many useful discussions in connection with this research. This work was supported by the Air Force Office of Scientific Research under Grant AFOSR-81-0082.

References

1. A. Armand, A.A. Sawchuk, T.C. Strand, B.H. Soffer, and D. Boswell, "Real-time Parallel Analog-to-Digital Conversion," Opt. Let., vol. 5, pp. 129-131, 1980.
2. P. Chavel, A.A. Sawchuk, T.C. Strand, A.R. Tanguay, Jr., and B.H. Soffer "Optical Logic with Variable-Grating-Mode Liquid-Crystal Devices," Opt. Let, vol. 5, pp. 398-400, 1980.
3. A.A. Sawchuk, T.C. Strand, and A.R. Tanguay, Jr., "Nonlinear Real-Time Optical Signal Processing," USCIPI Report 1080, USC Image Processing Institute, 1982.
4. B.K. Jenkins, A.A. Sawchuk, and T.C. Strand, "Sequential Optical Logic Implementation" J. Opt. Soc. Am., vol. 72, 1721 A, 1982; "Sequential Optical Logic Implementation," to be submitted to Appl. Opt..
5. J. Grinberg, A. Jacobson, W. Bleha, L. Miller, L. Fraas, D. Boswell, and D. Myer, Opt. Eng., vol. 14, pp. 217-225, 1975.
6. U. Efron, B.H. Soffer, M.J. Little, J. Grinberg, and M.A. Monahan, "Applications of Silicon Liquid Crystal Spatial Light Modulators for Optical Data Processing," SPIE Proc. Advances in Optical Information Proc., vol. 388, 1983.
7. H.M. Gibbs, S.L. McCall, and T.N.C. Venkatesan, "Optical Bistable Devices: The Basic Components of All-Optical Systems," Opt. Eng., vol. 19, pp. 463-468.
8. E. Abraham, C.T. Seaton, and S.D. Smith, "The Optical Computer," Scientific American, vol. 248, no. 2, pp. 85-93, February 1983.
9. C.B. Burckhardt, "A Simplification of Lee's Method of Generating Holograms by Computer," Appl. Opt., vol. 9, no. 8, p. 1949, 1970.
10. A. Huang, "Design for an Optical General Purpose Digital Computer," in Proc. of the 1980 International Computing Conference Book 2, pp. 119-123, 1980 (SPIE vol. 232).
11. S. Lowenthal and P. Chavel, "Reduction of the Number of Samples in Computer Holograms for Image Processing," Appl. Opt., vol. 13, pp. 718-720, 1974.

1.3 Variable Grating Mode Liquid Crystal Devices

The variable grating mode (VGM) liquid crystal device has been further studied experimentally [4-16]. This work has been in conjunction with the device development work being done at Hughes Research Laboratories.

An important area of research on the Variable Grating Mode Liquid Crystal Light Valve is concerned with a fundamental understanding of the origin of the "variable grating" effect. A wide variety of studies have been performed on electrically addressed VGM cells (no intervening photoconductive layer), in which diffraction order polarization and intensity were measured as a function of input polarization and applied cell voltage and the results correlated with observations of the VGM structure under polarized illumination in a polarizing microscope, as well as the with various theoretical models of the VGM domain structure.

Two recent papers summarizing these results are included here. The first paper "Physical Characterization of the Variable Grating Mode Liquid Crystal Device" by A.R. Tanguay, Jr., C.S. Wu, P. Chavel, T.C. Strand and A.A. Sawchuk, has been accepted for publication in Optical Engineering, special issue on Spatial Light Modulators: Fundamental Characteristics, November/December 1983. This paper summarizes the physical principles of operation of VGM devices and describes work in: a) experimental measurements of the Jones matrix describing

polarized light propagation through the VGM cell; b) the thickness dependence of the molecular orientation angles; c) understanding of the physical constraints on the VGM response time; and d.) the possibility of a VGM device with ac bias.

A second paper "Polarization Properties of the Variable Grating Mode Liquid Crystal Device" by A.R. Tanguay, Jr., P. Chavel, T.C. Strand and C.S. Wu, has been submitted to Optics Letters for publication and is also included here. This paper contains detailed results on the spatial distribution of the orientation of liquid crystal molecules in a VGM device. Experimental measurements of the polarization properties of light diffracted by the liquid crystal birefringent phase grating have been made as a function of the applied voltage across the cell.

PHYSICAL CHARACTERIZATION OF THE VARIABLE GRATING MODE LIQUID CRYSTAL DEVICE

A.R. Tanguay, Jr., C.S. Wu, P. Chavel†, T.C. Strand‡, and A.A. Sawchuk

Image Processing Institute, and Departments of Electrical Engineering and Materials Science
University of Southern California
Los Angeles, California 90089

and

B.H. Soffer
Hughes Research Laboratories, 3011 Malibu Canyon Road
Malibu, California 90265

†Permanent Address: Institut d'Optique, Université de Paris sud, BP 43, 91406 Orsay Cedex, France

‡Present Address: IBM Corporation, 5600 Cottle Road, San Jose, California, 95193

Abstract

The physical principles of operation of the Variable Grating Mode Liquid Crystal Device are described. The VGM device is capable of performing a two-dimensional intensity-to-spatial frequency conversion, which in turn allows the implementation of a wide range of nonlinear optical processing and computing functions. The device utilizes certain nematic liquid crystal mixtures that are observed to form variable frequency diffraction gratings under the influence of an applied bias voltage. Both fundamental and technological limitations to device performance characteristics are discussed.

Physical Characterization of the Variable Grating Mode Liquid Crystal Device

I. Introduction

A wide variety of one- and two-dimensional operations are necessary for full-scale implementation of parallel optical processing and computing systems. Incoherent-to-coherent conversions are often required for algorithms involving spectrum analysis and modification, correlation, convolution, and holographic image formation, particularly when the information to be processed is available only in time-sequential or matrix-addressed raster format. A number of one- and two-dimensional spatial light modulators capable of this type of image transduction are described within this Special Issue [1-4] as well as in several review articles [5-8].

Other, equally important processing and computing functions such as logic operations, programmable matrix addressing, binary addition, linearity compensation, and input-output nonlinearities (e.g., exponentials, logarithms, power laws, thresholds, level slices, and level restoration) have proven particularly difficult to implement. All of these functions, on the other hand, can be implemented by means of some form of intensity-to-position encoding in conjunction with either fixed (single function) or programmable (multi-function) masks. This general statement follows from the realization that all of the functions listed above are special cases of data-dependent multiplications, in

which the input value (e.g., pixel intensity) selects the appropriate multiplier (e.g., mask location) to obtain the desired product (e.g., output intensity).

The Variable Grating Mode Liquid Crystal Device (VGM LCD) [9-12] transforms input intensities to spatial positions when used in conjunction with a Fourier transform lens. The nature of this image transformation can be realized in the following manner. The VGM LCD primarily consists of a photoconductive layer in series with a layer of nematic liquid crystal mixture. A dc bias voltage is applied across the device to provide a voltage division between the two layers. Within a given image pixel, the input intensity decays the voltage across the photoconductive layer and correspondingly enhances the voltage across the liquid crystal layer. The photoconductor thus implements an intensity-to-voltage conversion. The nematic liquid crystal mixture employed in the device has the unusual property that the alignment of the liquid crystal molecules, which is homogeneous in the quiescent state, exhibits spatially periodic modulation when a bias voltage is applied across the layer. This modulation results in a birefringent phase grating [13] characterized by a spatial frequency that depends linearly on the applied voltage. The effect of the liquid crystal layer is thus to implement a voltage-to-spatial frequency conversion. If both layers are considered together, the entire device is thus seen to perform an image-wise intensity-to-spatial frequency conversion, which can be modified to the more general

intensity-to-position transformation by placing a Fourier transform lens behind the VGM LCD. Collimated readout illumination normally incident on the device (at a wavelength of photoconductive insensitivity) is angle-encoded within each image pixel by diffraction from each induced phase grating, and subsequently angle-to-position mapped by the Fourier transform lens into its focal plane.

This type of process is shown schematically in Fig. 1, in which the input image is assumed to consist of two separate regions of differing intensity. The VGM LCD encodes both regions with different spatial frequencies, resulting in separated diffraction orders in the filter (Fourier) plane. Insertion of an appropriate spatial filter or programmable mask (not shown in Fig. 1) into the Fourier plane allows the separated orders to be selectively modified to implement any desired data-dependent multiplication or point nonlinearity. In the reconstructed output image, all regions of equal input intensity are modified identically irrespective of their location in the input image field. Thus, all of the data-dependent multiplications are performed in parallel. Functional programmability is achieved by replacement or reprogramming of the Fourier plane mask, which need only be a low resolution device with a total number of resolution elements equal to the number of grey levels required to be processed.

The overall input-output characteristic of nonlinear

function implementation utilizing the VGM LCD is shown schematically in Fig. 2, by specifying sequentially the nature of the transformations from input intensity to spatial frequency within the VGM LCD, from spatial frequency to spatial filter amplitude transmittance in the Fourier transform plane, and from output amplitude to output intensity (usually by means of square law detection). The overall nonlinearity achieved can be easily compensated for the functional dependences of the separate steps by adjustment of the selected spatial filter transmittance function.

The VGM LCD has thus far been utilized to perform a wide variety of parallel nonlinear point transformations, including *level slicing* [9,10,12], binary logic functions (AND, OR, NOR, etc.) [10,11,12], and full binary addition (inputs: two addend bit planes and one carry bit plane; outputs: sum bit plane and carry bit plane)[11]. The purpose of this paper is to describe the physical principles of operation of the Variable Grating MOde Liquid Crystal Device, identifying areas of strength and weakness, and differentiating limitations to current device performance thought to be fundamental in origin from those that are seemingly technological. Section II consists of a more detailed description of the device, its operating mode, and its operational properties. The fundamental origins of these operational properties are examined in Section III, in which the natural focus will be the physical mechanism of the variable grating mode effect in nematic liquid crystal mixtures.

Experimental and theoretical efforts to elucidate the nature of this mechanism are described in Section IV, concluding with several important but as yet unanswered questions.

II. Device Description and Operational Mode

A number of important aspects of device construction and device operation are reviewed in this Section. A more complete description of these concepts has appeared previously [9-12].

The critical element of the VGM LCD is a thin (4-12 μm) layer of nematic liquid crystal mixture [12] that exhibits a periodic modulation of the liquid crystal director, and hence of the index ellipsoid, under application of an electric field normal to the plane of the layer. By means of suitable preferential alignment techniques [9,12], the quiescent state of the liquid crystal is homogeneous (parallel to the plane of the layer). As will be discussed in Section IV, this periodic variation of the principal axes of the dielectric tensor gives rise to a birefringent phase grating characterized by striking and unique optical properties [14]. The grating can be visualized in a polarizing microscope, as shown in Fig. 3, by utilizing the birefringence properties of the periodic perturbation. Distinct polarizer/analyzer combinations give rise to remarkably different grating images, as can be seen by comparison of Figs. 3(a) and 3(b) (see Section IV). Furthermore, the grating period is observed experimentally to be related inversely to the applied voltage across the layer. Above the

threshold for domain formation, therefore, the spatial frequency of the grating is a linear function of the voltage across the layer, as shown for a variety of nematic liquid crystal mixtures in Fig. 4.

This voltage-to-spatial frequency transformation can be optically addressed by means of a photoconductor placed in series with the liquid crystal layer, as shown in Fig. 5 and described in the previous Section. The photoconductive layer employed in devices constructed thus far is comprised of evaporated or ion-beam sputtered zinc sulfide (ZnS), chosen to optimize the impedance match with the liquid crystal layer ($\rho > 10^{10} \Omega$-cm). The layer thicknesses employed were of order 1.5-5 μm. As shown in Fig. 5, the photoconductive and liquid crystal layers are sandwiched between indium tin oxide (ITO) - coated 1.2 cm thick glass optical flats. The liquid crystal layer thickness is determined by a perimeter mylar spacer.

In operation, a dc bias voltage is applied between the indium tin oxide electrodes, of order 40-150 V. The input image to be spatial frequency encoded is focused on the ZnS photoconductor, producing image-wise modulation of the local voltage across the liquid crystal layer, thus effecting a parallel intensity-to-spatial frequency conversion. The high lateral impedance of the thin film layers allows high resolution images to be processed with low pixel-to-pixel cross-talk. The device sensitivity is optimized for exposure at blue and near

ultraviolet wavelengths due to the peak photosensitivity of zinc sulfide in that spectral region. Quasi-nondestructive readout can be accomplished at wavelengths beyond the photoconductivity edge, such as that of the He-Ne laser (6328 Å). Image erasure occurs with removal of the input image, within the dielectric and liquid crystal relaxation times of the device (see Section III). To date, all VGM LCDs that we have constructed have been designed for transmissive readout, although reflective readout is possible with incorporation of an appropriate dielectric mirror. Such a configuration would have the advantage of fully separating the reading and writing functions, allowing for increased effective optical gain.

III. Fundamental Origins of the Operational Properties

As was mentioned in Section II, the operational properties of the VGM LCD are primarily determined by the variable grating mode effect exhibited by the nematic mixture liquid crystal layer. The current state of knowledge concerning the physical origin of this unique effect is summarized in Section IV. In this Section, we outline a number of key factors and considerations which affect several important device properties, in order to provide both focus and a frame of reference for the succeeding Section. These device properties include the accessible range of spatial frequencies, the number of accessible grey levels, the functional dependence of diffraction efficiency on applied voltage, maximum diffraction efficiency, response

time, device uniformity, device input sensitivity, and device operational lifetime.

The accessible range of spatial frequencies extends from the threshold for grating formation at the low end to the onset of dynamic scattering induced by high electric fields at the high end, as shown in Fig. 4. For phenyl benzoate mixtures with slightly negative dielectric anisotropy (< -0.30) such as HRL 2N40 [15], this range extends from approximately 200 line pairs/mm to over 600 line pairs/mm. In order to avoid overlap of higher diffracted orders from lower spatial frequencies with lower diffracted orders from higher spatial frequencies, the maximum range that can be processed (uniquely assigned to specific grey levels) spans a factor of two in spatial frequency. For example, a useable range in HRL 2N40 extends from 300 line pairs/mm to 600 line pairs/mm without order overlap. This accessible range can be extended by an additional factor of two by utilizing the orthogonal polarization behavior of alternating diffracted orders, as described in Section IV. Hence, the accessible range of spatial frequencies observed in several of the nematic liquid crystal mixtures tested so far is sufficient for optimized grey scale processing. It should be noted that although the maximum number of resolution elements that can be processed is linearly proportional to the highest spatial frequency utilized for devices of a given size (see discussion below), use of significantly larger spatial frequencies begins to place stringent requirements on the Fourier transform lens due to

f-number reduction. For example, to utilize a spatial frequency range of 600 line pairs/mm requires the output optics to have an f-number less than 1.2 (or less than 2.6 if the lens is displaced off axis to accept only the positive diffracted orders). This is primarily a pragmatic limitation rather than a fundamental one, as VGM effects have been observed at spatial frequencies exceeding 1000 line pairs/mm [16].

The number of accessible grey levels that lead to well-separated diffraction orders in the filter plane is limited by the ratio of the frequency range between VGM harmonics to the object spectrum bandwidth, as shown in Fig. 6. The object spectrum bandwidth is in turn limited primarily by two effects: spot size due to diffraction from finite-sized pixel apertures, and grating imperfections that cause local deviations from uniform spatial frequency. The first effect is fundamental and has been treated previously [10]. The principal result of this analysis is the inequality

$$b\nu_o \geq 2N \qquad (1)$$

in which b is the pixel width, ν_o is the lowest useable VGM spatial frequency, and N is the desired number of distinguishable grey levels. This inequality requires that the pixel size contain at least 2N periods of the lowest grating frequency if N grey levels are to be processed. For example, a 256x256 pixel image could be processed with 32 distinguishable grey levels on a 50 mm square device with ν_o = 300 line pairs/mm. An additional

restriction arises from scattering effects due to grating imperfections, which tend to further increase the size of the diffracted orders. The most common type of imperfection observed in these devices is the joining or splitting of grating lines, as shown in the photomicrograph in Fig. 7. The origin of these "disclinations" is not at present understood, although the density of occurrence of such imperfections is directly related to the quality of substrate preparation.

A typical measurement of the functional dependence of diffraction efficiency on the applied voltage across the VGM liquid crystal layer is shown in Fig. 8. Since the applied voltage is linearly related to the induced grating spatial frequency, this relationship is illustrative of the dependence of the diffraction efficiency on spatial frequency as well. To first order, the nature of this dependence is not important to the implementation of optical processing functions, since any variation in diffraction efficiency with spatial frequency can be linearized by insertion of an appropriate multiplicative filter in the focal plane of the Fourier transform lens. In any case, the theoretical functional dependence can be derived only from knowledge of the relationship between the induced orientational angles of the liquid crystal director and the applied voltage across the layer. This relationship is discussed further in the subsequent Section.

The maximum diffraction efficiency that can be achieved at a

given spatial frequency and applied voltage depends fundamentally on the magnitude of the anisotropy in the index of refraction ($\Delta n \equiv n_e - n_o$, with n_e the extraordinary refractive index for polarization parallel to the molecular axis and n_o the ordinary refractive index for polarization perpendicular to the molecular axis), the magnitude of the periodic angular reorientation of the liquid crystal director, and the thickness of the VGM liquid crystal layer. Full periodic reorientation of the index ellipsoid from homogeneous (parallel to the substrate) alignment to homeotropic (perpendicular) alignment for HRL 2N40 ($\Delta n = 0.15$) in a 6 μm cell read out at 6328 Å gives rise to an optical phase modulation of approximately 9 radians. Hence, the maximum diffraction efficiency is fundamentally limited to that expected for a pure sinusoidal phase grating [17]. In practice, full reorientation is typically not achieved before the onset of dynamic scattering, although reorientation angles of 45° are thought at present to be commonly reached (see Section IV). As can be seen from Fig. 8, typical second order diffraction efficiencies are of order 20%. This order is larger than the first diffracted order due to the peculiar nature of the birefringent phase grating formed by the VGM distortion (details are given for this phenomenon in Section IV).

The response time of the cell is a critical parameter that directly affects the achievable overall processing throughput rate. At present it is the major factor inhibiting widespread incorporation of VGM devices in optical processing systems. The

risetime for grating formation from below to above threshold varies from mixture to mixture, but is typically of order one second. The response time for grating change in response to a step increase in applied voltage (corresponding to a step increase in grating spatial frequency) is typically of order a fraction of a second [18]. The response time of the photoconductive voltage division across the liquid crystal layer is not a significant factor by orders of magnitude relative to the reorientation response time, so that eventual improvements in VGM LCD response time will accrue only by advances in the state of understanding of the physical origin of the VGM effect and the dynamical nature of the grating reorientation process, followed by appropriate modification of the device operational mode to enhance the rate of molecular reorientation and/or a search for a nematic liquid crystal mixture with physical characteristics optimized for dynamic VGM effects.

The input sensitivity of the VGM LCD, defined as the input (writing) intensity per unit area per unit change in grating spatial frequency, is determined by a number of factors. These include the slope of induced grating spatial frequency as a function of applied voltage for the particular nematic liquid crystal mixture employed, the wavelength dependence of the photoconductive layer photosensitivity, and the cell switching ratio (fractional increase in voltage across the liquid crystal layer from illumination at the threshold for grating formation to saturation). The first factor (liquid crystal response slope)

varies significantly from mixture to mixture (see Fig. 4). Of the VGM nematic liquid crystal mixtures investigated to date, HRL 2N40 has proved to be nearly optimum in this regard. It is not yet clear what fundamentally influences and eventually limits this parameter. The photosensitivity of the photoconductive layer is determined primarily by the choice of photoconductive material (limited to those that can be appropriately impedance-matched to the liquid crystal layer), method and quality of thin film deposition, layer thickness, spectral width and central wavelength of the exposure (writing) illumination, and the operational bias voltage employed. The cell switching ratio is a function of the series impedance of the liquid crystal layer, the impedance of the unilluminated photoconductive layer, and the impedance of the photoconductive layer under saturation illumination. In addition, the cell switching ratio will be altered by incorporation of surfactant layers to improve liquid crystal quiescent alignment, and of a dielectric mirror in the reflective readout device structure. At this stage of the device development, the input sensitivity of the VGM LCD has not been optimized. A typical value of 15($\mu W/cm^2$)·(mm/line pair) was obtained with a VGM LCD consisting of a 6 μm layer of HRL 2N40 in series with a 5 μm thick evaporated ZnS layer that had been polished and rubbed with surfactant polyvinyl alcohol, operated at 160 VDC and illuminated in the passband 410 to 550 nm [9].

The uniformity of VGM LCD response depends inherently on technological issues, including uniformity of layer thicknesses,

homogeneous mixing of the liquid crystal material employed, and the as-deposited spatial dependence of photoconductive sensitivity. Whereas it is relatively straightforward to construct electrically-activated VGM cells (see Section IV) that exhibit a high degree of spatial uniformity, deposition of a photoconductive layer with equivalent spatial homogeneity has proven more difficult. Nonuniformity of the device response characteristic can be a contributing factor in the establishment of the maximum number of accessible grey levels discussed previously. In experimental devices constructed thus far, device uniformity has not proven to be the limiting factor. In any case, it is expected that response nonuniformities can be minimized significantly by improvements in the photoconductive layer deposition process.

The lifetimes of experimentally constructed VGM LCDs have ranged from less than a week to over a year. The causes of VGM device failure have not yet been extensively studied, although several contributing factors can be identified. These factors include the purity and composition of the liquid crystal mixture employed, the nature of the liquid crystal/photoconductive layer interface, the integrity of the device sealing process, and the device operational history. Since the VGM effect requires a dc applied voltage, unidirectional ion poisoning may contribute to gradual device degradation.

IV. Physical Origin of the Variable Grating Mode Effect

As can be clearly understood from the discussion presented in Section III, a vast majority of the important device operational properties depend critically on the detailed nature of the grating formation and dynamic reorientation process. The elucidation of the fundamental nature of the grating (molecular orientation angles as a function of applied voltage across the liquid crystal layer) and of the physical mechanism that gives rise to the observed periodic instability and its reorientation dynamics has been a subject of considerable experimental and theoretical interest [11,16,19-30]. In this Section, the present state of understanding of the VGM effect is described, and a number of important unresolved questions are presented.

The grating produced by the periodic spatial reorientation of the nematic liquid crystal molecules is quite unusual, giving rise to striking polarization-dependent properties [11]. These diffraction effects can be investigated in an electrically-activated VGM cell with no intervening photoconductive layer, as shown in Fig. 9. The orientation of the grating is such that the grating wavevector is perpendicular to the direction of unperturbed alignment, which is homogeneous and induced by unidirectional rubbing or ion beam milling. That is, the periodic modulation direction is perpendicular to the initial (zero applied bias) liquid crystal director (long molecular axis), as shown in the polarization micrographs

(Fig. 3).

For all linear input polarization angles, the even and odd diffraction orders are found to be essentially linearly polarized. In addition, the even diffraction orders are nearly linearly polarized parallel to the "domains" comprising the VGM grating, as shown in Fig. 10. For input polarization perpendicular to the domains, the even orders are found to be almost fully extinguished. On the other hand, the odd diffraction orders are nearly linearly polarized with a major axis that rotates counterclockwise at the same rate as the input polarization is rotated clockwise. This effect is the same as that produced by a half-wave plate oriented at 45° with respect to the grating wavevector. For input polarization at 45° to the wavevector, all orders are observed in the far field diffraction pattern. An analyzer placed on the output side of the VGM device can be rotated to extinguish the even orders (when oriented parallel to the grating wavevector) or the odd orders (when oriented at -45° to the grating wavevector).

These unusual polarization properties have recently been utilized to determine the spatial distribution of the molecular orientation within the VGM liquid crystal layer [11]. The polarization dependence of the diffraction phenomena is directly related to the formation of a birefringent phase grating [13], in which the principal axis of the index ellipsoid varies periodically both in the plane of the grating (characterized by

an orientation angle α) and normal to the plane of the grating (characterized by an orientation angle η). The angular coordinates are as shown in Fig. 9.

The polarization properties of light diffracted by the liquid crystal birefringent phase grating can be summarized by means of a transfer matrix that connects the output polarization at each point (x,y) on the rear surface of the liquid crystal layer with the input polarization at the front surface of the liquid crystal layer. On the basis of the experimental observations, this matrix must be of the form:

$$\begin{bmatrix} A_o + A(x;p) & B(x;2p) \\ C(x;2p) & D_o + D(x;p) \end{bmatrix} \tag{2}$$

in which the notation A(x;p) indicates that the complex amplitude A varies in the x direction with periodic repetition distance p. For uniaxial liquid crystal molecules at an arbitrary orientation (α,η), assumed uniform throughout the layer thickness at a given coordinate in the x direction, the Jones matrix can be determined by appropriate rotations of the index ellipsoid, which yields:

$$\begin{bmatrix} 1 - \sin^2\alpha(1 - e^{j\phi}) & \sin\alpha\cos\alpha(1 - e^{j\phi}) \\ \sin\alpha\cos\alpha(1 - e^{j\phi}) & 1 - \cos^2\alpha(1 - e^{j\phi}) \end{bmatrix} \tag{3}$$

where

$$\phi \equiv \frac{2\pi t}{\lambda}\left\{\left[\frac{\sin^2\eta}{n_o^2} + \frac{\cos^2\eta}{n_e^2}\right]^{-\frac{1}{2}} - n_o\right\}$$

in which t is the liquid crystal layer thickness, n_o is the ordinary index of refraction, n_e is the extraordinary index of refraction, and λ is the wavelength of readout illumination employed. The angles α and η are assumed to be periodic functions of x and independent of y and z. Measurement of the intensities in each diffraction order for a minimum set of polarizer/analyzer orientations uniquely determines the magnitudes of the Fourier components of the polarization transfer matrix. These experimentally derived values can then be compared with the theoretically calculated coefficients of Eq. (3) (by harmonic expansion) for different possible assumptions concerning the spatial distribution of the orientation angles α and η. An example of such a comparison between theory and experiment is shown in Fig. 11, under the assumption that the spatial dependences of α and η are given by

$$\alpha = \alpha_{max} \cos\frac{2\pi x}{\Lambda} \qquad \eta = \pm\eta_{max} \sin\frac{2\pi x}{\Lambda} \tag{4}$$

This procedure allows the extraction of the maximum orientational

excursion angles $\alpha_o(V)$ and $\eta_o(V)$ as functions of the applied bias voltage above the threshold for grating formation, as shown in Fig. 12(α_o) and Fig. 13(η_o). In each case, subject to the assumed form of α and η implicit in Eq. 4, it is observed that the maximum excursion angles both in and out of the plane of the grating seem to increase as the logarithm of the applied voltage.

The spatial distribution of the ends of the liquid crystal molecules described by Eq. 4 is approximately cycloidal. Such a dependence of the angles α and η on the spatial coordinate x has been predicted by direct minimization of the free energy in a similar nematic liquid crystal system [21]. This particular solution is obtained by incorporation of the converse flexoelectric effect in the expression for the free energy [13,31,33]. The flexoelectric effect describes a strain-induced polarization that arises due to molecular shape effects in conjunction with a nonzero dipole moment as shown schematically in Fig.14. The converse flexoelectric effect thus pertains to a polarization-induced strain within the liquid crystal layer, which can result in a periodic molecular reorientation characterized by a linear dispersion relation between the grating wavevector and the applied field, as is observed experimentally. Including the dielectric, distortion, and flexoelectric contribution to the free energy yields an expression of the form:

$$
\begin{aligned}
F_{VGM} &= \int \left(F_{dielectric} + F_{distortion} + F_{flexoelectric} \right) dV \\
&= F_o - \frac{1}{8\pi} \int (\varepsilon_e - \varepsilon_o)(\underline{E} \cdot \hat{n})^2 dV \\
&\quad + \frac{1}{2} \int \Big[K_1 (\nabla \cdot \hat{n})^2 + K_2 (\hat{n} \cdot \nabla \times \hat{n})^2 \\
&\qquad + K_3 (\hat{n} \times \nabla \times \hat{n})^2 \Big] dV \\
&\quad - \int \left[e_1 (\nabla \cdot \hat{n})(\hat{n} \cdot \underline{E}) + e_3 \left[\left((\nabla \times \hat{n}) \times \hat{n} \right) \cdot \underline{E} \right] \right] dV
\end{aligned}
\tag{5}
$$

in which K_1, K_2, and K_3 are the elastic constants for splay, twist, and bend deformations, respectively; $\hat{n}$ is the liquid crystal director, $\underline{E}$ is the applied electric field, ε_e and ε_o are principal components of the dielectric tensor of the liquid crystal, and e_1 and e_3 are flexoelectric coefficients [31]. Minimization of F_{VGM} with respect to the orientation angles α and η of the director, subject to fully pinned boundary conditions at both substrate surfaces, and with the simplifying assumption that $K_1 = K_2 = K$, yields [21]:

$$
\begin{aligned}
\alpha &= \alpha_o \cos(kx) \cos(\pi z/t) \\
\eta &= \eta_o \sin(kx) \cos(\pi z/t)
\end{aligned}
\tag{6}
$$

in which k is the grating wavevector and t the liquid crystal

layer thickness. This solution generates a dispersion relation between E and k of the form:

$$E^2 = \left(\frac{K}{e^*}\right)^2 \cdot \frac{\left(k^2 + (\pi/t)^2\right)^2}{k^2 + \mu\left(k^2 + (\pi/t)^2\right)} \qquad (7)$$

in which $e^* \equiv e_1 - e_3$, $\mu \equiv (\epsilon_a K/4\pi e^{*2})$, and $\epsilon_a \equiv \epsilon_e - \epsilon_o$. The dispersion relation is linear when $k >> \pi/t$, as shown in Fig. 15 (compare with the experimental relationship shown in Fig. 4).

The origin of the periodic instability in VGM liquid crystals has not yet been established beyond doubt, although the accumulated evidence points strongly toward the converse flexoelectric effect. This assignment is also intuitively appealing, since the VGM effect is observed only in liquid crystal mixtures with slightly negative dielectric anisotropy [12], for which both the dielectric and distortion contributions to the free energy increase for deviations from uniform alignment. The addition of the flexoelectric term counteracts these effects, producing a free energy minimum at non-zero distortion angles. Furthermore, this model predicts a static periodic perturbation; no hydrodynamic or electrohydrodynamic effects are observed in our test cells.

The dynamics of grating formation, reorientation, and relaxation are subjects of ongoing experimental and theoretical investigation. Understanding of the basic physical principles

underlying these effects is vital to the success of efforts to improve the VGM LCD response time.

A number of spatial discontinuities can be observed within the liquid crystal layer, similar in appearance to crystallographic dislocations (see Fig. 7). The "dislocation" density increases with time as each VGM device deteriorates, and strongly depends on the manner in which the applied bias is brought from below to above the threshold of grating formation. In some cases, as the applied bias across an electrically activated cell is increased or decreased, the "dislocations" propagate past each other while the grating period decreases or increases, respectively. Dislocations with opposite orientations propagate in opposite directions until a new stable equilibrium situation is achieved. It is not yet clear whether these "dislocations" represent true disclinations, for which the liquid crystal director is discontinuous near the defect, or whether they are in fact alternative local continuous solutions to the free energy minimization, perhaps induced by an as yet undiscovered perturbation.

A large number of research directions have been described in the foregoing. In addition, several others are worthy of note. First, numerous experimental measurements of the off-diagonal elements in the Jones matrix describing polarized light propagation through the VGM cell have revealed a significant asymmetry not predicted by the uniaxial model. The origin of

this "B/C" asymmetry effect has not yet been elucidated. Second, the thickness dependence of the molecular orientation angles α and η has not been fully established. The solution proposed [21] in Eq. 6 assumes full surface pinning at the substrate boundaries, and represents the lowest order z-dependent mode. The polarization-dependent diffracted order measurements described herein do not provide clear differentiation between a uniform z-dependence and the lowest order mode. Third, the nature of the transient solutions to the free energy minimization incorporating molecular dynamic and viscosity effects has not been treated. Solution of this problem is key to response time optimization of the VGM liquid crystal device. Fourth, it is not yet clear whether a nematic liquid crystal mixture can be found that exhibits a useful VGM effect under ac bias. Such a mixture may provide significant immunity from long-term ion-poisoning effects. Finally, it should be emphasized that the variable grating mode liquid crystal effect provides only one possible means of achieving parallel intensity-to-position encoding. The processing potential of the intensity-to-position algorithm should provide more than adequate inducement to intensify the search for alternative implementations.

ACKNOWLEDGEMENTS

The authors gratefully acknowledge the contributions of D. Boswell, A.M. Lackner, and J.D. Margerum (H.R.L.), and K. Sherman and G. Edwards (U.S.C.). This research was supported

by the U.S. Air Force Office of Scientific Research, Electronics and Solid State Sciences Division, under grant AFOSR-81-0082 at the University of Southern California and contract F49620-81-C-0086 at Hughes Research Laboratories.

REFERENCES

1. R.V. Johnson, D.L. Hecht, R.A. Sprague, L.N. Flores, D.L. Steinmetz, and W.D. Turner, Opt. Eng. Special Issue on Spatial Light Modulators: Fundamental Considerations, 22(6), (1983).

2. D.L. Pape and L.J. Hornbeck, Opt. Eng. Special Issue on Spatial Light Modulators: Fundamental Considerations, 22(6), (1983).

3. U. Efron, P.O. Braatz, M.J. Little, R.N. Schwartz, and J. Grinberg, Opt. Eng. Special Issue on Spatial Light Modulators: Fundamental Considerations, 22(6), (1983).

4. C. Warde and J. Thackera, Opt. Eng. Special Issue on Spatial Light Modulators: Fundamental Considerations, 22(6), (1983).

5. D. Casasent, Proc. IEEE, 65, 143-157, (1977).

6. S. Lipson, "Recyclable Incoherent-to-Coherent Image Converters", in Advances in Holography, N. Farhat, Ed., Marcel Dekker, New York, (1979).

7. G. Knight, "Interface Devices and Memory Materials", in Optical Data Processing, S.H. Lee, Ed., Springer-Verlag, Heidelberg, Germany, (1976).

8. A.R. Tanguay, Jr., Proc. ARO Workshop on Future Directions for Optical Information Processing, Texas Tech University, Lubbock, Texas, 52-76, (1980).

9. B. Soffer, D. Boswell, A.M. Lackner, A.R. Tanguay, Jr., T.C. Strand, and A.A. Sawchuk, Proc. SPIE, 218, 81-87, (1980).

10. P. Chavel, A.A. Sawchuk, T.C. Strand, A.R. Tanguay, Jr., D. Boswell, A.M. Lackner, and B.H. Soffer, Proc. SPIE, 232, 128-136, (1980).

11. P. Chavel, A.A. Sawchuk, T.C. Strand, A.R. Tanguay, Jr., and B.H. Soffer, Opt. Eng., 5, 398-400, (1980).

12. B.H. Soffer, J.D. Margerum, A.M. Lackner, D. Boswell, A.R. Tanguay, Jr., T.C. Strand, A.A. Sawchuk, and P. Chavel, Mol. Cryst. Liq. Cryst., 70, 145-161, (1981).

13. A.R. Tanguay, Jr., submitted for publication in Opt. Lett.

14. A.R. Tanguay, Jr., P. Chavel, T.C. Strand, C.S. Wu, and B.H. Soffer, submitted for publication in Opt. Lett.

15. J.B. Margerum, J.E. Jensen, and A.M. Lackner, Mol. Cryst. Liq. Cryst., 68, 137-156, (1981).

16. W. Greubel and U. Wolff, Appl. Phys. Lett., 19(7), 213-215, (1971).

17. J.W. Goodman, Introduction to Fourier Optics, McGraw-Hill, New York, 1968.

18. B.H. Soffer, "Real-Time Implementation of Nonlinear Optical Processing Functions", Annual Technical Report on AFOSR F49620-81-C-0086, (1982).

19. R.B. Meyer, Phys. Rev. Lett., 22(18), 918-921, (1969).

20. A.I. Derzhanski, A.G. Petrov, Chr. P. Khinov, and B.L. Markovski, Bulg. J. Phys., 2, 165-174, (1974).

21. Yu. P. Bobylev and S.A. Pikin, Sov. Phys. JETP, 45(1), 195-198, (1977).

22. Yu. P. Bobylev, V.G. Chigrinov, and S.A. Pikin, J. de Phys., 40, suppl. 4, C3-331 - C3-333, (1979).

23. S.A. Pikin, Mol. Cryst. Liq. Cryst., 63, 181-192, (1981).

24. J.M. Pollack and J.B. Flannery, Society for Information Display 1976 Intern. Symp. Digest, 143-144, (1976).

25. J.M. Pollack and J.B. Flannery, in Liquid Crystals and Ordered Fluids, J.F. Johnson and R.E. Porter, Eds., Plenum Press, New York, 2, 557-571, (1974).

26. J.M. Pollack and J.B. Flannery, in Liquid Crystals and Ordered Fluids, J.F. Johnson and R.E. Porter, Eds., Plenum Press, New York, 3, 421-442, (1978).

27. L.K. Vistin', Sov. Phys.-Dok., 15(10), 908-910, (1971).

28. L.K. Vistin', Sov. Phys.-Cryst., 15(3), 514-515, (1970).

29. A. Derzhanski, A.G. Petrov, and M.D. Mitov, J. de Phys., 39, 273-285, (1978).

30. M.I. Barnik, L.M. Blinov, A.N. Trufanov, and B.A. Umanski, J. de Phys., 39, 417-422, (1978).

31. P.G. de Gennes, The Physics of Liquid Crystals, Oxford University Press, London, 97-101, (1974).

32. J. Prost and J.P. Marcerou, J. de Phys., 38, 315-324, (1977).

33. J. Prost and P.S. Pershan, J. Appl. Phys., 47, 2298-2312, (1976).

FIGURE CAPTIONS

Figure 1 Experimental arrangement for demonstration of intensity-to-position encoding by means of an intensity-to-spatial frequency conversion in a VGM LCD.

Figure 2 VGM nonlinear processing. The overall input-output characteristic can be found by stepping through the successive nonlinear transformations including (1) the intensity-to-spatial frequency conversion, (2) spatial filtering, and (3) intensity detection.

Figure 3 Polarization photomicrographs of the liquid crystal domain pattern in an electrically activated cell. In (a), the polarizer was oriented at 90°, and the analyzer at 90°, with respect to the grating wavevector. In (b), the polarizer was oriented at 90°, and the analyzer at 10°, with respect to the grating wavevector. The unit vector $\hat{n}_{QA}$ denotes the direction of quiescent alignment, and $\underline{k}_G$ indicates the direction of the grating wavevector.

Figure 4 VGM spatial frequency as a function of applied voltage for various nematic liquid crystal mixtures.

Figure 5 Schematic diagram of the VGM Liquid Crystal Device. Current devices are read out in transmission at a wavelength of photoconductive insensitivity.

Figure 6 Grey level resolution. The number of accessible grey levels is limited by the ratio of the separation between VGM harmonics to the object spectrum bandwidth.

Figure 7 Polarization photomicrograph of a VGM liquid crystal layer exhibiting a number of grating discontinuities (circled).

Figure 8 Diffraction efficiency as a function of applied voltage across a nematic liquid crystal mixture of phenyl benzoates (HRL 2N40). The layer thickness was approximately 6 μm as defined by a perimeter mylar spacer.

Figure 9 Variable grating mode liquid crystal test geometry showing the cartesian coordinate system referred to in the text as well as the molecular orientation angles α and η. This configuration was utilized in the polarized light diffraction efficiency and photomicroscopy experiments.

Figure 10 The polarization behavior of VGM diffracted orders, with illumination normal to the plane of the liquid crystal layer. The left hand column indicates the input polarization associated with each row of output polarizations. The inset shows the corresponding orientation of the VGM grating.

Figure 11 Measured diffracted order intensities as a function of theoretical intensities calculated from the uniaxial VGM model described in the text.

Figure 12 The in-plane molecular orientation angle (α_o) as a function of the applied dc bias voltage across the cell (V) (see Fig. 5).

Figure 13 The out-of-plane molecular orientation angle (η_o) as

a function of the applied dc bias voltage across the cell (V) (see Fig. 5).

Figure 14 Schematic diagram illustrating a possible mechanism for the occurrence of the flexoelectric effect due to a shape anisotropy in liquid crystal molecules with a permanent dipole moment. In (a), the molecular orientations are randomly distributed, resulting in zero net polarization. In (b), the applied distortion induces a shape-dependent molecular realignment, resulting in a net polarization. (After Ref. [31]).

Figure 15 Resultant theoretical dispersion relation for liquid crystal parameters corresponding to HRL 2N40 phenyl benzoate mixture (see Eq. 7), subject to the assumption that $K_1 = K_2 = K$.

AD-A142 619 NONLINEAR REAL-TIME OPTICAL SIGNAL PROCESSING(U) 2/2
UNIVERSITY OF SOUTHERN CALIFORNIA LOS ANGELES IMAGE
PROCESSIN.. A A SAWCHUK ET AL. 01 DEC 83 USCIPI-1100
UNCLASSIFIED AFOSR-TR-84-0538 AFOSR-81-0082 F/G 20/6 NL

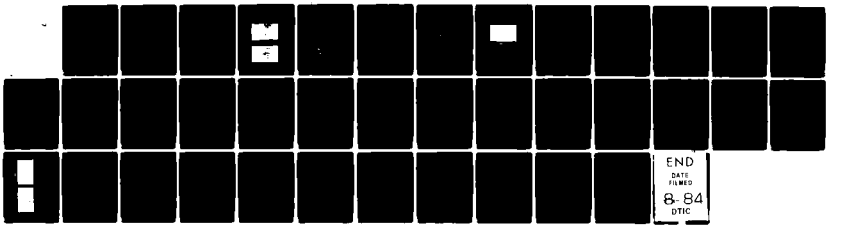

END
DATE FILMED
8-84
DTIC

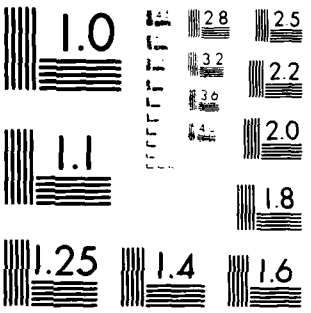

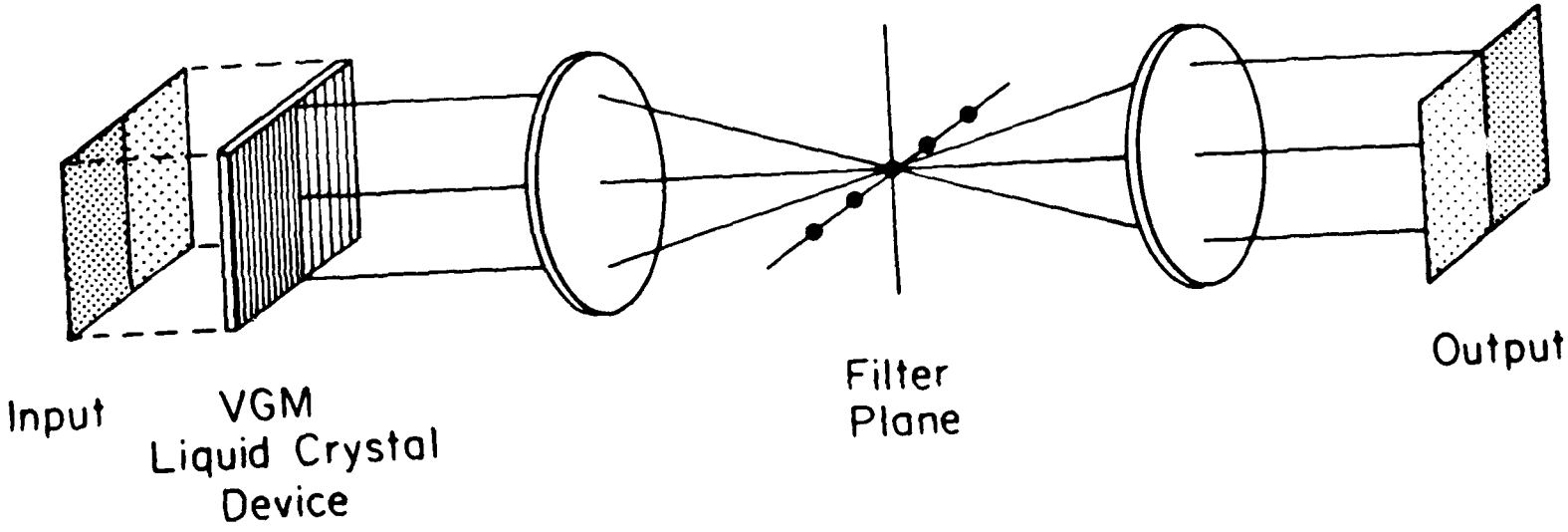

FIGURE 1

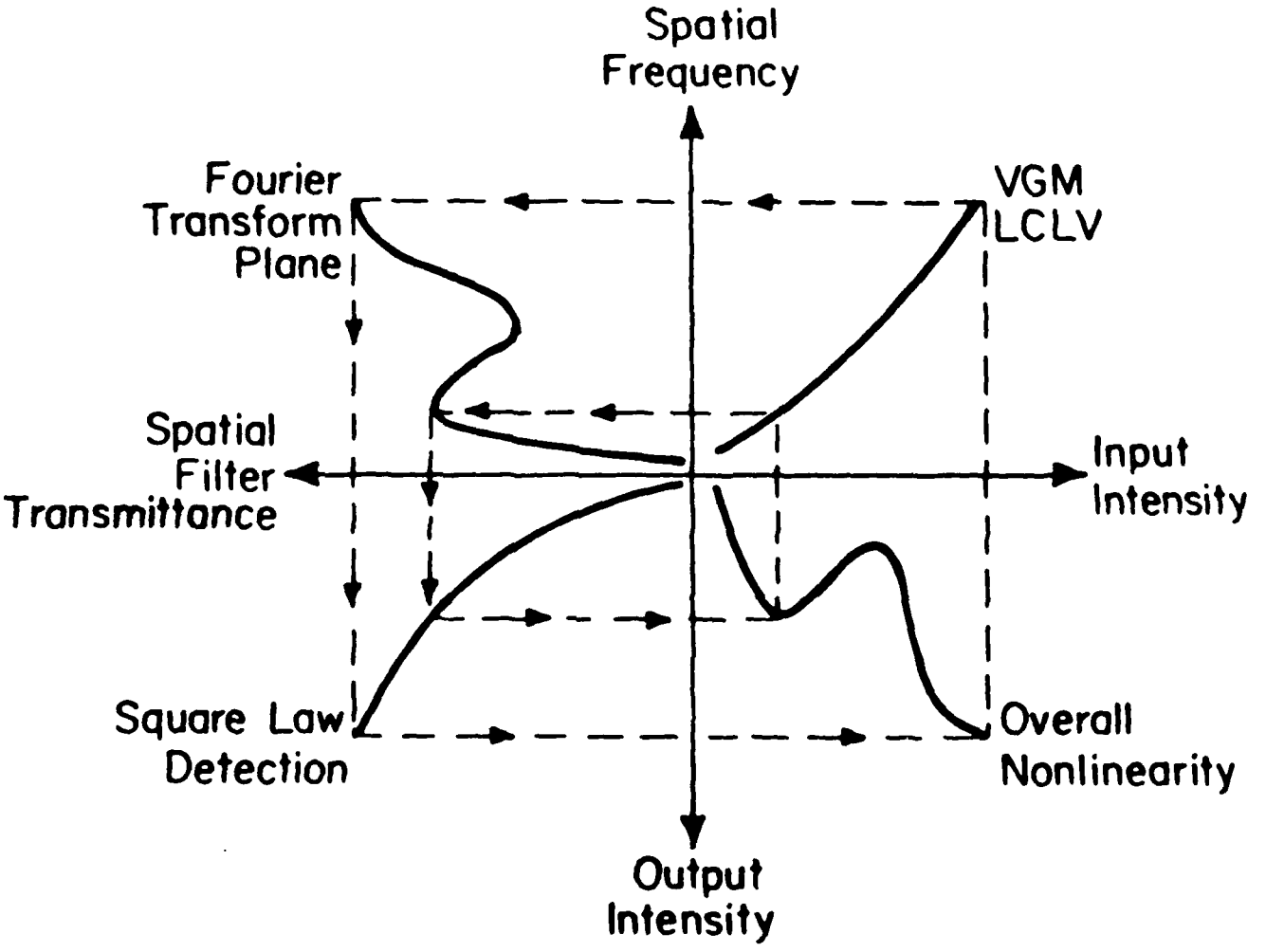

Nonlinear Processing with a Variable-Grating-Mode LCLV

FIGURE 2

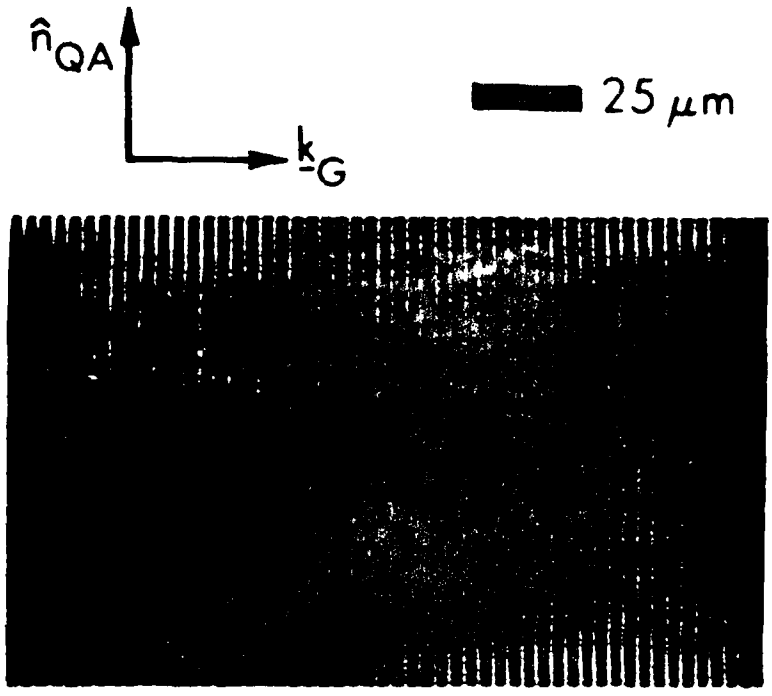

(a)

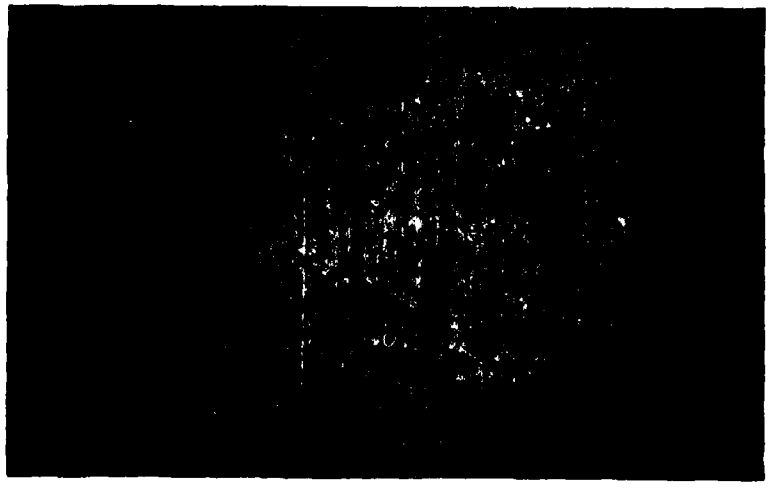

(b)

FIGURE 3

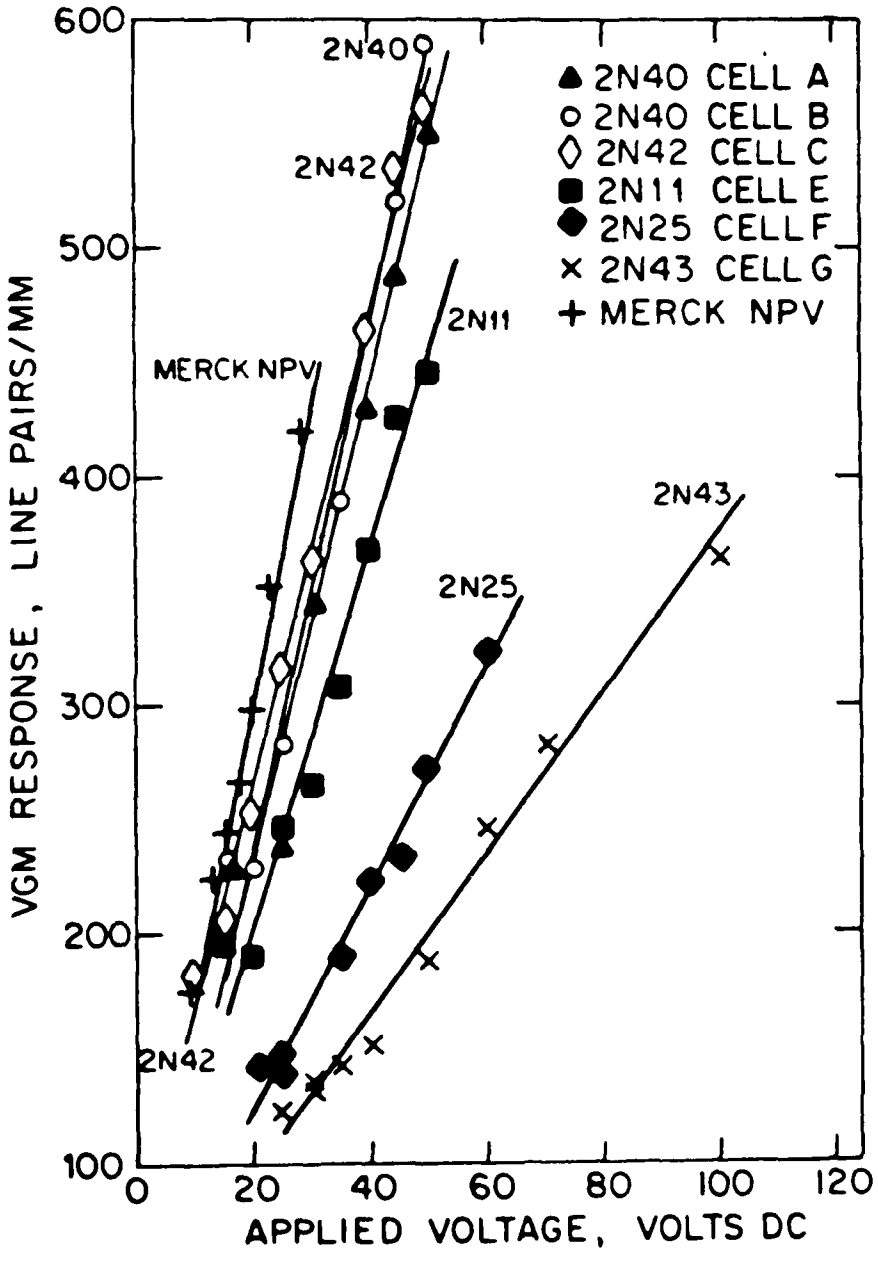

VGM VOLTAGE DEPENDENCE FOR VARIOUS LCs.

FIGURE 4

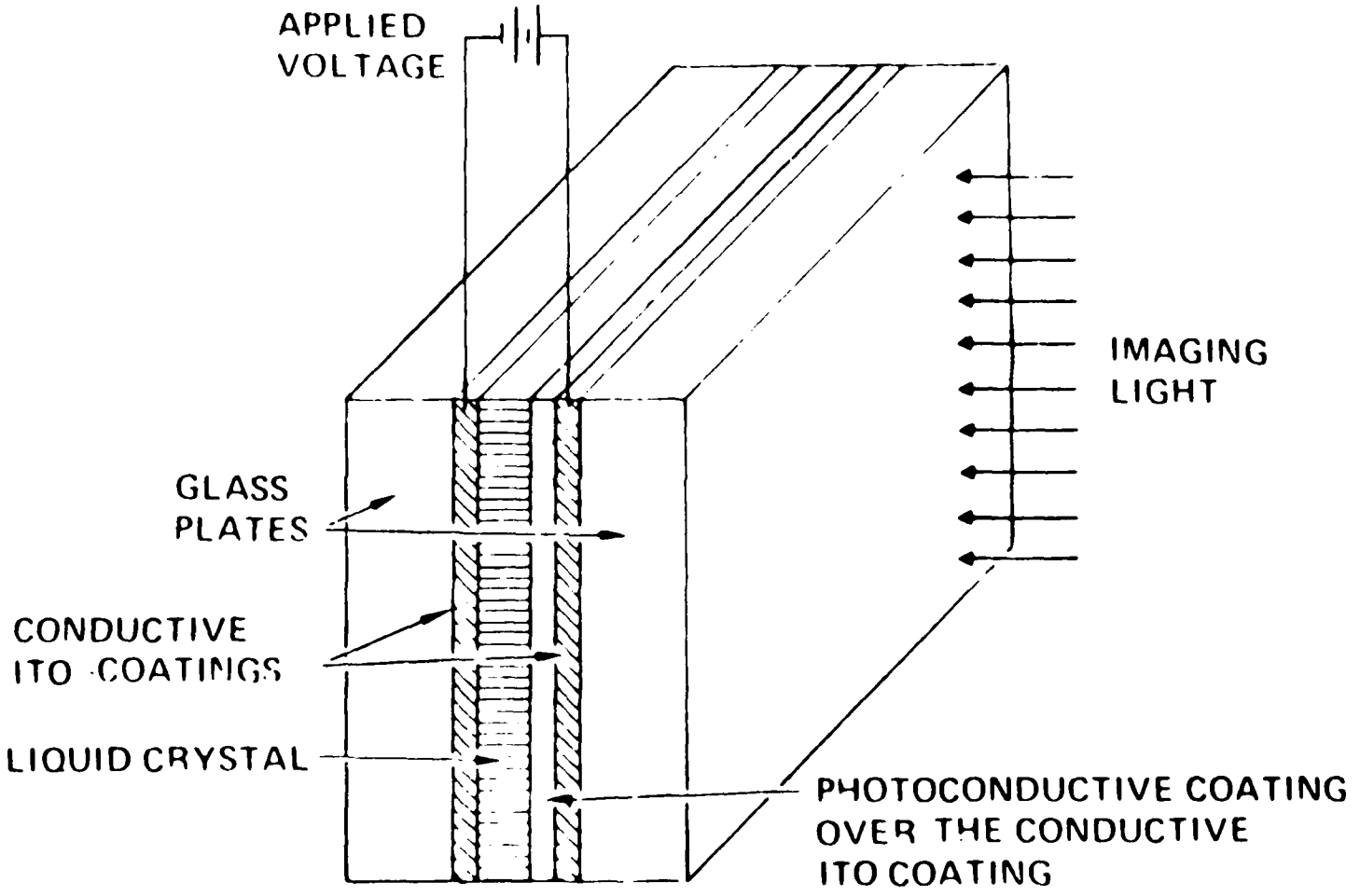
APPLIED
VOLTAGE
IMAGING
LIGHT
GLASS
PLATES
CONDUCTIVE
ITO COATINGS
LIQUID CRYSTAL
PHOTOCONDUCTIVE COATING
OVER THE CONDUCTIVE
ITO COATING

FIGURE 5

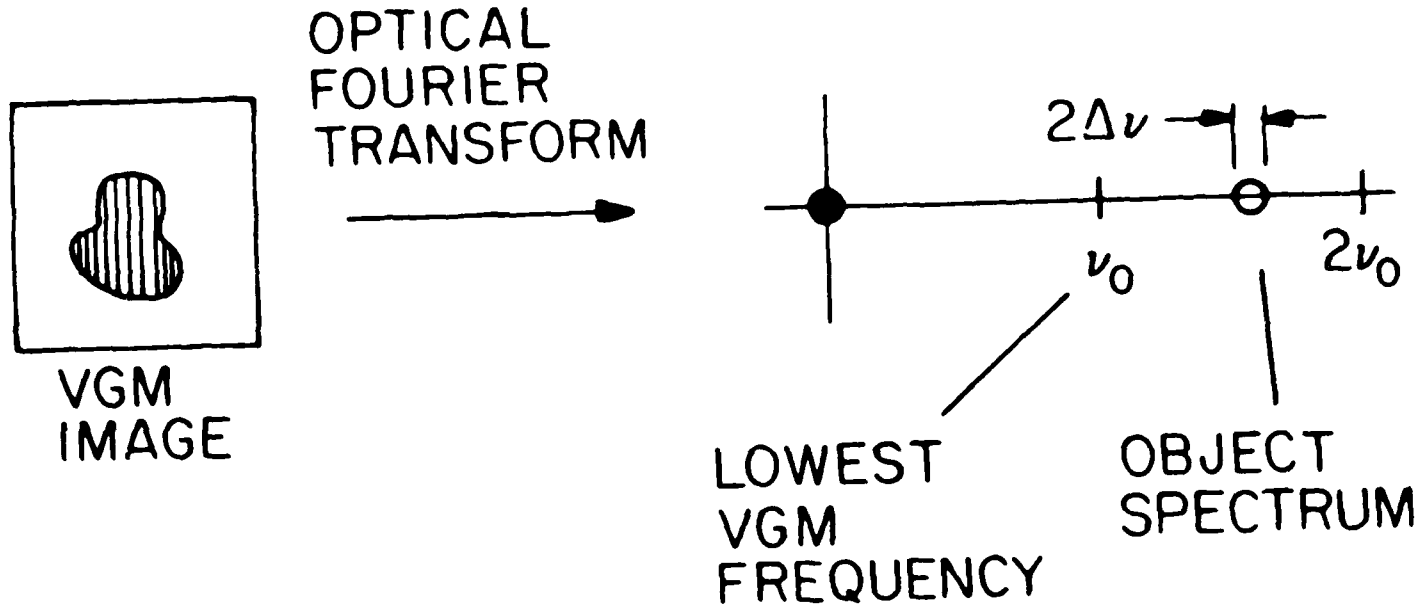
OPTICAL
FOURIER
TRANSFORM
VGM
IMAGE
2Δν
ν0
2ν0
LOWEST
VGM
FREQUENCY
OBJECT
SPECTRUM

FIGURE 6

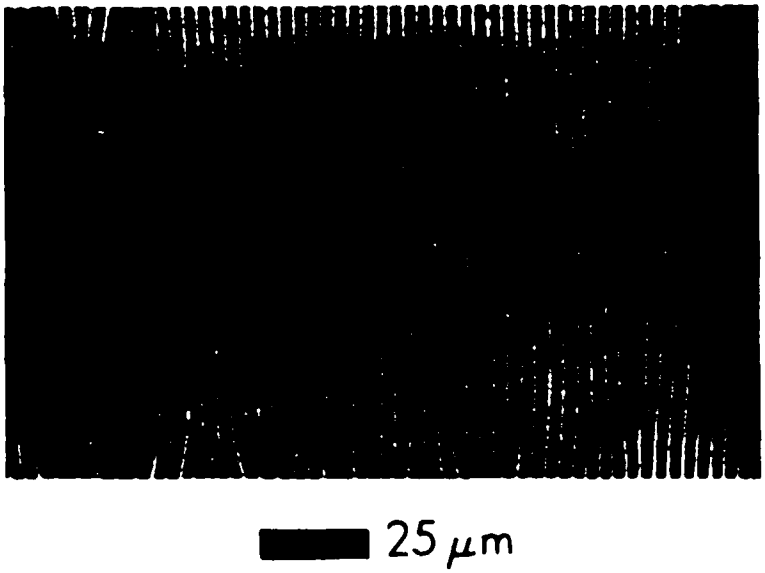

FIGURE 7

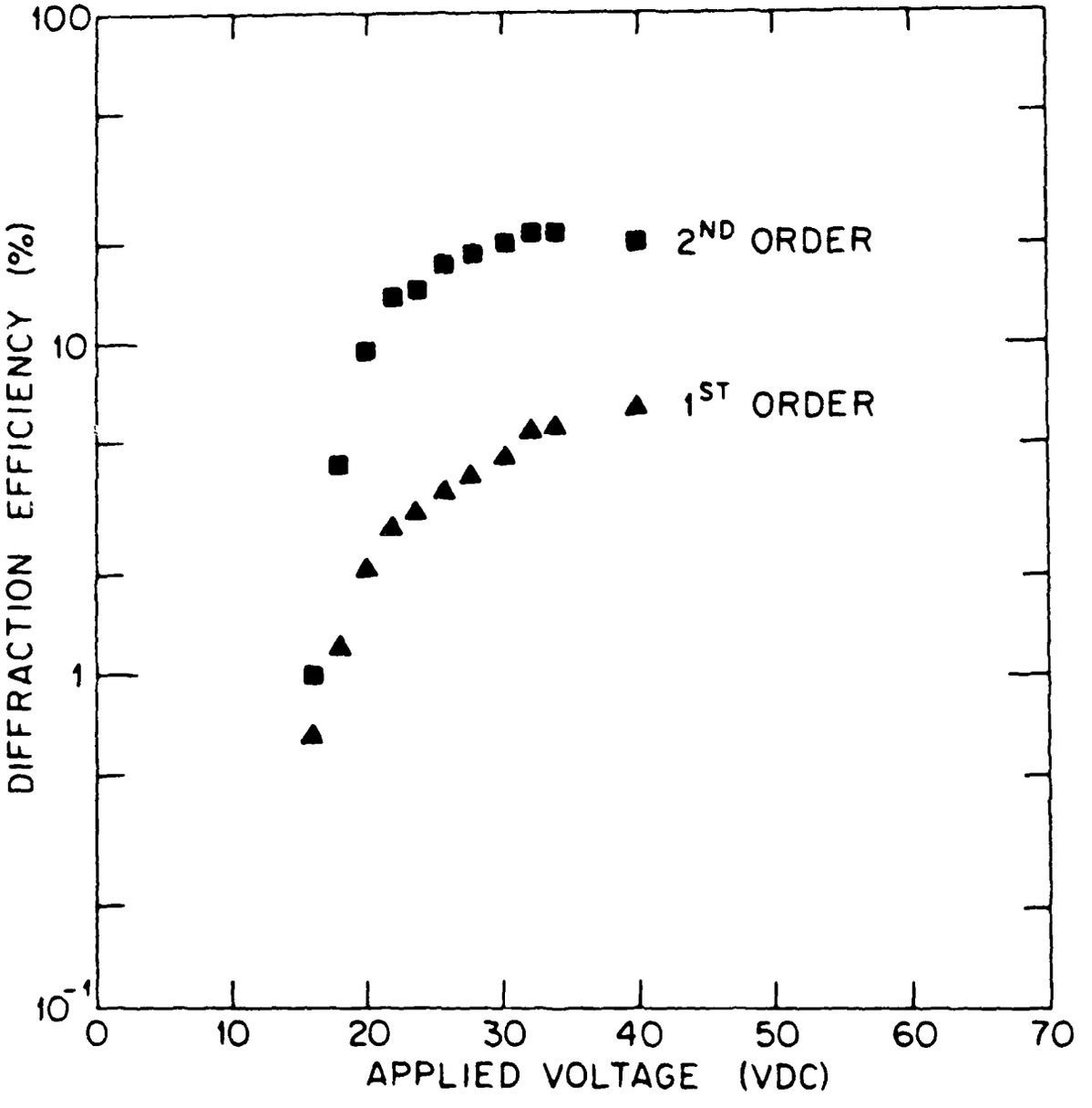
100
10
1
10^{-1}
DIFFRACTION EFFICIENCY (%)
2ND ORDER
1ST ORDER
0
10
20
30
40
50
60
70
APPLIED VOLTAGE (VDC)

FIGURE 8

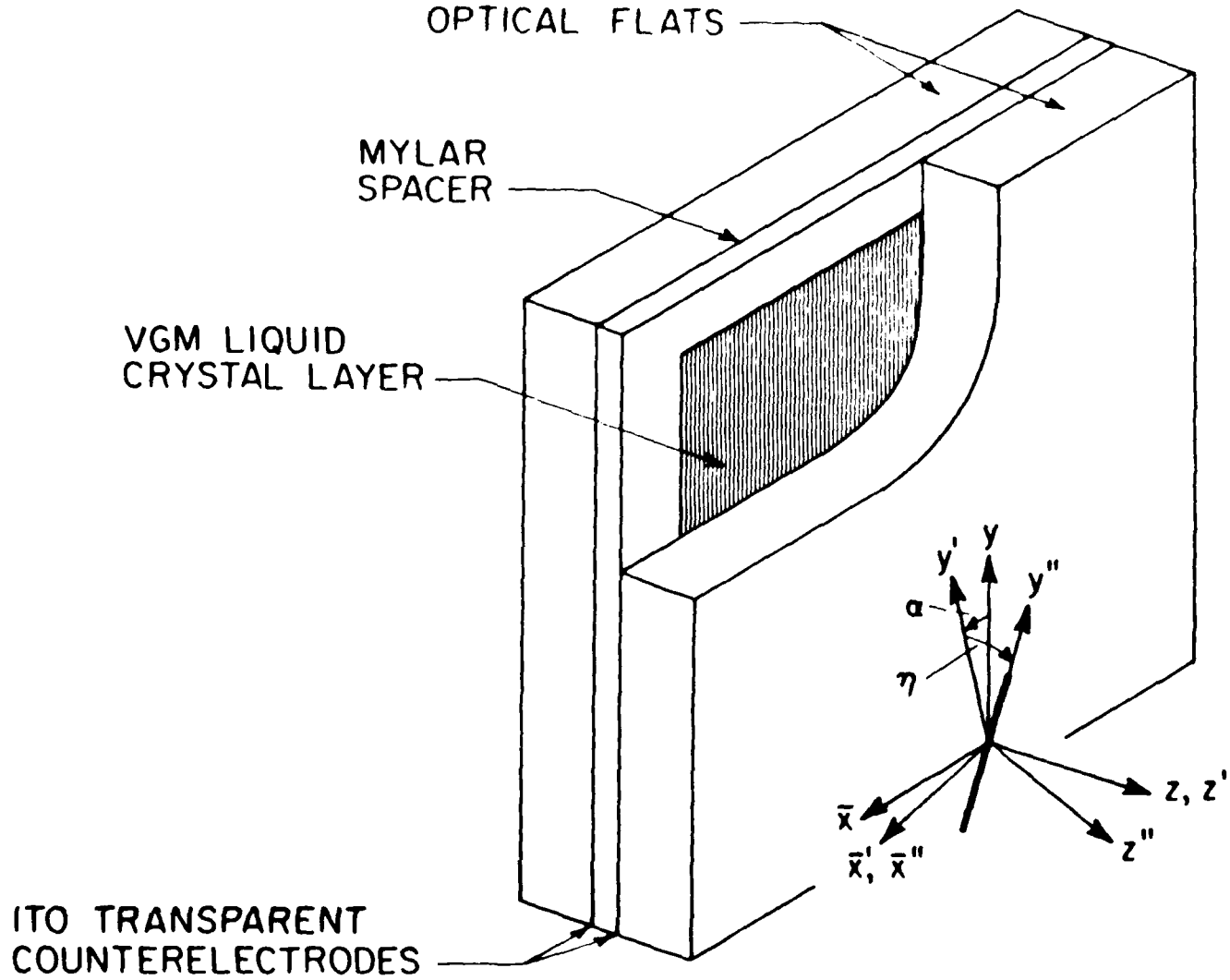
OPTICAL FLATS
MYLAR SPACER
VGM LIQUID CRYSTAL LAYER
ITO TRANSPARENT COUNTERELECTRODES
y'
y
y"
α
η
z, z'
z"
x̄
x̄', x̄"

FIGURE 9

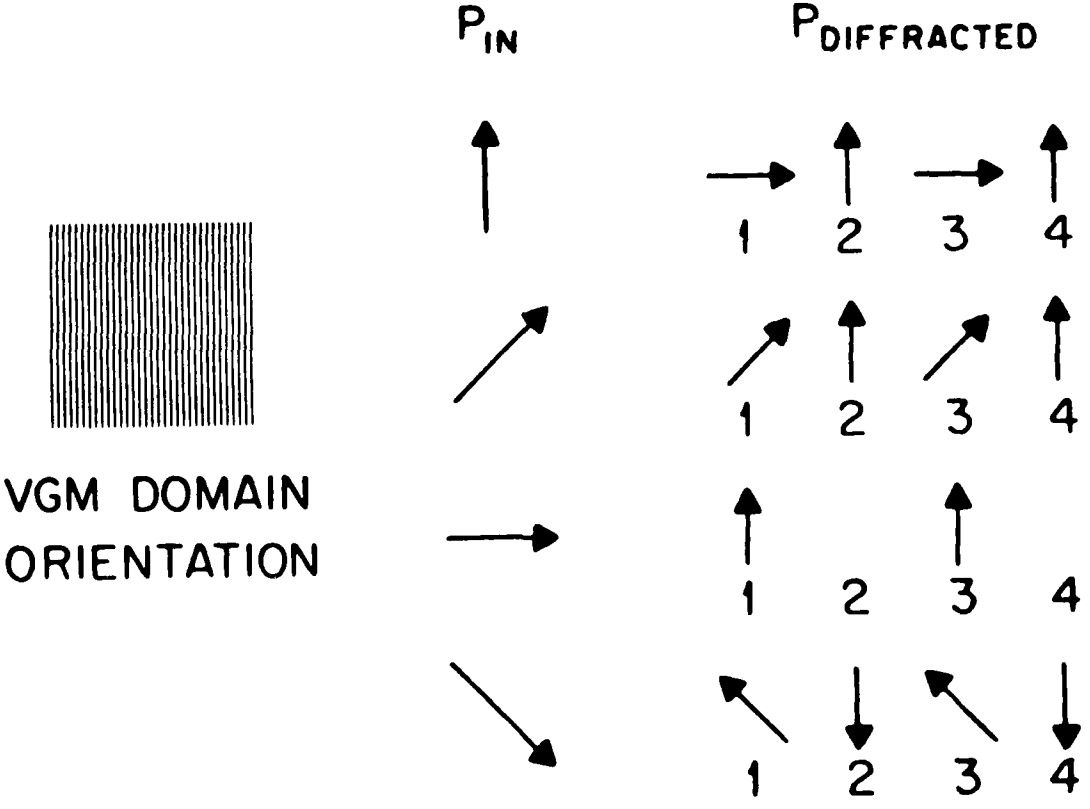
VGM DOMAIN
ORIENTATION
P_{IN}
$P_{DIFFRACTED}$
1 2 3 4
1 2 3 4
1 2 3 4
1 2 3 4

FIGURE 10

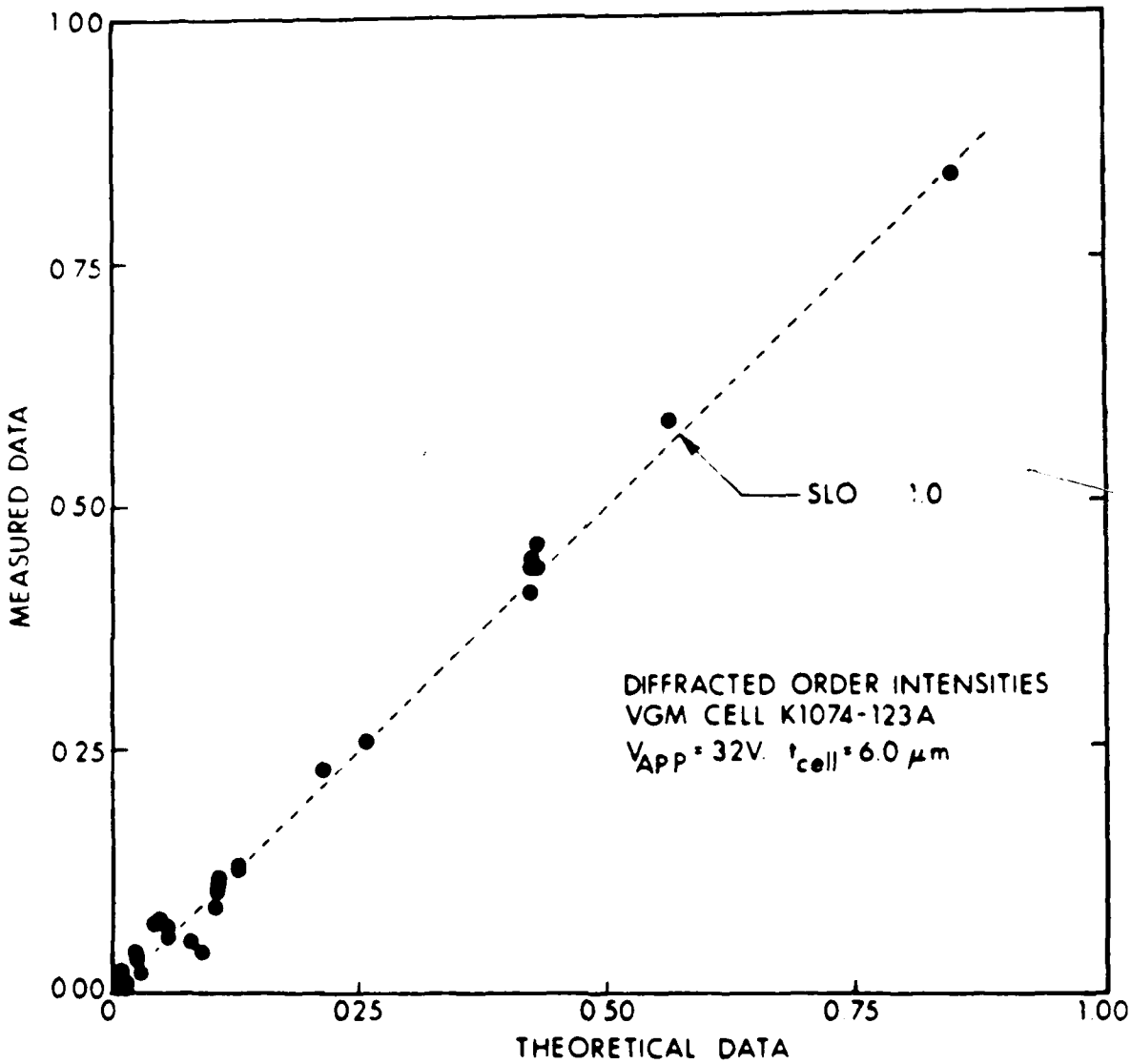
1.00
0.75
0.50
0.25
0.00
0
0.25
0.50
0.75
1.00
MEASURED DATA
THEORETICAL DATA
SLO 1.0
DIFFRACTED ORDER INTENSITIES
VGM CELL K1074-123A
V_{APP} = 32V. t_{cell} = 6.0 μm

FIGURE 11

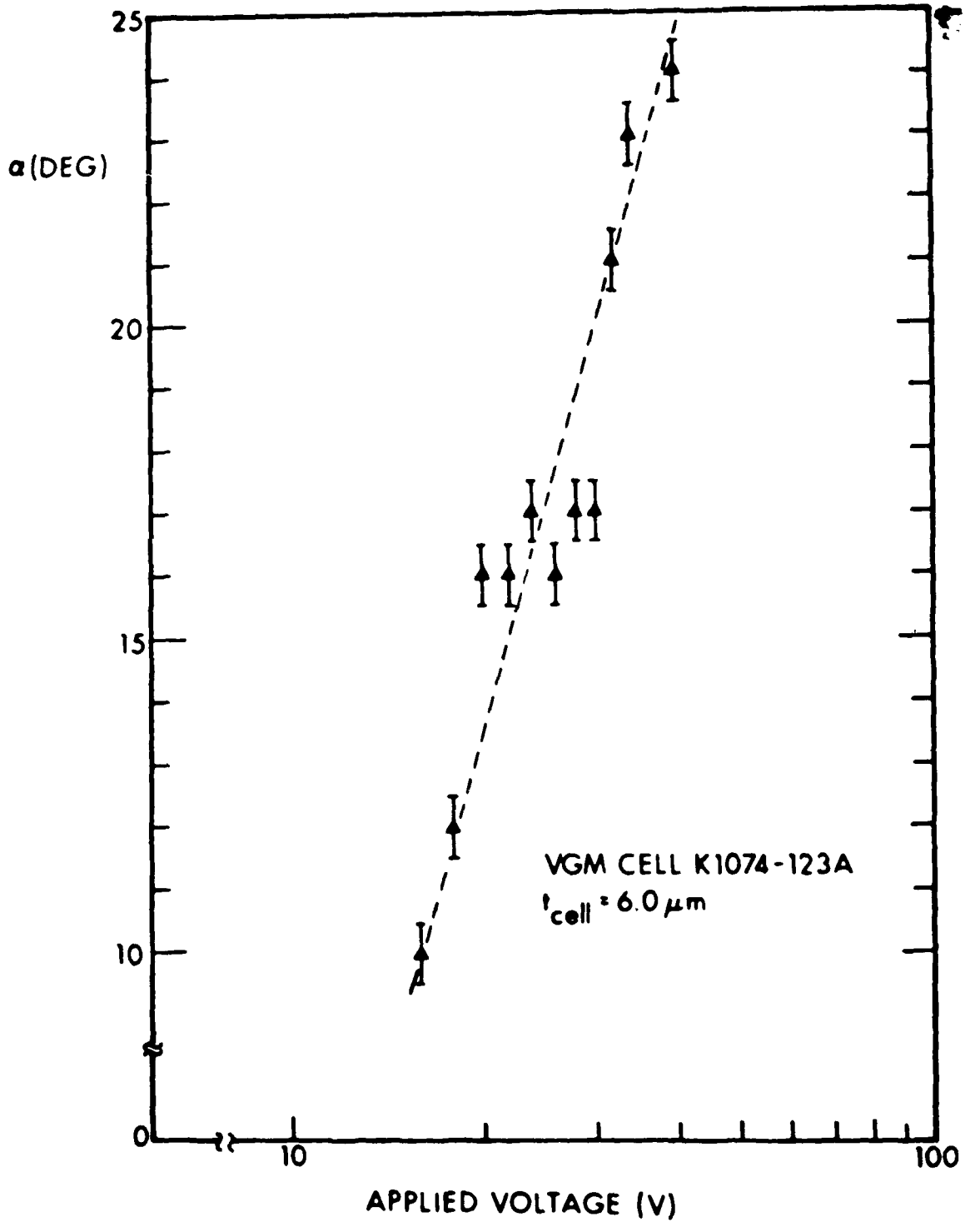
25
20
15
10
0
α(DEG)
10
100
APPLIED VOLTAGE (V)
VGM CELL K1074-123A
$t_{cell} = 6.0\,\mu m$

FIGURE 12

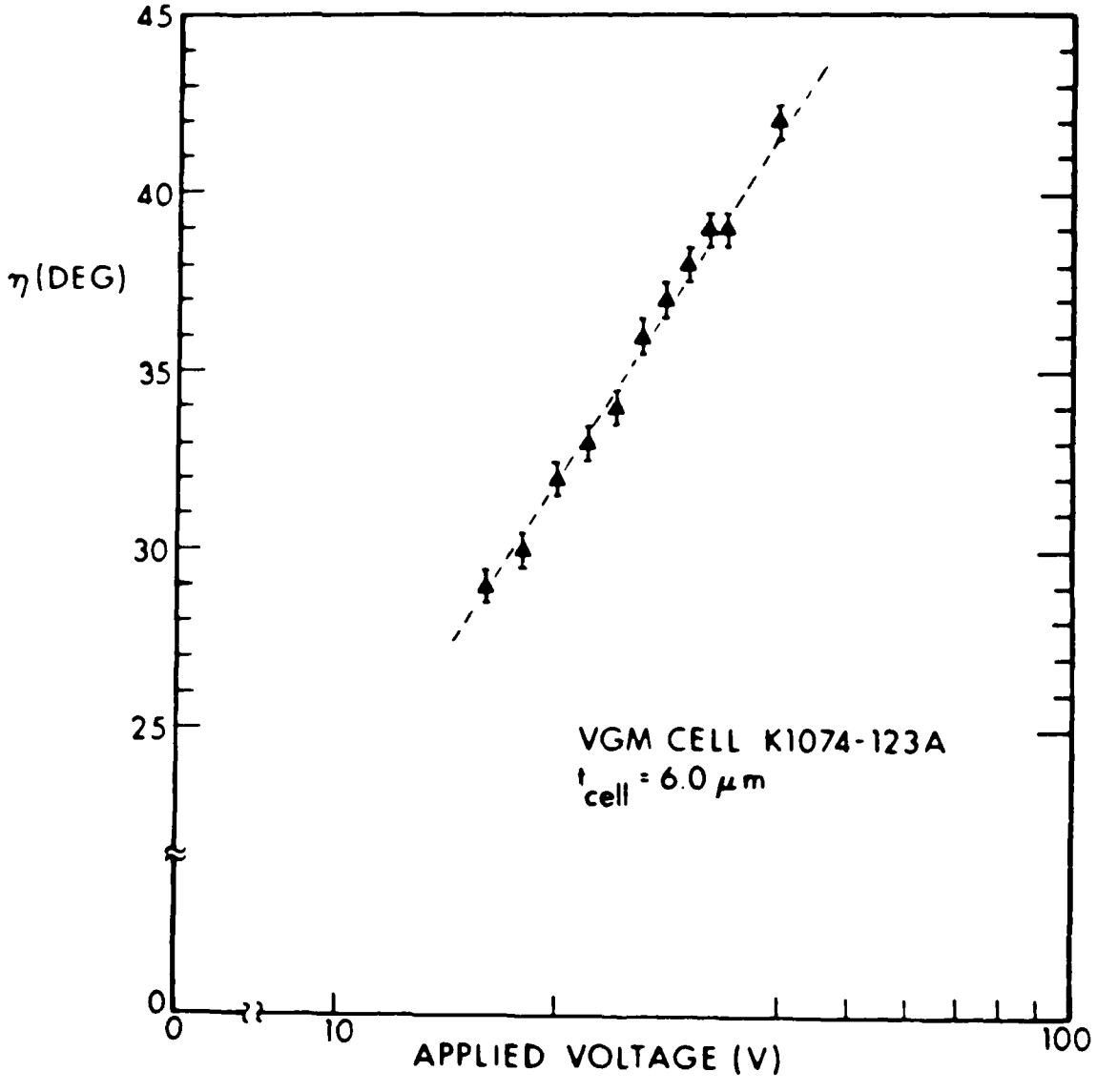
45
40
35
30
25
0
η(DEG)
0
10
100
APPLIED VOLTAGE (V)
VGM CELL K1074-123A
t_{cell} = 6.0 μm

FIGURE 13

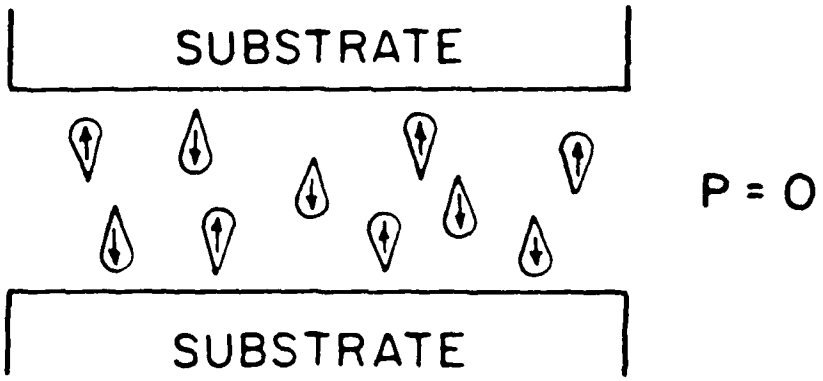

(a)

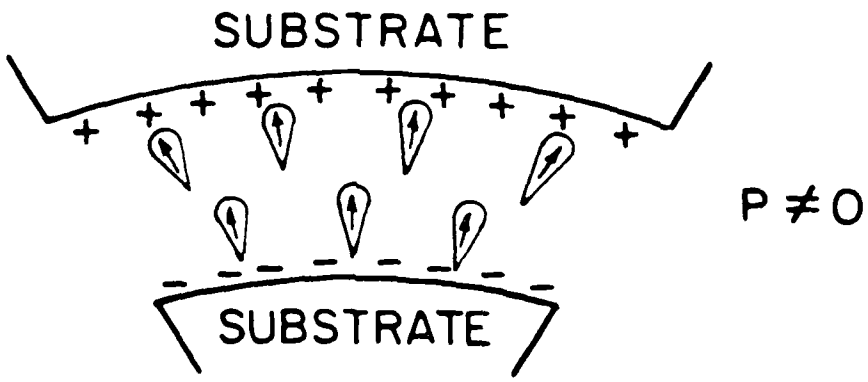

(b)

FIGURE 14

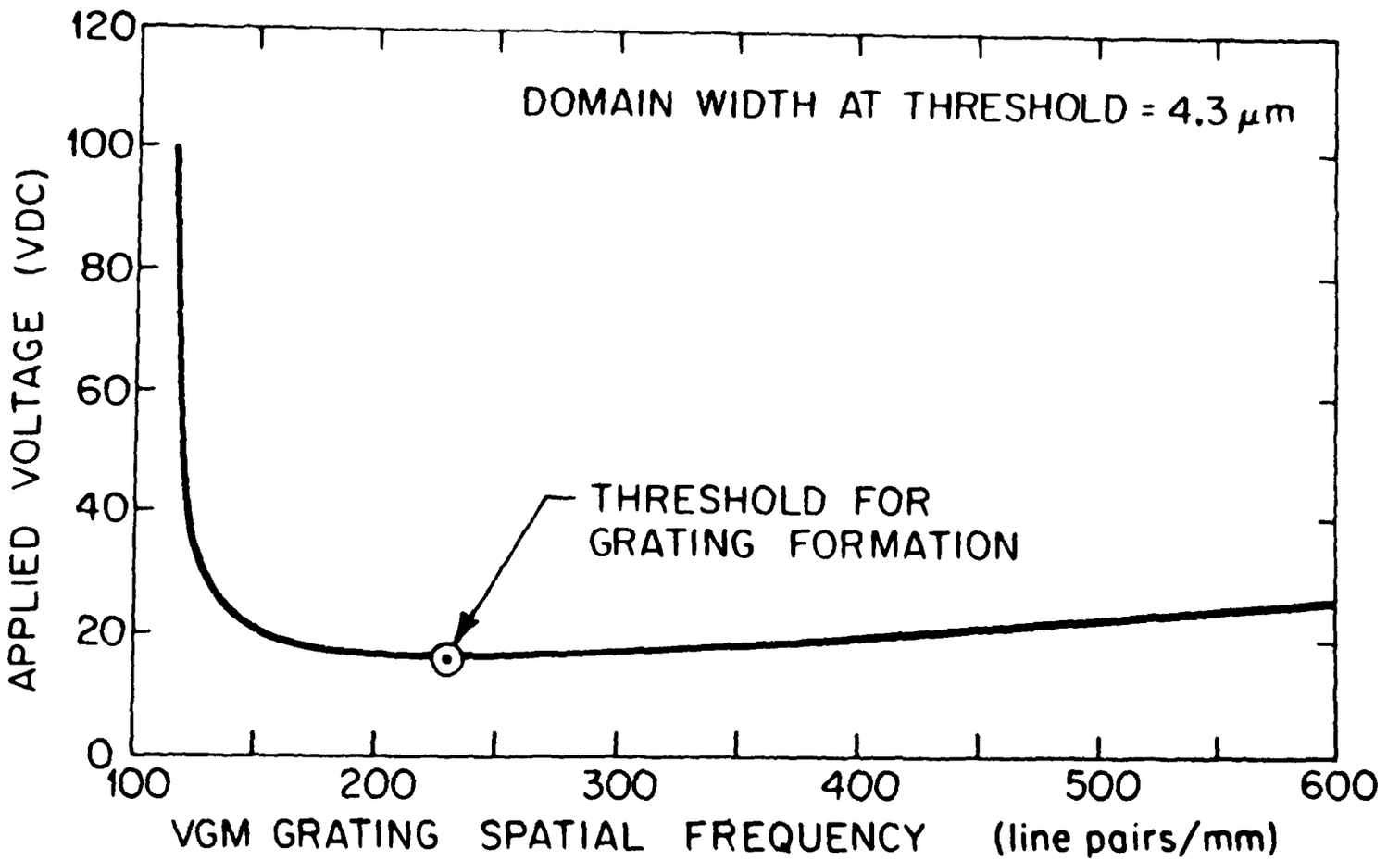
DOMAIN WIDTH AT THRESHOLD = 4.3 μm
THRESHOLD FOR
GRATING FORMATION
APPLIED VOLTAGE (VDC)
120
100
80
60
40
20
0
100
200
300
400
500
600
VGM GRATING SPATIAL FREQUENCY (line pairs/mm)

FIGURE 15

POLARIZATION PROPERTIES OF THE VARIABLE GRATING MODE LIQUID CRYSTAL DEVICE

A.R. Tanguay, Jr., P. Chavel†, T.C. Strand*, and C.S. Wu
Image Processing Institute, and Departments of Electrical Engineering and Materials Science,
University of Southern California, Los Angeles, California 90089
and
B.H. Soffer
Hughes Research Laboratories, 3011 Malibu Canyon Road,
Malibu, California 90265

ABSTRACT

The spatial distribution of the molecular orientation within the liquid crystal layer of the Variable Grating Mode (VGM) Liquid Crystal Device has been determined as a function of the applied voltage across the cell by measurement of the polarization properties of light diffracted by the liquid crystal birefringent phase grating.

† Permanent Address: Institut d'Optique, Université de Paris sud, BP 43, 91406 Orsay Cedex, France

* Present Address: IBM Corporation, 5600 Cottle Road, San Jose, California 95193

POLARIZATION PROPERTIES OF THE VARIABLE GRATING MODE LIQUID CRYSTAL DEVICE

The Variable Grating Mode (VGM) Liquid Crystal Device is a two-dimensional spatial light modulator that is capable of implementing an intensity-to-spatial frequency conversion over an input image field [1]. In this process, the intensity variations in an input image distribution are converted to local spatial frequency variations in a phase grating structure within the liquid crystal layer. As a direct result of this intensity-to-spatial frequency transduction, programmable spatial filtering of the converted image results in selected modifications of the input intensities. Utilizing this device concept, a wide variety of optical processing and computing functions have been demonstrated, including linearity compensation and nonlinear function implementation, thresholding, level slicing, binary logic (AND, OR, NOR, etc.), full binary addition, and matrix addressing operations [1-3]. The operation of this photoactivated device has been described in detail previously [4].

An important area of research on the VGM liquid crystal device is concerned with a fundamental understanding of the origin of the "variable grating" effect, in which a thin layer of nematic liquid crystal sandwiched between transparent conductive coatings (Fig. 1)

is observed to exhibit a periodic refractive index anisotropy under application of an applied dc bias voltage between the electrodes. This index modulation results in the formation of a birefringent phase grating [5] characterized by a fundamental spatial frequency that depends on the magnitude of the voltage across the liquid crystal layer. The orientation of the grating is such that the grating wavevector is perpendicular to the direction of unperturbed alignment, which is homogeneous and induced by unidirectional rubbing or ion beam milling. That is, the periodic modulation direction is perpendicular to the initial (zero applied bias) liquid crystal director (long molecular axis), as shown in the polarization micrographs (Fig. 2).

The polarization behavior of light diffracted from this birefringent phase grating is quite striking. For all linear input polarization angles, the even and odd diffraction orders are found to be essentially linearly polarized. In addition, the even diffraction orders are linearly polarized parallel to the "domains" comprising the VGM grating, as shown in Fig. 3. For input polarization perpendicular to the domains, the even orders are found to be almost fully extinguished. On the other hand, the odd diffraction orders are linearly polarized with a major axis that rotates counterclockwise at the same rate as the input polarization is rotated clockwise. This effect is the same as that produced by a half-wave plate oriented at 45° to the grating wavevector. For input polarization at 45° to the wavevector, all orders are observed in the far field diffraction pattern. For this situation,

an analyzer placed on the output side of the VGM device can be rotated to extinguish the even orders (when oriented parallel to the grating vector) or the odd orders (when oriented at -45° to the grating wavevector). Above the voltage threshold for grating formation, the intensities of the diffracted orders increase dramatically as a function of increasing applied voltage (increasing spatial frequency), and asymptotically saturate.

Observations of the variable grating mode structure in the polarizing microscope provide correlating evidence for the diffraction phenomena described above. For input polarization perpendicular to the grating wavevector, the periodic modulation is observed through a parallel analyzer to have a principal grating period p which corresponds to the measured diffraction angles of the even orders (see Figure 2(a)). For input polarization parallel to the grating wave vector, the periodic modulation is observed through a perpendicular analyzer to have a period 2p which corresponds to the measured diffraction angles of all orders. Other input polarization orientations produce apparent superposition of the p and 2p gratings as shown in Fig. 2(b), in agreement with the diffraction experiment results. These experiments are performed with the focus set at the upper surface of the liquid crystal layer. The grating contrast can be altered, and in some cases reversed, by adjusting the focal plane to lie within or below the liquid crystal layer.

The polarization properties of light diffracted by the liquid crystal birefringent phase grating can be summarized by means of a transfer matrix that connects the output polarization at the rear surface of the liquid crystal layer with the input polarization at the front surface of the liquid crystal layer. On the basis of the experimental observations, this matrix must be of the form:

$$\begin{bmatrix} A_o + A(x;p) & B(x;2p) \\ C(x;2p) & D_o + D(x;p) \end{bmatrix} \tag{1}$$

in which the notation A(x,p) indicates that the complex amplitude A varies in the x direction with periodic repetition distance p. Fourier expansion of the transfer matrix yields the complex amplitudes A_n, B_n, C_n, and D_n which completely specify the contributions of each component of the input polarization to the observed polarization of the n^{th} diffracted order:

$$\begin{bmatrix} A & B \\ C & D \end{bmatrix} = \sum_{n=-\infty}^{\infty} e^{j2\pi xn/\Lambda} \begin{bmatrix} A_n & B_n \\ C_n & D_n \end{bmatrix} \tag{2}$$

where $\Lambda = 2p$ is the fundamental (lowest order) grating wavelength.

The polarization transfer matrix can be calculated by considering the uniaxial liquid crystal molecules at a given spatial coordinate x to be characterized by a twist angle α in the plane of the grating, followed by a tilt angle η out of the plane of the grating. The Jones matrix for this case can be determined

by appropriate rotations of the index ellipsoid, which yield:

$$\begin{bmatrix} 1 - \sin^2\alpha(1 - e^{j\phi}) & \sin\alpha\cos\alpha(1 - e^{j\phi}) \\ \sin\alpha\cos\alpha(1 - e^{j\phi}) & 1 - \cos^2\alpha(1 - e^{j\phi}) \end{bmatrix} \tag{3}$$

where

$$\phi \equiv \frac{2\pi t}{\lambda}\left\{\left[\frac{\sin^2\eta}{n_o^2} + \frac{\cos^2\eta}{n_e^2}\right]^{-\frac{1}{2}} - n_o\right\}$$

in which t is the liquid crystal layer thickness, n_o is the ordinary refractive index, n_e is the extraordinary refractive index, and λ is the wavelength of readout illumination employed. A uniform phase factor in Eq. (3) has been suppressed. The angles α and η are assumed to be periodic functions of x and independent of y and z; since the index ellipsoid will in general have its principal axes skewed relative to the original coordinate system, the polarization transfer matrix is not diagonal.

Measurement of the intensities in each diffraction order for a minimum set of polarizer/analyzer orientations uniquely determine the values of $|A_n|^2$, $|B_n|^2$, $|C_n|^2$, and $|D_n|^2$. These experimentally derived values can then be compared with the theoretically calculated coefficients of Eq. (3) (utilizing the harmonic expansion of Eq. (2)) for different possible assumptions concerning the spatial distribution of the orientation angles α and η. Consideration of simple harmonic motion of the out-of-plane angle

can be shown to explain the polarization behavior of the even diffracted orders [5], while similar motion of the in-plane angle α yields the polarization behavior of the odd diffracted orders [5]. Hence as a trial solution we may take:

$$\alpha = \alpha_{max} \cos \frac{2\pi x}{\Lambda} \qquad \eta = \pm \eta_{max} \sin \frac{2\pi x}{\Lambda} \qquad (4)$$

The spatial distribution in the x-direction of the ends of the liquid crystal molecules at a given z-coordinate as described by Eq. 4 is cycloidal in nature.

An example of such a comparison between theory and experiment for a large number of diffracted orders is shown in Fig. 4. In this experiment, the VGM liquid crystal utilized was a phenyl benzoate mixture (Hughes 2N40 [1]), the cell thickness was 6.0 μm, and the applied voltage was 32 VDC. To obtain the data shown in this Figure, α_{max} and η_{max} have been utilized as the only adjustable parameters. The assumed simple harmonic spatial dependence of the angles α and η is justified by the quality of fit evident in Fig. 4. In addition, such a dependence of the angles α and η on the spatial coordinate x has been predicted by direct minimization of the free energy in a similar nematic liquid crystal system [6].

The fitting procedure described above allows the extraction of the maximum orientational excursion angles $\alpha_{max}(V)$ and $\eta_{max}(V)$ as functions of the applied bias voltage above the threshold for

grating formation, as shown in Fig. 5 ($\eta_{max}(V)$) and in Fig. 6 ($\theta_{max}(V)$). In each case, it is observed that the maximum excursion angles both in and out of the plane of the grating seem to increase as the logarithm of the applied voltage.

Numerous experimental measurements of the off-diagonal elements in the Jones matrix describing polarized light propagation through the VGM cell have revealed a significant asymmetry not predicted by the uniaxial model. The origin of this "B/C" asymmetry effect is under continuing investigation.

In conclusion, we have utilized the polarization properties of the diffracted orders from a liquid crystal birefringent phase grating to deduce the spatial distribution of the molecular orientation within the liquid crystal layer.

ACKNOWLEDGEMENTS

The authors gratefully acknowledge the contributions of D. Boswell, A.M. Lackner, and J.D. Margerum (H.R.L.), and A.A. Sawchuk (U.S.C.). This research was supported by the U.S. Air Force Office of Scientific Research, Electronics and Solid State Sciences Division, under grant AFOSR-81-0082 at the University of Southern California and contract F49620-81-C-0086 at Hughes Research Laboratories.

REFERENCES

1. B.H. Soffer, J.D. Margerum, A.M. Lackner, D. Boswell, A.R. Tanguay, Jr., T.C. Strand, A.A. Sawchuk, and P. Chavel, Mol. Cryst. Liq. Cryst., 70, 145-161, 1981.

2. P. Chavel, A.A. Sawchuk, T.C. Strand, A.R. Tanguay, Jr., and B.H. Soffer, Opt. Lett., 5, 398-400, 1980.

3. B.H. Soffer, D. Boswell, A.M. Lackner, P. Chavel, A.A. Sawchuk, T.C. Strand, and A.R. Tanguay, Jr., Proc. Soc. Photo-Opt. Instrum. Eng., 232, 128-136, 1980.

4. B.H. Soffer, D. Boswell, A.M. Lackner, A.R. Tanguay, Jr., T.C. Strand, and A.A. Sawchuk, Proc. Soc. Photo-Opt. Instrum. Eng., 218, 81-87, 1980.

5. A.R. Tanguay, Jr., Opt. Lett., (in press), 1983.

6. Yu. P. Bobylev and S.A. Pikin, Sov. Phys. JETP, 45, 195-198, 1977.

FIGURE CAPTIONS

Figure 1 Variable grating mode liquid crystal test geometry showing the cartesian coordinate system referred to in the text as well as the molecular orientation angles α and η. This configuration was utilized in the polarized light diffraction efficiency and photomicroscopy experiments.

Figure 2 Polarization micrographs of the liquid crystal domain pattern in an electrically activated cell. In (A), the polarizer was oriented at 90°, and the analyzer at 90°, with respect to the grating wavevector. In (B), the polarizer was oriented at 90°, and the analyzer at 10°, with respect to the grating wavevector.

Figure 3 The polarization behavior of VGM diffracted orders. The left hand column indicates the input polarization associated with each row of output polarizations. The inset shows the direction of VGM domain orientation.

Figure 4 Measured diffracted order intensities as a function of theoretical intensities calculated from the uniaxial VGM model described in the text.

Figure 5 The out-of-plane molecular orientation angle, η, as a function of the applied dc bias voltage across the cell, V.

Figure 6 The in-plane molecular orientation angle, α, as a function of the applied dc bias voltage across the cell, V.

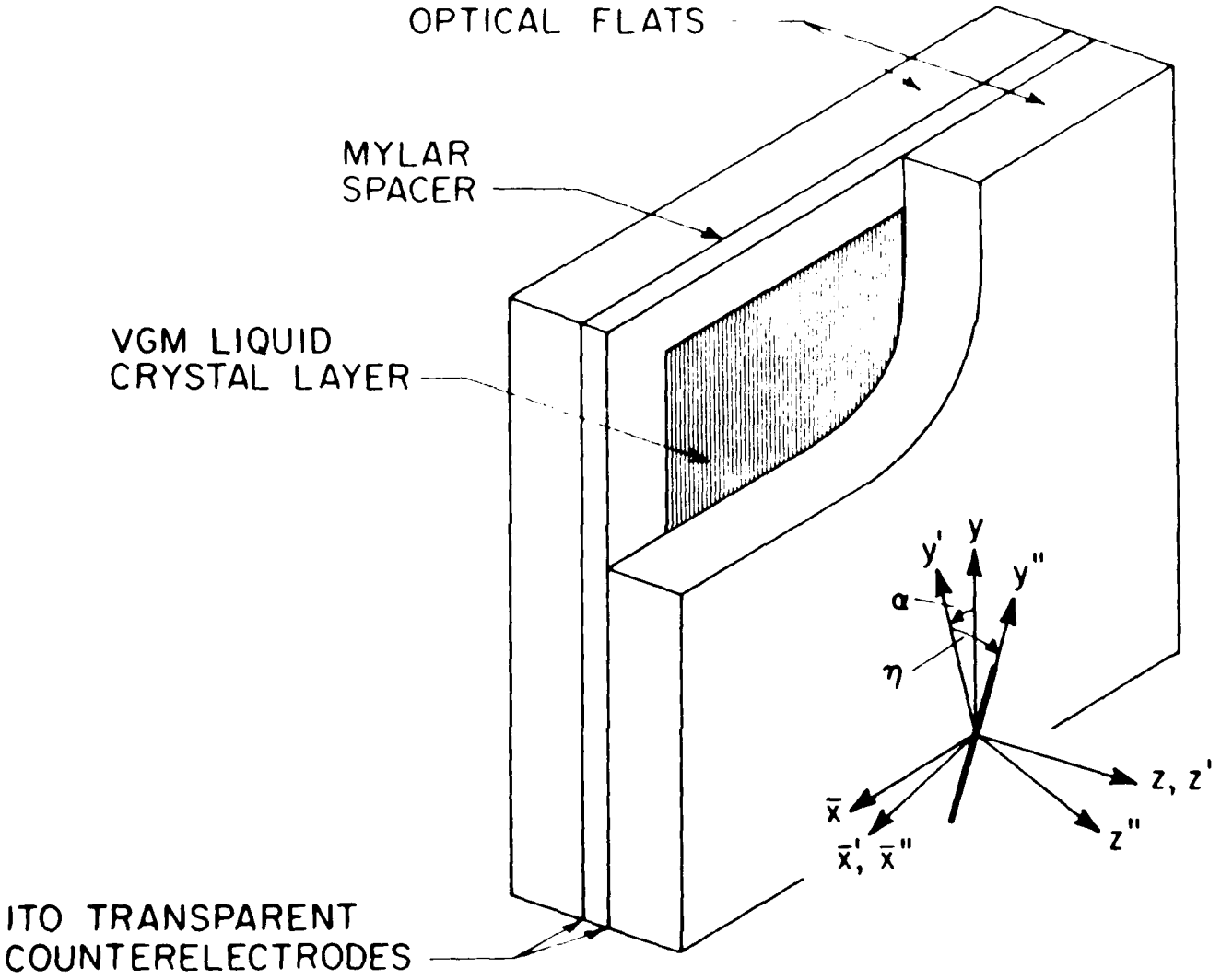
OPTICAL FLATS
MYLAR
SPACER
VGM LIQUID
CRYSTAL LAYER
ITO TRANSPARENT
COUNTERELECTRODES
y'
y
y"
α
η
z, z'
z"
x̄
x̄', x̄"

FIGURE 1

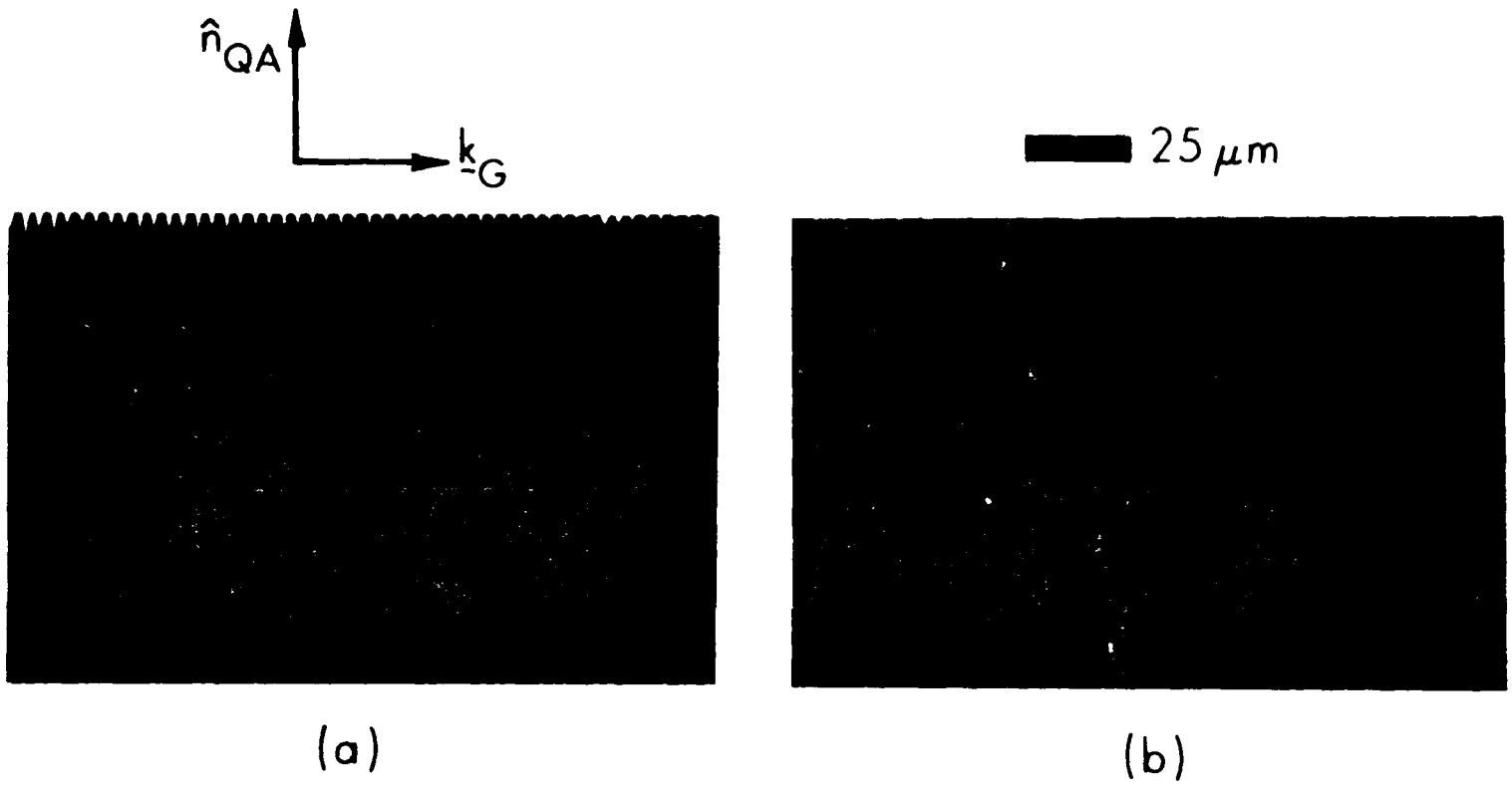

FIGURE 2

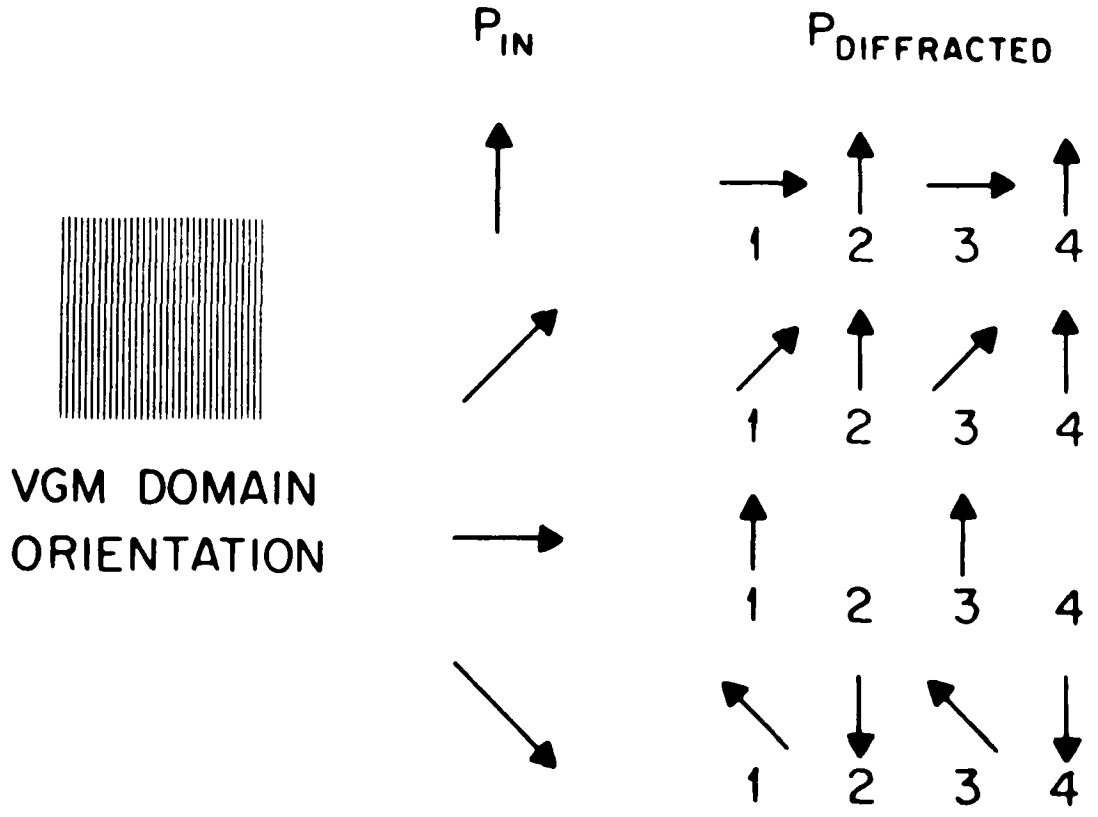
VGM DOMAIN
ORIENTATION
P IN
P DIFFRACTED
1 2 3 4
1 2 3 4
1 2 3 4
1 2 3 4

FIGURE 3

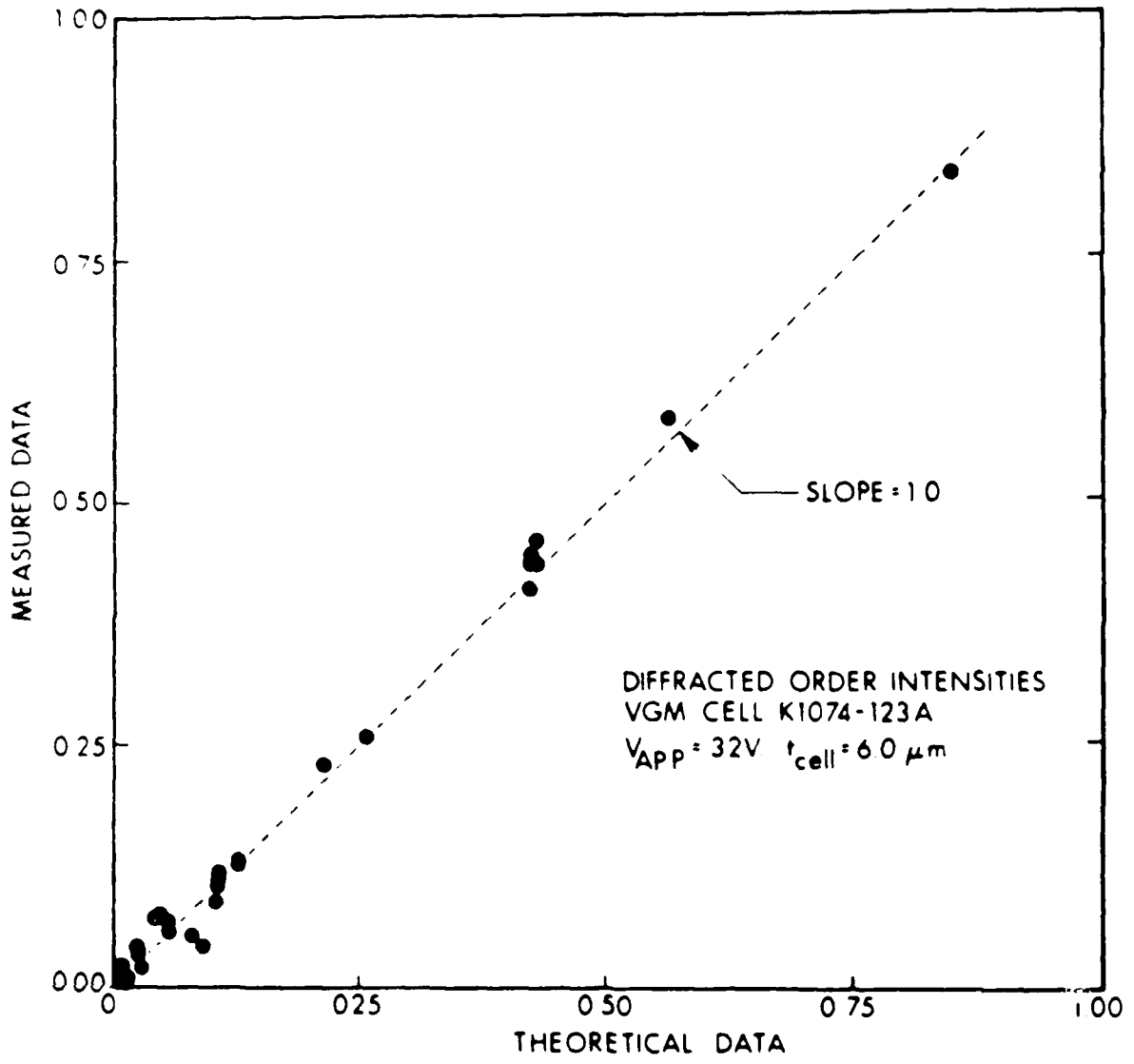
1 00
0 75
0 50
0 25
0 00
MEASURED DATA
0
025
0 50
0 75
1 00
THEORETICAL DATA
SLOPE = 1 0
DIFFRACTED ORDER INTENSITIES
VGM CELL K1074-123A
V_{APP} = 32V t_{cell} = 6 0 μm

FIGURE 4

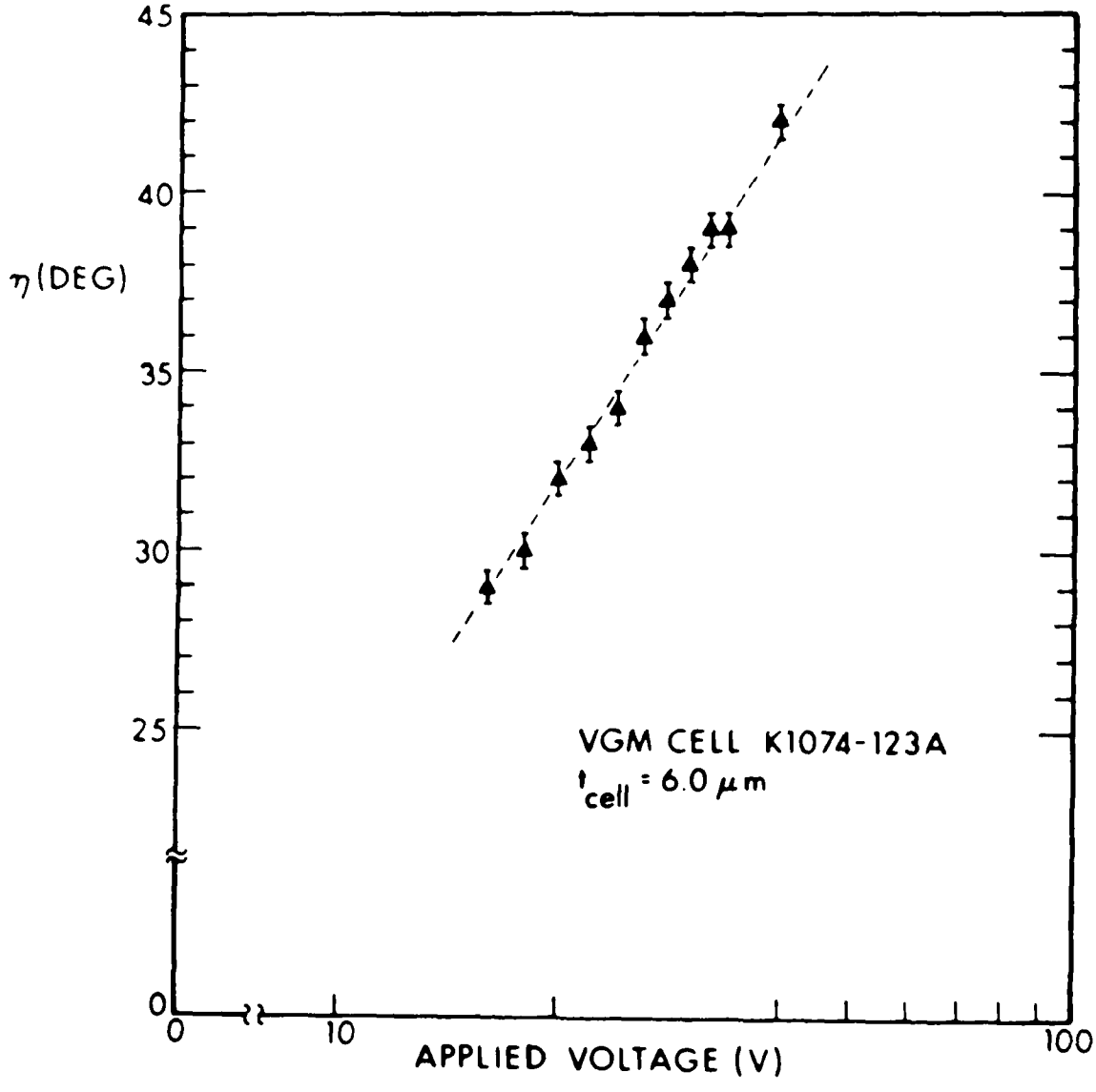
45
40
35
30
25
0
0
10
100
η(DEG)
APPLIED VOLTAGE (V)
VGM CELL K1074-123A
t_{cell} = 6.0 μm

FIGURE 5

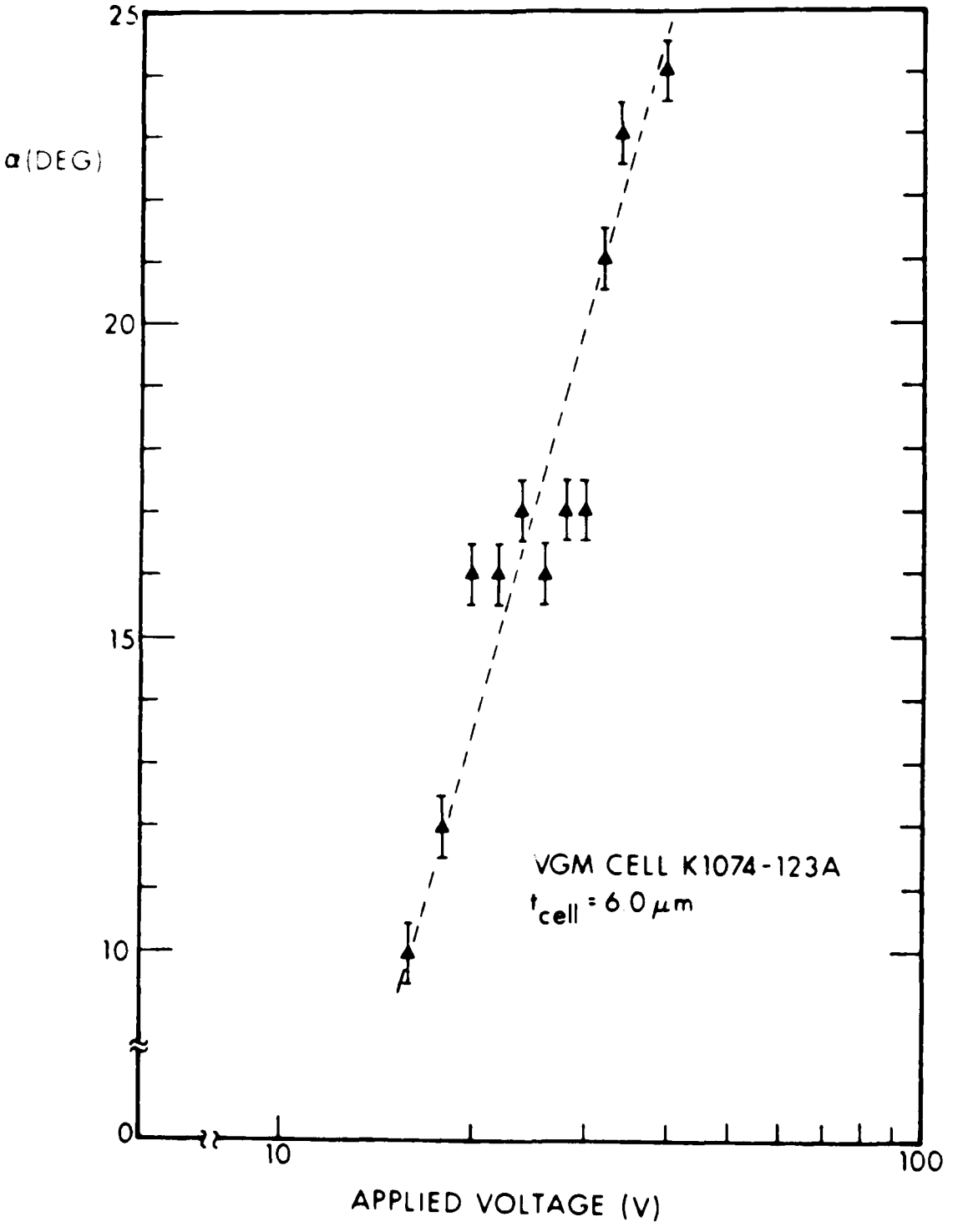
25
20
15
10
0
α(DEG)
10
100
APPLIED VOLTAGE (V)
VGM CELL K1074-123A
$t_{cell} = 6.0\,\mu m$

FIGURE 6

1.4 References

1. A.A. Sawchuk and T.C. Strand, "Fourier Optics in Nonlinear Signal Processing," Ch 9 of Applications of Optical Fourier Transform, H. Stark, ed., Academic, New York, 1981.

2. A. Armand, A.A. Sawchuk, T.C. Strand, B.H. Soffer and D. Boswell, "Real-time Parallel Optical Analog-to-Digital Conversion," Optics Letters, vol. 5, pp. 129-131, 1980.

3. P. Chavel, A.A. Sawchuk, T.C. Strand, A.R. Tanguay, Jr., and B.H. Soffer, "Optical Logic with Variable-Grating-Mode Liquid-Crystal Devices," Optics Letters, vol. 5, pp. 398-400, 1980.

4. B.H. Soffer, J.D. Margerum, A.M. Lackner, D. Boswell, A.A. Sawchuk, T.C. Strand, A.R. Tanguay, Jr., and P. Chavel, "Variable Grating Mode Liquid Crystal Device for Optical Processing and Computing," Molecular Crystals and Liquid Crystals, vol. 70, pp. 145-161.

5. A.A. Sawchuk, "Intensity-to-spatial Frequency Transformations," Proceedings Society of Photo-Optical Instrumentation Engineers Advanced Institute of Transformations in Optical Signal Processing, Seattle, (February 1981).

6. A.A. Sawchuk, "Recent Developments in Optical and Digital Processing," Proceedings Workshop on Optical Information Processing, Centro de Investigaciones en Optica, Cuernavaca, Mexico, (January 1982).

7. A.R. Tanguay, Jr., P. Chavel, T.C. Strand, J. Wu, and B.H. Soffer, "Physical Characterization of the Variable Grating Model Liquid Crystal Devices," SPIE Proc. Advances in Optical Information Processing, vol. 388, (January 1983).

8. A.R. Tanguay, Jr., P. Chavel, T.C. Strand, and J.S. Wu, "Polarization Properties of the Variable Grating Mode Liquid Crystal Device," to be submitted to Applied Optics.

9. A.R. Tanguay, Jr., T.C. Strand, P. Chavel, A.A. Sawchuk, and B.H. Soffer, "Theoretical and Experimental Polarization Properties of the Variable Grating Mode Liquid Crystal Structure," presented at 1981 Annual Meeting, Optical Society of America, Orlando, Florida, October 1981, Journal of the Optical Society of America, vol. 71, p. 1630, (December 1981).

10. A.R. Tanguay, Jr., "Recent Progress in Spatial Light Modulators for Coherent Optical Processing Applications," 1982 Gordon Conference on Holography and Optical Information Processing, Plymouth, New Hampshire, 1982.

11. A.R. Tanguay, Jr., "Polarization Properties of Birefringent Phase Gratings," presented at 1982 Annual Meeting, Optical Society of America, Tucson, Arizona, October 1982: Journal of the Optical Society of America, vol. 72, (1982).

12. A.R. Tanguay, Jr., "Spatial Light Modulators for Real Time Optical Processing," Proc. ARO Workshop on Future Directions for Optical Information Processing, pp. 52-76, Lubbock, Texas, May, 1980.

13. P.G. de Gennes, The Physics of Liquid Crystals Claredon Press, Oxford, (1975).

14. Yu P. Bobylev and S.A. Pikin, "Threshold Piezoelectric Instability in a Liquid Crystal," Sov. Phys. JETP, vol. 45, pp. 195-198, (1977).

15. R.B. Meyer, Phys. Rev. Lett., vol. 22, 918, (1969).

16. P. Auborg, J.P. Huignard, N. Hareng, and R.A. Mullen, "Liquid Crystal Light Valve Using Bulk Monocrystalline $Bi_{12}SiO_{20}$ as the Photoconductive Material," Appl. Opt., vol. 21, 3706-3711, (1982).

2. PROFESSIONAL PERSONNEL

The following individuals contributed to the research effort supported by this grant from the April 15, 1981 starting date.

1. Alexander A. Sawchuk, Professor, Department of Electrical Engineering, Director - Image Processing Institute, Principal Investigator.

2. Timothy C. Strand, Research Associate Professor, Image Processing Institute, Senior Investigator.

3. Armand R. Tanguay, Jr., Associate Professor, Departments of Electrical Engineering and Materials Science, and Image Processing Institute, Senior Investigator.

4. Pierre H. Chavel, Visiting Research Scientist, Image Processing Institute (on leave from Institut d'Optique, Orsay, France).

5. Robert Forchheimer, Visiting Research Scientist, Image Processing Institute (on leave from Linkoping University, Linkoping, Sweden).

6. Keith Jenkins, Research Assistant, Ph.D. Candidate, Department of Electrical Engineering.

7. John Wu, Research Assistant, Ph.D. Candidate, Department of Electrical Engineering.

3. PUBLICATIONS

This section lists written publications resulting from AFOSR support of this project from the April 15, 1981 starting date.

1. A.A. Sawchuk and T.C. Strand, "Fourier Optics in Nonlinear Signal Processing," Ch. 9 of Applications of Optical Fourier Transforms, H. Stark, ed., Academic, New York, (1981).

2. A. Armand, A.A. Sawchuk and T.C. Strand, "Nonlinear Optical Processing with Halftones: Accurate Predictions for Degradation and Compensation," to be submitted to Applied Optics.

3. A. Armand, A.A. Sawchuk, T.C. Strand, and B.H. Soffer, "Real-Time Parallel Logarithmic Filtering," Optics Letters, vol. 7, pp. 451-453, (September 1982).

4. B.H. Soffer, J.D. Margerum, A.M. Lackner, D. Boswell, A.A. Sawchuk, A.R. Tanguay, Jr., T.C. Strand, and P. Chavel, "Variable Grating Mode Liquid Crystal Device for Optical Processing and Computing," Molecular Crystals and Liquid Crystals, vol. 70, pp. 145-161, (1981).

5. A.A. Sawchuk, "Intensity-to-Spatial Frequency Transformations," Proceedings Society of Photo-Optical Instrumentation Engineers Advanced Institute on Transformations in Optical Signal Processing, Seattle, (February 1981).

6. A.A. Sawchuk, "Recent Developments in Optical and Digital Processing," Proceedings Workshop on Optical Information Processing, Centro de Investigaciones en Optica, Cuernavaca, Mexico, (January 1982).

7. A.R. Tanguay, Jr., C.S. Wu, P. Chavel, T.C. Strand, A.A. Sawchuk, and B.H. Soffer, "Physical Characterization of the Variable Grating Mode Liquid Crystal Device," SPIE Proc. Advances in Optical Information Processing, vol. 388, (January 1983).

8. A.R. Tanguay, Jr., P. Chavel, T.C. Strand, C.S. Wu, and B.H. Soffer, "Polarization Properties of the Variable Grating Model Liquid Crystal Device," submitted to Optics Letters.

9. P. Chavel, R. Forchheimer, B.K. Jenkins, A.A. Sawchuk, and T.C. Strand, "Architectures for a Sequential Optical Logic Processor," Proceedings 10th International Optical Computing Conference, IEEE Cat. No. 83CH1880-4, pp. 6-12, (April 1983).

10. A.R.Tanguay, Jr., C.S. Wu, P. Chavel, T.C. Strand, and A.A. Sawchuk, "Physical Characterization of the Variable Grating Mode Liquid Crystal Device", Optical Engineering, Vol. 22, (November/December 1983), to appear.

11. B.K. Jenkins, A.A. Sawchuk, T.C. Strand, R. Forchheimer,and B.H. Soffer, "Sequential Optical Logic Implementation," submitted to Applied Optics.

12. B.K. Jenkins and T.C. Strand, "Computer-Generated Holograms for Space-Variant Interconnections in Optical Logic Systems, "SPIE Proc., vol. 437, (August 1983).

13. B.K. Jenkins, P. Chavel, R. Forchheimer, A.A. Sawchuk and T.C. Strand," Architectural Implications of Digital Optical Processors", submitted to Applied Optics.

4. ORAL PRESENTATIONS

This section lists oral presentations at meetings and conferences describing research supported by this grant from the April 15, 1981 starting date.

1. A.R. Tanguay, Jr., T.C. Strand, P. Chavel, A.A. Sawchuk and B.H. Soffer, "Theoretical and Experimental Polarization Properties of the Variable Grating Mode Liquid Crystal Structure," presented at 1981 Annual Meeting, Optical Society of America, Orlando, Florida, October 1981, Journal of the Optical Society of America, vol. 71, p. 1630, (December 1981).

2. A.R. Tanguay, Jr., "Recent Progress in Spatial Light Modulators for Coherent Optical Processing Applications," 1982 Gordon Research Conference on Holography and Optical Information Processing, Plymouth, New Hampshire, (1982), (Invited Paper).

3. A.R. Tanguay, Jr., "Polarization Properties of Birefringent Phase Gratings," 1982 Gordon Research Conference on Holography and Optical Information Processing, Plymouth, New Hampshire, (1982), (Invited Paper).

4. B.K. Jenkins, A.A. Sawchuk, T.C. Strand, and B.H. Soffer, "Sequential Optical Logic Implementation," presented at 1982 Annual Meeting, Optical Society of America, Tucson, Arizona, October 1982; Journal of the Optical Society of America, vol. 72, p. 1721, (1982).

5. A.R. Tanguay, Jr., "Polarization Properties of Birefringent Phase Gratings," presented at 1982 Annual Meeting, Optical Society of America, Tucson, Arizona, October 1982; Journal of the Optical Society of America, Vol. 72, p. 1832, (1982).

6. B.K. Jenkins, A.A. Sawchuk, T.C. Strand, "Spatial Light Modulator Requirements for Sequential Optical Logic," presented at 1983 Annual Meeting, Optical Society of America, New Orleans, October 1983; Journal of the Optical Society of America, Vol. 73, (1983).

7. A.A. Sawchuk and T.C. Strand, "Digital Optical Computing Techniques", presented at 1983 Annual Meeting, Optical Society of America, New Orleans, October 1983; Journal of the Optical Society of America, Vol. 73, (1983).